University of Sussex

Exploiting symmetry and criticality in quantum sensing and quantum simulation

Samuel Fernández Lorenzo

Submitted for the degree of Doctor of Philosophy

University of Sussex

February 2018

To Kathryn,
the one who believed.

Declaration

I hereby declare that this thesis has not been and will not be submitted in whole or in part to another University for the award of any other degree.

This thesis is written based on the following publications:

- *Topological phases of shaken quantum Ising lattices.* S. Fernández-Lorenzo, J.J. García-Ripoll, D. Porras. New J. Phys. 18 (2), 023030 (2016). I contributed to the mathematical aspects of this paper under the guidance of D. Porras. J.J. García-Ripoll helped with the coding for the numerical analysis and wrote the section *Ultracold bosons in optical lattices.* D. Porras wrote the implementation in Rydberg atoms, section *Rydberg atoms in optical lattices.*

- *Quantum sensing close to a dissipative phase transition: Symmetry breaking and criticality as metrological resources.* S. Fernández-Lorenzo, D. Porras. Phys. Rev. A 96 (1), 013817 (2017). I contributed to the mathematical aspects of this paper, under the guidance of D.Porras, who also wrote the implementation in trapped ions, section *Physical implementations.*

- *Heisenberg scaling with classical long-range correlations.* S. Fernández-Lorenzo, J.A. Dunningham, D. Porras. Phys. Rev. A 97 (2), 023843 (2018). I contributed to all aspects of this paper, with other authors giving comments and advice.

Signature:

Samuel Fernández Lorenzo

UNIVERSITY OF SUSSEX

Samuel Fernández Lorenzo, Doctor of Philosophy

Exploiting symmetry and criticality in quantum sensing and quantum simulation

Summary

Decoherence and errors appear among the main challenges to implement successful quantum technologies. In this thesis I discuss the application of some general tools and principles that may be valuable resources to develop robust technologies, with applications in quantum sensing and quantum simulation.

Firstly, we employ suitable periodically driving fields acting on the Ising model in order to tailor spin-spin interactions depending on the spatial direction of the bonds. In this way, we are able to simulate the quantum compass model on a square lattice. This system exhibits topological order and a doubly degenerate ground state protected against local noise. A possible implementation of this proposal is outlined for atomic quantum simulators.

Secondly, we exploit two general working principles based on spontaneous symmetry breaking and criticality that may be beneficial to achieve robust quantum sensors, particularly appropriate for quantum optical dissipative systems. A concrete application is given for a minimal model: a single qubit laser. It is shown how the precision in parameter estimation is enhanced as the incoherent pumping acting on the qubit increases, and also when the system is close to the lasing critical point.

Finally, classical long-range correlations in lattice systems are shown to provide us with an additional resource to be used in robust sensing schemes. The previous setup is extended to a lattice of single qubit lasers where interactions are incoherent. Under the right conditions, we show that a Heisenberg scaling with the number of probes can be accomplished.

Acknowledgements

Ever since I was 15 years old, I dreamt of becoming a Doctor of Philosophy in Physics at some point in my life. If that old dream comes true, it is because of the opportunity that my supervisor, Diego Porras, gave me some years ago to begin my scientific career. For that I will be indelibly grateful to him. Not only I have learned a great deal from his enormous scientific insight, but he also gave me the space and time to develop my own scientific ideas. It has been an honor to work with Diego.

I feel also privileged for having carried out my research at the University of Sussex, which provided me with a warm and comfortable environment to focus on what was really important: Science. My time in Brighton has been undoubtedly intense, where I have lived incredibly positive experiences, and also really difficult moments. But after all, it has been a fruitful experience that life granted me to become the person who I wanted to be.

My work has benefited greatly from the contribution of Juan José García Ripoll and Jacob Dunningham, to whom I can only express my gratitude and admiration for their help.

I would also like to thank some people that have contributed, in some way, to help me complete this long adventure towards my PhD.

First and foremost, I want to thank my parents for the support and respect they showed through my journey to become a Physicist first, and afterwards during these last years away from home. Even though they would probably have chosen another lifestyle for me, they allowed me to follow my own path. Their encouragement have been also important many times.

I had the enormous privilege to meet and enjoy a priceless friendship with one the most incredible human beings I ever met: Kathryn Alice Burrows. There are no words that could possibly describe how much she helped me during my time in Brighton, and how much her faith has inspired me to become the very best version

of myself. I will never be able to repay her emotional and intellectual support. Also, she did an excellent job in proofreading this thesis.

I feel greatly thankful to Mikel Sanz, who has been a mentor for me and from whom I have learned so much about being a scientist and the scientific career. His passion for Science and his timely emotional support have been also key at some crucial moments. Also, I must thank Carlos Navarrete for his valuable advise whenever I required it.

Alicia Moreno gave me the love that many times I was craving for and I couldn't enjoy. I could not be more grateful for her illuminating presence in my life.

Cris (Lunastica) was a fresh injection of energy and passion during the last year. Her loving character, her enormous capacity to listen to me and her encouragement have been extremely important during many tough moments.

Even though our lives took different routes some time ago, a warm thank you goes to Angélica, as she also was part of this dream and supported it with her love.

Pedro Nevado and Jesús Rubio, with their help whenever necessary, also deserve my gratitude. Charlie Nation took the time to proofread this thesis, for which I'm very grateful to him.

Last but not least, I want to thank all those people who, one way or another, made my days in Brighton challenging, as they unintentionally gave me the keys to welcome the present moment.

Contents

List of Figures

Part I

Introduction and research context

Chapter 1

Quantum technologies

We live in fascinating and rapidly evolving times. For some decades now, we are immersed in the so-called information age, in which information has become one of our most valuable commodities, and the acute need for more powerful information technologies increases every day. As a result, the supply and demand of data is pushing the limits of our technological resources at a level that reach, or even surpass, the capabilities offered by our most advanced classical devices. This is happening in all aspects regarding information, whether acquisition, storage, processing or communication.

In response to this increasing demand, huge investments and research have been made to boost the potential of our classical technologies in order to manage large amounts of information as well as to increase our computational power. Firstly, our capacity to collect information has increased enormously, to the extent that we sometimes struggle to process it in conventional ways. The different methods to deal with this problem have even originated a discipline in itself, the recently popular *Big Data* [1], and its applications probably go unnoticed for many. For example, up to zettabytes of information concerning our likings and preferences is now commonly stored and evaluated by many companies like Amazon or Youtube to create recommender systems that suggest similar products likely to appeal to us. In the future, this tendency to acquire and use our personal information will probably be manifested in our daily life by the so-called *Internet of Things* (IoT) [2], a network of home appliances, vehicles and other items embedded with electronics that enable them to connect and exchange data. For business purposes, tools like *Google ana-*

lytics are already very popular to track and report website traffic, based on which a company may act accordingly to improve its marketing strategy. Secondly, our computational power has increased unceasingly thanks to the progress made in supercomputing and parallel computing, which for example has been used to unveil the secrets of the human genome. Lastly, we are witnessing the far-reaching revolution in the way we process information, brought about by the so-called *Artificial Intelligence* (A.I) [3], which makes use of cunning coding strategies like machine learning, neural networks or deep learning, with multiple applications ranging from image recognition to self-driving cars. All these new technologies lie at the forefront of the upcoming social and economic revolution, whose exciting and fast advances often pop up in the media.

In spite of all these advances, the computational power of classical computing has also its own limits. Fulfilling Moore's law prediction, we are now reaching a point where it will be impossible to miniaturize further our transistors to produce more powerful computer chips [4], as we will be reaching the scale of molecules and atoms, where classical physics is not a valid description of matter and light and quantum mechanics takes over. The ultimate frontier of computation will be given by our ability to control a totally different type of information: *quantum information* [5]. Single particles are not easily isolated from their surrounding environment and they lose their quantum properties soon after they interact with the outside world. Luckily, in the last decades a formidable progress has been carried out regarding the control of quantum systems in all its aspects. Namely, tremendous advances have been made in isolating, manipulating and detecting at the single quantum level.

More specifically, pioneering research was made by Serge Haroche (2012 Nobel Prize) and his group in Paris concerning trapping and controlling the particle of light: the photon [6–8]. They employed small cavities where photons could bounce back and forth between superconducting mirrors. These mirrors are so reflective that a single photon can be trapped inside for almost a tenth of a second before it is lost or absorbed. During its lifetime, several quantum operations can be performed with the trapped photon and test fundamental light matter interaction effects such as the quantum Rabi oscillations [9]. Regarding the manipulation of atoms or ions, leading groups like David Wineland's group (2012 Nobel Prize) in Boulder (USA) [10–12]

and R. Blatt's (Innsbruck, Austria) [13] developed techniques to trap electrically charged atoms or ions with electric fields. The particles are isolated from heat and radiation by performing the experiments in vacuum at extremely low temperatures. A laser beam can be used to suppress the ion's thermal motion and prepare its ground state (laser cooling), allowing the study of quantum phenomena. Additionally, the use of optical lattices to create artificial crystals has been launched experimentally from groups led by I. Bloch (Mainz, Germany) [14], T.Esslinger (Zurich, Suiza) [15] or R. Grimm (Insbruck, Austria) [16].

Figure 1.1: An IBM cryostat wired for a 50-qubit processor. [Source IBM [17]]

Aside from the efforts to expand our technologies in the classical realm, a more sophisticated line of research, less known to the general public, profits from the aforementioned taming of quantum systems. The essential idea behind this approach is

to use the exotic laws of quantum mechanics to our advantage, which could in principle expand our capabilities in ways that classical technologies cannot. A new wave of ideas, possible implementations, proof-of-principle experiments and prototypes have flooded the research activity within the quantum realm during the last years. In a few cases, these technologies have taken a leap to become commercial products, such as various quantum random number generators [18], the IBM 20-qubit quantum computer [19] (Fig. 1.1), or quantum cryptographic systems [20, 21]. Still, from an industrial point of view, quantum technologies are still in their infancy, although recent governmental initiatives, such as the Quantum Technology Flagship in the E.U. [22] or the U.K. National Quantum Technologies Program [23], aim to push them forward and take the lead in their future growth and economic impact. Quantum technologies promise to significantly advance the previously mentioned aspects of information: acquisition, storage, processing and communication. In the following we shall give a big picture of the different quantum technologies along with a brief description of their aims.

- **Acquisition**
  - ***Quantum clocks***: a precise measurement of time is vital in our society, and it is the basis to sustain or improve many other technologies. Current developments in this field have originated devices that are more precise than previous atomic clocks used as international standard [24]. This technology is regarded as a short term goal with potential applications in defense, telecommunications and finance.
  - ***Quantum random number generators***: a source of random numbers is a fundamental resource in science and engineering. Computer simulation and cryptography are among its fields of applications. The intrinsic randomness that is found in quantum mechanics may be used as a perfect source of entropy to count with an unlimited random number generator [18].
  - ***Quantum sensing***: quantum sensing employs quantum resources such as entanglement or squeezing to achieve some enhancement in sensor characteristics, like precision or efficiency [25–27]. This is another short-

term technology with a wide variety of potential applications: gravity mapping for creating three dimensional maps of the density of material [28], measurement of electric signals from the brain [29], accelerometers and gyroscopes [30, 31] for naval or underground navigation, or magnetic sensors of high resolution [32].

- ***Quantum enhanced imaging***: this technology exploits quantum correlations and resources, typically quantum states of light, in order to achieve image resolutions beyond what is possible with classical optics [33, 34]. Possible applications range from improving microscopes and telescopes to medical imaging.

- **Storage**

  - ***Quantum memories***: the need for storing classical bits has its quantum counterpart in the pursuit of having systems able to store quantum information rather than classical information. Systems of atoms and trapped ions are good candidates because they are able to preserve their quantum state for long periods of time under correct isolating conditions. Quantum memories are key elements for other more complex developments of quantum technologies, such as quantum computation or quantum networks [35, 36].

- **Processing**

  - ***Quantum computation***: managing quantum information offers the possibility of achieving a computational power that, in some cases, is capable of surpassing the computational power of the most advanced classical computers [5]. This is a sought-after technology that demands a huge technical effort in order to keep the fragile quantum information protected from noise and decoherence, so it is still considered as a long-term goal. Quantum computing would provide us with a universal simulator of the physics of a wide class of quantum systems which are intractable otherwise. Additionally, it would allow the implementation of quantum algorithms that fundamentally surpass the capabilities of classical computing, such as the Shor algorithm for integer factorization [37] or the Grover algorithm for searching in an unordered database [38].

  - ***Quantum simulation***: as resource-demanding as quantum computing is, quantum simulation emerges as a short-term solution to simulate a restricted class of quantum systems that are difficult or even impossible to simulate in classical computers. The essential idea behind quantum simulation is to use a fully controllable quantum system cleverly designed to mimic other less controllable quantum system dynamics [39, 40].
  - ***Quantum artificial intelligence***: echoing modern approaches rooted in the field of artificial intelligence, quantum artificial intelligence aims to develop algorithms and technologies that accomplish some enhancement with respect to their classical counterparts. This field includes latest efforts regarding quantum machine learning [41] and quantum neural networks [42].

- **Communication**

  - ***Quantum communication***: in this field we encounter solutions to the transmission of quantum information itself, for example, quantum teleportation protocols, or efficient transmission of classical information, like the superdense coding protocol that allows the transmission of two bits by means of a qubit [4].
  - ***Quantum cryptography***: quantum cryptography promises secure methods to transmit information protected against a possible interceptor [21]. While some commercial applications have been tested [20], large scale implementation of these technologies still faces significant challenges.

Naturally, all these exciting prospects come at a price. In many cases, the potential benefits of quantum technologies are limited by the robustness against errors and the survival of the fragile quantum states for a sufficiently long period of time (coherence time). In the latter case, such loss of quantumness, known as *decoherence*, transforms a useful quantum state into a classical state that frequently (although not always) destroys the advantage with respect to purely classical devices. For acquisition purposes, the enhancement that quantum states of light offer in quantum sensing and imaging is normally lost as soon as decoherence comes into play. A simple example is given by the incoherent loss of a photon in a NOON

state, well-known in optical interferometry for leading to a Heisenberg scaling, which rapidly becomes a worthless mixed state [43]. Similarly, for processing purposes, these issues are currently the main enemy to combat in quantum computation so as to achieve the so-called *quantum supremacy*, where a quantum computer may prove to solve classically intractable problems. For this reason, different companies are in the beginning of a race to accomplish longer coherence times and fault tolerant quantum computation. A first approach to tackle this problem is given by quantum error correction algorithms [44]. Current quantum computers, like the IBM 16-qubit processor, are built in this way. An alternative direction is to take advantage of certain exotic symmetry properties displayed by well-chosen models and interactions. These systems open the door to construct topologically protected states that are naturally robust against local errors. This last approach, although more difficult to implement with the state-of-the-art technologies, is considered as the long term goal pursued by companies like Google or Microsoft.

One of the main motivations of this thesis is to examine mechanisms that help to surpass the limitations brought about by the presence of decoherence and errors. Concretely, we focus our study within the fields of quantum simulation and quantum sensing. To this end, we shall merge ideas and methods that normally show up within the fields of many-body physics and condensed matter physics with well-established results in the fields of quantum sensing and simulation. Namely, the concepts of spontaneous symmetry breaking, long-range order, topological order or criticality will be used as powerful conceptual tools to organize the analysis and interpretation of our results. The ideas introduced in this work may contribute, for example, to implement topologically protected quantum memories, as well as sensing schemes robust against decoherence and errors in quantum optical dissipative systems.

Part II

Background theory

Chapter 2

Quantum systems

2.1 Quantum degrees of freedom

2.1.1 The superposition principle

What is so special about quantum mechanics? The fundamental distinction between classical and quantum mechanics lies in the intrinsic probabilistic behaviour of the degrees of freedom in a certain system. Our intuition, built on our everyday experience in the classical world, suggests that the outcome of any measurement of any observable (i.e., a property of a system) is defined even before the measurement is performed on the system. A deterministic theory, like Newtonian or Hamiltonian mechanics, gives a perfectly well-defined value to any observable at any time. In many cases, nevertheless, we do not have complete knowledge of the system degrees of freedom so as to work with a deterministic and exhaustive description of its dynamics. This is the case, for instance, of a system consisting of many degrees of freedom, like a fluid or a solid, or non-integrable systems exhibiting chaotic behaviour and extreme sensitivity to initial conditions. In those cases one has to rely on statistical methods to be able to give significant and useful predictions. A simple example would be the result of tossing a coin, which could come up a head or a tail, or in the computational jargon, '1' or '0'. However, one must notice that the use of probabilistic methods in these cases is the result of our lack of knowledge over the system, but not the lack of definition of their properties. In other words, by having enough information when tossing a coin, one should be able to predict the outcome

using Newtonian mechanics.

A totally different scenario appears in quantum mechanics, where it is found that some properties are intrinsically ill-defined, at least until some measurement is performed over the system. In contrast to a classical coin, the result, heads or tails, is not defined until the measurement is performed. This fact has profound consequences in the statistical results of experiments involving quantum degrees of freedom. Because of this, we need to use a radically different mathematical approach to correctly describe the intrinsic ill-definition of reality. Traditionally this is done by the use of Hilbert spaces and the superposition principle [45]. While in classical physics the space of states is represented by a manifold in some phase space, in quantum physics we resort to a Hilbert space $\mathcal{H}$. While a possible outcome of an experiment is represented by a point in the phase space in classical mechanics, a possible outcome will be represented by an additional dimension in the Hilbert space. By doing so, an ill-defined state will be given by a vector (ket) $|\Psi\rangle$ expressed as a certain linear combination of the possible outcomes. A quantum coin, a *qubit* in the jargon of the quantum information theory, with equal probability for heads and tails will be denoted by the following normalized state ($|\langle\Psi|\Psi\rangle|^2 = 1$),

$$|\Psi\rangle = \frac{1}{\sqrt{2}}(|1\rangle + |0\rangle). \tag{2.1}$$

The probability distribution is then obtained from the rule $p(r) = |\langle r|\Psi\rangle|^2$, with r being '1' or '0'. While an observable in classical physics is represented by a function in the system phase space, in quantum physics it is mathematically represented by an appropriate operator $\hat{O}$, whose eigenvalues $\hat{O}|\Psi\rangle = o|\Psi\rangle$ match the possible values of that observable. The reason is twofold; first, the operator representation is a compact tool to gather both the quantisation and the continuity regarding the possible values of the observable. Both cases are contained in the spectrum of the operator, which could be discrete and/or continuous. Second, the fact that some operators, say $\hat{A}$ and $\hat{B}$, do not commute in the general case ($[\hat{A}, \hat{B}] \neq 0$) accounts for the observation that the result of an experiment depends on the order followed when measuring those observables. The position and linear momentum of a particle is a canonical example of such bizarre phenomenon. This is again an indirect manifestation of the intrinsic ill-definition of some properties in a system. Bearing in mind all these considerations, the system state $|\Psi\rangle$ is not limited to give

the probability distribution of merely one observable, but it can also be used as a generator of the probability distribution of any observable by squaring the projection of each eigenvector $|o_j\rangle$ onto the normalized system state $|\Psi\rangle$,

$$p(o_j) = |\langle o_j|\Psi\rangle|^2. \tag{2.2}$$

Conversely, the set of eigenvectors $\{|o_j\rangle\}$ of an observable serves as a *basis* to express the system state $|\Psi\rangle$ as a linear superposition of the possible outcomes. In any case, the probability distributions obtained will exhibit statistical fluctuations that reflect the intrinsic quantum uncertainty of reality.

In some cases, the independent nature of the observables at play allows us to obtain the same result regardless of the order followed in the measurement, mathematically expressed as commuting operators $[\hat{O}_i, \hat{O}_j] = 0$. This could be the case, for example, of the different position components $\hat{X}_i$ of a particle, where it is irrelevant which one is measured first, so we have $[\hat{X}_i, \hat{X}_j] = 0$.

In full generality, a system will consist of different simpler subsystems, each with its own Hilbert space $\mathcal{H}_j$. The way to correctly add up degrees of freedom in quantum mechanics is by using a tensor product of the Hilbert spaces of each subsystem, such that the total Hilbert space $\mathcal{H}$ becomes,

$$\mathcal{H} = \otimes_j \mathcal{H}_j. \tag{2.3}$$

Notice that the dimension of the total Hilbert space is the product of the dimensions of each subsystem. For example, the Hilbert space of a collection of N qubits will be of dimension $\dim(\mathcal{H}) = 2^N$, where each qubit has dimension 2. This can be understood simply as a manifestation of the fundamental counting principle of probability theory, where we need to take into account all possible combinations of outcomes. The result of this is an exponential explosion of the dimension of our Hilbert space, with profound consequences as we shall discuss in chapter 5. The superposition principle has further bizarre consequences with regards to these composite systems, as nothing prevents us from having a superposition of outcomes related to spatially *distant* observables. A canonical example is the Bell state of two distant qubits located at positions A and B,

$$|\Phi^+\rangle = \frac{1}{\sqrt{2}}(|0\rangle_A \otimes |0\rangle_B + |1\rangle_A \otimes |1\rangle_B). \tag{2.4}$$

When a such a system is prepared in the state $|\Phi^+\rangle$, the result of local measurements will be *non-locally* correlated, a phenomenon that has no classical counterpart. This effect is popularly known as *entanglement*.

Finally, we require a rule to obtain the dynamical evolution of the properties of a system. One can choose to put this evolution in the generator of the probability distributions, i.e., the state $|\Psi\rangle$, or the observables themselves. The former is known as the Schrödinger picture and the latter the Heisenberg picture. For a closed system the evolution is given in terms of the Hamiltonian $\hat{H}$, and follows the Schrödinger equation [45],

$$i\hbar\frac{d}{dt}|\Psi\rangle = \hat{H}|\Psi\rangle. \tag{2.5}$$

The Hamiltonian is an operator that represents the system energy, and its eigenvalues are invariant under unitary transformations $\hat{U}$ such that $\hat{H}' = \hat{U}^\dagger\hat{H}\hat{U}$. In some cases it will be useful to express our system in a rotating reference frame, mathematically described by a time-dependent unitary operator $\hat{U}(t)$. It is simple to prove that the transformed state $|\Psi'\rangle = \hat{U}(t)|\Psi\rangle$ evolves according to the new Hamiltonian $\hat{H}_U$, such that

$$\hat{H}_U = \hat{U}^\dagger(t)\hat{H}\hat{U}(t) + i\frac{d\hat{U}^\dagger}{dt}\hat{U}(t). \tag{2.6}$$

The use of these rotating pictures will be omnipresent in this thesis, which are used to simplify notably the description of the dynamics.

The Schrödinger equation can be extended to time-dependent Hamiltonians $\hat{H} = \hat{H}(t)$, which come out typically in cases where the system is subjected to time-dependent external potentials. We shall make use of these potentials in chapter 8 in the form of periodic driving fields. The state evolution is obtained from the Schrödinger equation by formally integrating equation (2.5). In the case that the Hamiltonian commutes with itself at different times, i.e., $[\hat{H(t)}, \hat{H(t')}] = 0$, this integration can be formally expressed as [45],

$$|\Psi(t)\rangle = \exp\left(-\frac{i}{\hbar}\int_{t_0}^{t}\hat{H}(t')dt'\right)|\Psi(0)\rangle, \tag{2.7}$$

with $|\Psi(t)\rangle$ and $|\Psi(0)\rangle$ being the state at times t and 0 respectively. Equation (2.7) will come up in section 8.4 when integrating the effect of periodic driving fields acting on the system.

2.1.2 Density operator formalism

The previous formalism allows us to take into account the uncertainty derived from the quantum statistical fluctuations of a system. However, in a general scenario, we shall encounter two sources of statistical fluctuations within the same system: quantum fluctuations arising from the intrinsic ill-definition of nature as well as classical statistical fluctuations as a consequence of our lack of knowledge about the system. Thus, we need to extend the previous formalism to incorporate both sources of uncertainty at the same time. One way to do so is by means of the density operator formalism [45]. Instead of a ket in a Hilbert space, the system state will be mathematically represented by an operator defined as

$$\hat{\rho} = \sum_j p_j |\Psi_j\rangle\langle\Psi_j|, \tag{2.8}$$

where p_j are probability weights to account for the fact that we do not know which of the states $|\Psi_j\rangle$ the system is in.

The density operator must satisfy three essential conditions to be a valid description of a physical state. Namely, it must be self-adjoint, $\hat{\rho}^\dagger = \hat{\rho}$, positive semi-definite, $p_j > 0$ and with trace one, $\mathrm{Tr}\{\hat{\rho}\} = 1$. Quantum states that possess classical fluctuations are known as *mixed states*, in contrast to the *pure states* represented by kets. For instance, our quantum coin will be represented with the following density operator,

$$\hat{\rho} = \frac{1}{2}(|0\rangle\langle 0| + |1\rangle\langle 1| + |0\rangle\langle 1| + |1\rangle\langle 0|), \tag{2.9}$$

in contrast to the classical mixture

$$\hat{\rho} = \frac{1}{2}(|0\rangle\langle 0| + |1\rangle\langle 1|). \tag{2.10}$$

The diagonal elements, such as $|0\rangle\langle 0|$ are known as *populations* while the nondiagonal terms, like $|0\rangle\langle 1|$ are known as *coherences*. Diagonal terms account for the classical probability distributions while the coherences store the information concerning the quantum superpositions. Finally, the Schrödinger equation is likewise updated into the density operator formalism, adopting the form[1]

$$\dot{\rho} = \frac{d}{dt}\rho = -\frac{i}{\hbar}[H, \rho]. \tag{2.11}$$

Equation (2.11) is known as the von-Neumann equation [45].

[1] From now on we shall drop the hat symbol when writing operators.

2.1.3 Spin degrees of freedom

The simplest case of a quantum degree of freedom is given by a spin-1/2 degree of freedom, which is formally equivalent to a *qubit*. The Hilbert space representing the space of states of such a system is simply $\mathcal{C}^2$.

Originally, the concept of spin was introduced as an internal degree of freedom of the electron, associated to its magnetic momentum and with two possible outcomes, up $|\uparrow\rangle$ and down $|\downarrow\rangle$. The Pauli matrices, defined as

$$\sigma^x = \begin{pmatrix} 0 & 1 \\ 1 & 0 \end{pmatrix}, \quad \sigma^y = \begin{pmatrix} 0 & -i \\ i & 0 \end{pmatrix}, \quad \sigma^z = \begin{pmatrix} 1 & 0 \\ 0 & -1 \end{pmatrix}, \tag{2.12}$$

and which satisfy the algebra of an angular momentum,

$$[\sigma^x, \sigma^y] = 2i\sigma^z, \quad [\sigma^y, \sigma^z] = 2i\sigma^x, \quad [\sigma^z, \sigma^x] = 2i\sigma^y, \tag{2.13}$$

were used to represent observables in this Hilbert space.

As any operator in $\mathcal{C}^2$ can be expressed as a linear combination of the Pauli matrices, a spin is also used to describe other degrees of freedom with two possible outcomes (pseudospin). This could be the case of an atom in which only two energy levels are taken into account, or two relevant charge or flux levels in circuit quantum electrodynamics (circuit QED) [46, 47]. These states will be referred in this thesis as the ground $|g\rangle$ and excited $|e\rangle$ states. In this way, a spin will be widely used to describe relevant degrees of freedom of matter, although it could very well describe additional aspects of light like its polarization states.

A paradigmatic model with interacting spin degrees of freedom is the Ising model, which is a spin Hamiltonian firstly introduced to describe quantum magnetic phenomena like ferromagnetism and antiferromagnetism. The Hamiltonian of the Ising model reads [48],

$$H_{\text{Ising}} = -J \sum_{<\boldsymbol{i},\boldsymbol{j}>} \sigma^z_{\boldsymbol{i}} \sigma^z_{\boldsymbol{j}} - \Gamma \sum_{\boldsymbol{j}} \sigma^x_j. \tag{2.14}$$

The spins are assumed to lie on a lattice (normally a square lattice) of dimension D, and the indices $\boldsymbol{i}, \boldsymbol{j}$ label lattice sites. Furthermore, the interactions are only for nearest-neighbour sites, denoted by $\langle \boldsymbol{i}, \boldsymbol{j} \rangle$. The term with Γ takes into account a transverse external field, which will be set to zero in chapter 8 ($\Gamma = 0$). In the case $J > 0$, the first term in the right-hand side of equation (2.14) favours

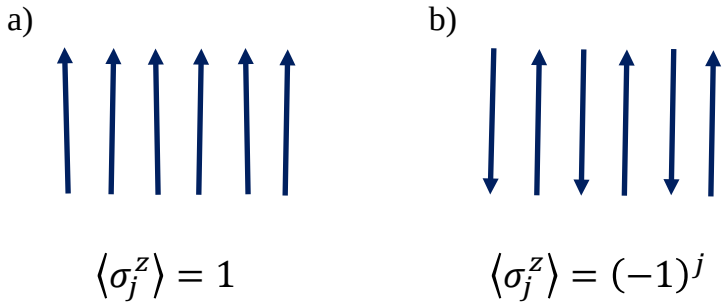

Figure 2.1: a) Ferromagnetic order in the Ising model. b) Antiferromagnetic order in the Ising model

ferromagnetic order in the z direction, as neighbouring sites tend to be aligned. Antiferromagnetic order is favoured if $J < 0$, with alternating spin orientations (see figure 2.1). Interactions are typically isotropic, like in the Ising model, where the couplings are independent of the spatial direction of the bonds. Nonetheless, this is not always the case. Generally speaking, 'compass models' refer to a broad type of lattice Hamiltonians in which the couplings between sites depend on the orientation of the bonds in the lattice [49]. This category includes famous instances such as the Kitaev's honeycomb model [50]. The simplest spin model of this kind was introduced by Kugel and Khomskii [51] to study certain interactions between orbital degrees of freedom in strongly correlated electron materials. The Hamiltonian is defined as follows,

$$H_{\text{Compass}} = -J_x \sum_{\boldsymbol{j}} \sigma^x_{\boldsymbol{j}} \sigma^x_{\boldsymbol{j}+\boldsymbol{e}_x} - J_y \sum_{\boldsymbol{j}} \sigma^y_{\boldsymbol{j}} \sigma^y_{\boldsymbol{j}+\boldsymbol{e}_y}. \tag{2.15}$$

In contrast to the Ising model, this model presents two competing tendencies: bonds along the y axis induce spin alignment along y ($\langle \sigma^y_{\boldsymbol{j}} \rangle \neq 0$), while bonds along the x axis induce spin alignment along x ($\langle \sigma^x_{\boldsymbol{j}} \rangle \neq 0$). We shall analyse this model in detail in chapter 8

2.1.4 Bosonic degrees of freedom

The lack of complete definition of reality has further mesmerizing consequences beyond what has been mentioned thus far. Specifically, unlike classical dynamics, where one can always distinguish each individual particle, quantum particles must

be treated as indistinguishable entities in many circumstances. We could say that to label particles is not as meaningful as we are accustomed to based on our classical intuition, and one must focus on the statistical consequences of those particles rather than their individual identification. We typically distinguish between bosons and fermions depending on how these indistinguishable particles behave with respect to the exchange of labels. In this thesis we will encounter only bosonic degrees of freedom, which are characterized by a state that is symmetric under permutation of indices [52]. These type of degrees of freedom appear typically in the quantum description of waves such as the electromagnetic fields or mechanical vibrations in a crystal. The quantisation of these fields give rise to bosonic excitations, known as phonons for mechanical waves and photons for the electromagnetic field.

The use of Slater determinants allows the symmetry properties of bosons and fermions to be taken into account; an approach followed in atomic or molecular physics where there are only a few particles. Nonetheless, a description where labels are employed to characterise quantum particles turns out to be tedious and impractical when the number of particles builds up. A more powerful mathematical tool is available in this situation, in which the focus is on how many particles are in a certain state rather than *which* particles occupy those states. This formalism is known as *second quantisation* (or number occupation representation), even though there is really nothing fundamentally new that is being quantised. The key element is the introduction of certain creation (a_j) and annihilation ($a_j^\dagger$) operators, which increase or decrease the number of particles in a certain state $|j\rangle$ labelled by the index j. It is important to stress that the meaning of the labels j depends on the particular context, and they could very well refer to different momentum states in a Fourier space, wave vectors, or sites in a lattice. Likewise, the number operator $n_j = a_j^\dagger a_j$ counts the number of particles in the state $|j\rangle$. These bosonic operators are mathematically defined by their algebra, specifically

$$[a_i, a_j] = 0, \tag{2.16}$$

$$[a_i, a_j^\dagger] = \delta_{i,j}, \tag{2.17}$$

$$[n_j, a_j] = -a_j, \tag{2.18}$$

$$[n_j, a_j^\dagger] = a_j^\dagger. \tag{2.19}$$

The above commutation relations automatically guarantee that we respect the symmetry properties of the system with respect to the permutation of indices. Finally, observables that were previously written in the first quantisation language demand to be re-expressed in the language of the second quantisation. This can be done again by using the creation and annihilation operators. Namely, one-body operators, like the kinetic energy or the potential energy created by an external field, will adopt the generic structure

$$T = \sum_{i,j} T_{i,j} a_i^\dagger a_j, \tag{2.20}$$

where the matrix $T_{i,j}$ essentially represents the hopping for annihilating and creating a particle in the states $|j\rangle$ and $|i\rangle$ respectively. Likewise, two-body operators accounting for interacting terms among bosons will be of the form,

$$V = \sum_{i,j} V_{i,j} a_i^\dagger a_k^\dagger a_j a_l. \tag{2.21}$$

2.2 Quantum optics

2.2.1 Light quantisation

In a classical description, the electromagnetic field can be expressed in terms of orthogonal modes with their characteristic spatial, temporal and polarization properties. These modes form a collection of independent harmonic oscillators. Hence, we shall associate separate Hilbert spaces for each of these modes in a quantum description of light, and one can prove that each mode will be quantised as a bosonic degree of freedom [52]. The total Hilbert space is obtained when taking the tensor product of these modes, the so-called *Fock space*. Hence, the most general M-mode state of light is represented by a density operator ρ in the Fock space, which can be written as

$$\rho = \sum_{n,n} \rho_{n,n} |n\rangle\langle n|, \tag{2.22}$$

where $n = \{n_1, n_2, \cdots, n_M\}$ and $|n\rangle = |n_1\rangle \otimes |n_2\rangle \otimes \cdots |n_M\rangle$. Each $|n_j\rangle$ represents a Fock state with exactly n_j photons. Fock states can in turn be expressed in terms of the creation and annihilation operators acting on the vacuum state $|0\rangle$, i.e, the

state with no photons, as follows,

$$|n_j\rangle = \frac{a_j^{\dagger n}}{\sqrt{n!}}|0\rangle, \quad a_j|n_j\rangle = \sqrt{n_j}|n_j-1\rangle, \quad a_j^\dagger|n_j\rangle = \sqrt{n_j+1}|n_j+1\rangle. \tag{2.23}$$

Also, the electric and the magnetic fields can be obtained through the *quadratures* of the field, defined as

$$X = a^\dagger + a, \tag{2.24}$$

$$P = i(a^\dagger - a). \tag{2.25}$$

In free space it is convenient to label the different modes with frequencies $\omega_{\vec{k}}$ by their corresponding wave vector $\vec{k}$ and polarization $\lambda = 1, 2$, so that the Hamiltonian is given by[2]

$$H_E = \sum_{\vec{k}} \sum_{\lambda=1,2} \omega_{\vec{k}} a_\lambda^\dagger(\vec{k}) a_\lambda(\vec{k}). \tag{2.26}$$

In the context of optical interferometry, in contrast, modes are distinguishable by their spatial separation, corresponding to different arms of an interferometer. In modern experiments of cavity QED, modes correspond to the quantised electromagnetic field within each cavity arranged in a lattice, in which case the label j denotes the lattice site. When cavities are allowed to exchange photons between neighbouring cavities, the evolution can be described by a tight-binding model in a Wannier basis [47, 53], analogous to the tight-binding model appearing in solid state physics, which reads as follows

$$H = -t \sum_{\langle i,j \rangle} \left(a_i a_j^\dagger + a_j a_i^\dagger \right). \tag{2.27}$$

The constant t quantifies the hopping rate between sites. This Hamiltonian will show up again in chapter 10.

2.2.2 Quantum states of light

The Fock states defined in equation (2.23) are the primary example of quantum states of light, characterised by having a definite number of photons. These states explicitly show a corpuscular nature in contrast to the wave theory of light from classical electrodynamics. Beyond these states, we find others that reflect both the classical and quantum aspects of light. If the Fock states are the most extreme

[2] The Planck's constant is set to be $\hbar = 1$ from now on.

case of states with quantum features, the coherent states of light would be the most similar to a classical description. In the mode representation, a single-mode coherent state can be defined as an eigenstate of its respective annihilation operator,

$$a|\alpha\rangle = \alpha|\alpha\rangle, \tag{2.28}$$

where α is a complex number with certain amplitude and phase. A multi-mode coherent state is simply the tensorial product of each single-mode coherent state, $|\boldsymbol{\alpha}\rangle = |\alpha_1\rangle \otimes |\alpha_2\rangle \otimes \cdots |\alpha_M\rangle$. In terms of the Fock states, a coherent state takes the form

$$|\alpha\rangle = \exp\left(-|\alpha|^2/2\right) \sum_{n=0}^{\infty} \frac{\alpha^n}{\sqrt{n!}} |n\rangle. \tag{2.29}$$

These are the states produced by any phase-stabilized laser, which have properties that resemble features of classical light [27]. For instance, a coherent state evolves in time identically to a classical wave amplitude. In particular, an optical phase delay ϕ turns the state $|\alpha\rangle$ into $|\alpha e^{i\phi}\rangle$. Coherent states, unlike Fock states, do not have a definite number of photons, but they follow a Poissonian distribution,

$$P(n) = e^{-|\alpha|^2} \frac{|\alpha|^{2n}}{n!}, \tag{2.30}$$

with average $\langle n\rangle = |\alpha|^2$ and standard deviation $\Delta n = |\alpha|$. The relative uncertainty $\Delta n/\langle n\rangle$ scales like $1/\sqrt{\langle n\rangle}$, this is, according to the shot noise limit (see section 6.2). It is a common jargon to call coherent states the classical states of light, however, their quantum character emerges when taking into account their instrinsic quantum fluctuations and non-orthogonality, which make them hard to distinguish for small amplitudes [54],

$$|\langle\alpha|\beta\rangle|^2 = \exp\left(-|\alpha - \beta|^2\right). \tag{2.31}$$

There exists a very useful tool to work with quantum states of light that, in many cases, facilitates enormously its description and enables its graphical representation. This tool is the representation in phase space, which allows us to work with functions rather than kets or operators. Such conversion arises as a result of the correspondence between the field quadratures X and P with the position and momentum, according to the quantisation of the electromagnetic field as a set of harmonic oscillators [52]. In this way we may compare quantum mechanics in phase space and classical statistical mechanics, where classical ensembles are represented

by probability distributions in phase space and the evolution is given by the Liouville equation [55].

Unlike statistical mechanics, the representation in phase space does not really lead to a probability distribution, as it may take negative values, even though it integrates to one over the whole phase space as a real distribution. This is the reason why these functions are referred as quasi-probability distributions, the non-positivity being a striking feature of their quantum nature. In this thesis we shall make use of the P-representation, introduced by Glauber and Surdashan [54, 56]. This representation utilizes a basis of coherent states, which are related to position and momentum via the relation,

$$\alpha = \frac{1}{2}(\langle X\rangle + i\langle P\rangle). \tag{2.32}$$

The P-representation is then defined in terms of the M-mode coherent state as,

$$\rho(t) = \int d^{2M}\boldsymbol{\alpha} P(\boldsymbol{\alpha}, \boldsymbol{\alpha}^*, t)|\boldsymbol{\alpha}\rangle\langle\boldsymbol{\alpha}|. \tag{2.33}$$

Having defined this representation, it is convenient to introduce some useful terminology that will appear in chapters 9 and 10. In general, we shall admit that a state ρ is a classical state of light if it admits a positive P-representation (equivalently, a mixture of coherent states), this is, $P > 0$. However, let us recall that, because of the non-orthogonality condition, a basis of coherent states is not a true basis, and it is said to be an over-complete basis. This means that even if a P-function behaved like a true probability distribution, it would not describe probabilities of mutually exclusive states [54]. Additionally, the P-representation may turn out to be more singular than a Dirac delta (which selects an element of the basis). Bearing in mind all these precautions, it is accepted to call classical states those that are positive and not more singular than a Dirac delta distribution. Fock states, with definite number of photons, are examples of highly non-classical states. In quantum optics, the so-called Gaussian state are also useful, which are by definition those represented by a Gaussian probability distribution in phase space. In our case, Gaussian states are those represented by Gaussian P-functions. Notice that, in the general case, Gaussian states are not classical states. This is for example the case of squeezed states, with many applications in quantum metrology [27]. Coherent states are special cases of Gaussian states, in which there are no correlations between the modes

and the relation $\Delta^2 X \Delta^2 P = 1$ is held.

2.2.3 Atom-light interactions

Atom-light interactions in quantum optics can be obtained by quantising the classical dipolar interaction $H_I = -\vec{d} \cdot \vec{E}(t)$, where $\vec{d}$ is the dipole moment $\vec{d} = -e\vec{r}$ and $\vec{E}(t)$ and oscillating electric field. The quantization comes after replacing the electric and position observables by their corresponding operators. When the atomic wave function is of the form $\Psi(\vec{r}) = a_g \Psi_g(\vec{r}) + a_e \Psi_e(\vec{r})$, the interaction can be written as [57],

$$H = \omega(a^\dagger a) + \frac{\omega_0}{2}\sigma^z + g(\vec{r}_m)(a + a^\dagger)\sigma^x \tag{2.34}$$

where $g(\vec{r}_m)$ incorporates the mode profile. If we move to a frame rotating at the atom and field frequencies we have $a \to a^\dagger e^{i\omega t}$ and $\sigma^+ \to \sigma^+ e^{i\omega_0 t}$, so the previous Hamiltonian becomes,

$$H = g(a\sigma^- e^{-i(\omega+\omega_0)t} + a^\dagger \sigma^+ e^{i(\omega+\omega_0)t} + a\sigma^+ e^{-i(\omega-\omega_0)t} + a^\dagger \sigma^- e^{i(\omega-\omega_0)t}). \tag{2.35}$$

In the proximity of the resonance condition, $|\omega - \omega_0| \ll \omega + \omega_0$, the quickly rotating terms can be neglected, an approximation known as the *Rotating Wave Approximation* (RWA), resulting in the famous Jaynes-Cummings model [57] after transforming back into the static picture,

$$H = \omega(a^\dagger a) + \frac{\omega_0}{2}\sigma^z + g(a\sigma^+ + a^\dagger \sigma^-). \tag{2.36}$$

In this thesis the Hamiltonian (2.36) will account for all the atom-light interactions considered, and we shall also assume perfect resonance $\omega = \omega_0$.

2.3 Symmetries in quantum systems

In 1956, Paul Dirac wrote a famous quote on a blackboard of the University of Moscow (an honour reserved for only the greatest visitors): '*A physical law must possess mathematical beauty*' [58]. It is probably in the connection between symmetry principles and its physical consequences, like the existence of conservation laws, where this beauty shines with special intensity.

Invariances and symmetry in Physics appeared firstly as a result of examining the relation between different coordinate systems or reference frames. For example, it was already well known in classical physics that certain local operations imply conservation laws, along with continuity equations when the symmetry group is continuous. Namely, invariance under spatial translations, temporal translations, and rotations result in the conservation of linear momentum, energy, and angular momentum respectively. In the context of classical electrodynamics, the invariance under certain local transformations (gauge transformations) were known to give rise to different but equivalent representations, and also the conservation of electric charge.

The role of symmetry in quantum physics becomes even more apparent because of the linear character of Hilbert space, which allows us to construct superpositions of states transforming as irreducible representations of symmetry groups. Generally speaking, a symmetry operation T transforms a state $|\Psi\rangle$ into another state $|\Psi'\rangle = T|\Psi\rangle$ in such a way that transition probabilities are conserved [59],

$$|\langle\Psi_2'|\Psi_1'\rangle|^2 = |\langle\Psi_2|\Psi_1\rangle|^2 = |\langle\Psi_2|T^\dagger T|\Psi_1\rangle|^2. \tag{2.37}$$

It follows from the previous equation that the operator must be unitary or antiunitary, $T^\dagger T = \mathbb{1}$. Unitary operators include well-known transformations as translations or rotations, while antiunitary operators can be used to represent time-reversal symmetry [45]. In some cases the dynamical equations, which are given the Hamiltonian H, will be invariant under the transformation T, hence $T^\dagger H T = H$, and thus,

$$HT = TH \Rightarrow [H, T] = 0. \tag{2.38}$$

Conversely, if equation (2.38) holds, energy eigenstates $|E_n\rangle$ connected though T will have the same energy since

$$H(T|E_n\rangle) = TH|E_n\rangle = E_n(T|E_n\rangle), \tag{2.39}$$

and the operators H and T will share a common basis of eigenstates.

When the symmetry operator actually connects different states, i.e., $|E_n'\rangle = T|E_n\rangle \neq |E_n\rangle$, the states $|E_n\rangle$ and $|E_n'\rangle$ are said to be degenerate. Let us then notice that a symmetry does not necessarily yields the existence of degeneracies at

all energies, but the presence of a degeneracy generally implies that there is a symmetry transformation acting at least on the subspace spanned by the corresponding degenerate states.

A first important classification of symmetries distinguishes between discrete and continuous symmetries. Continuous symmetries are those that differ infinitesimally from the identity transformation so we can write $T = \mathbb{1} - \epsilon G$, where G is known as the generator of the transformation [45]. The symmetry under label permutation for bosonic degrees of freedom discussed in section 2.1.4, or the aforementioned time-reversal symmetry are examples of discrete symmetries. The parity operator P will be frequently employed in chapter 8 (which will acquire different specific forms), and physically corresponds to an inversion operation such that, for example,

$$P^\dagger \sigma^z P = -\sigma^z. \tag{2.40}$$

In relatively recent years, new invariance principles with remarkable physical consequences have been found as a result of using nonlocal probes, which will come in handy when we discuss the notion of topological order in section 4.5. To take into account all scenarios, we shall introduce another classification of symmetries according to the spatial dimension d of the region where a minimal set of elements in the system is transformed under the symmetry group. Such region will be a subset $\mathcal{C}_\alpha$ of the complete D-dimensional lattice, so trivially we have $d \leq D$. Namely, we may distinguish between local gauge symmetries, gauge-like symmetries and global symmetries.

- *Local gauge symmetries*: the symmetry operators act locally so we have $d = 0$. These symmetries play a fundamental role in high-energy physics, and they can also be simulated in quantum simulators like trapped ions [60].

- *Gauge-like symmetries*: $d > 0$ and $d \leq D$. A simple example is given by the quantum compass model defined in section 2.1.3, where it is possible to find symmetries acting only on individual rows or columns of the lattice (see section 8.3).

- *Global symmetries*: the symmetry operators act globally so we have $d = D$, and the region $\mathcal{C}_\alpha$ becomes the full volume of the system. A canonical example

is the quantum Ising model, where the Hamiltonian is invariant under a global inversion (see section 4.4).

The physical consequences of having a system with global and Gauge-like symmetries will be explored in more detail in chapter 4.

Chapter 3

Dissipative quantum systems

3.1 Open quantum systems

Any introductory textbook on quantum mechanics mainly deals with isolated systems, i.e., systems for which the interaction with the rest of the universe (usually referred as the *environment*) can be neglected. This could be the case, for example, of an electron in free space or an isolated atom. A step forward consists of considering systems in thermal equilibrium with some bath, which can be used to study, for instance, properties from the bulk of a solid, such as heat capacity or conductivity. The mathematical tools from statistical mechanics tackle these situations. While in many cases the assumption of an isolated system constitutes a valid empirical approximation, it is generally impossible to isolate completely a system from its surroundings. Likewise, we would also like to explore phenomena beyond thermal equilibrium. Moreover, a complete description of reality needs to systematically encompass non-negligibly influences of the environment over a quantum system dynamics and vice versa. In this way, we can explore richer phenomena like the dynamics towards equilibrium, far-from equilibrium phenomena, or memory effects.

Theoretically one could think of dealing with the system S and the environment E as a whole isolated system, whose unitary dynamics would be then given by the Schrödinger equation [61]. The Hilbert space of the total system is mathematically represented by the tensor product space $\mathcal{H} = \mathcal{H}_S \otimes \mathcal{H}_E$. Typically, this Hamiltonian can be expressed in the form

$$H = H_S + H_E + H_I, \tag{3.1}$$

where H_S and H_E are the free Hamiltonians corresponding to the system and environment respectively, and H_I is the Hamiltonian describing the interaction between them. In practice, nonetheless, a detailed microscopic description of the dynamical evolution of the whole system (3.1) is not always available. Even so, this would provide us with a large irrelevant amount of information since we are really interested in the degrees of freedom of the system S. To this purpose, the theory of open quantum systems supplies the mathematical tools to take into account the influence of the environment on a particular system dynamics, which will in general result in having a non-unitary dynamics of the open system S.

Although the concept of environment is applicable to any dimension of a Hilbert space, we are frequently interested in an environment consisting of an infinite number of degrees of freedom (and being mathematically rigorous, a continuum of them). This property leads to an irreversible flux of matter or energy from the system into the environment as some information of the system dynamics gets lost in the infinite dimensional state space of the environment which never returns into the system. For this reason, this represents a suitable mathematical description of *dissipative dynamics*. The term *reservoir* refers to this type of environment, whereas the concepts of *bath* (or *heat bath*) are normally reserved for a reservoir which is in a thermal equilibrium state [61], i.e., $\rho_E = 1/Z_E \exp(-\beta H_E)$.

The essential mathematical tools employed to represent an open quantum system are given by the density operator formalism and the use of the so-called *partial trace*. Indeed, all the accessible information about the open quantum system is encoded in the *reduced density operator* (or reduced density matrix), which is defined as follows,

$$\rho_S = \mathrm{tr}_E \rho. \tag{3.2}$$

The operator ρ is the density matrix of the full system-plus-environment, and tr_E is a notation indicating a trace taken over the Hilbert space of the environment $\mathcal{H}_E$. Trivially, all the observables referring to the system S will be of the form $A \otimes I_E$, where A is an operator acting on the Hilbert space $\mathcal{H}_S$. Hence, it turns out that any expectation value can be calculated through a partial trace of the reduced density matrix,

$$\langle A \rangle = \mathrm{tr}_E\{A\rho_S\}. \tag{3.3}$$

Finally, the equation of motion for the reduced density matrix ρ_S is obtained simply

by taking the partial trace over the Liouville-von Neumann equation (2.11) of the whole system $S + E$,

$$\frac{d}{dt}\rho_S = -i\mathrm{tr}_\mathrm{E}[H, \rho(t)]. \tag{3.4}$$

Notice that after taking the partial trace in equation (3.4), the dynamics will be no longer unitary in the most general case. Consequently, the density operator formalism introduced in section 2.1.2 is essential to correctly capture the dynamics of an open quantum system, as the evolution of the system state has to encompass both pure and mixed states.

3.2 Quantum master equations

The exact dynamics of an open system given by equation (3.4) is ordinarily rather complicated to be solved analytically. We shall distinguish between two broad types of evolution: *Markovian* and *non-Markovian* [61]. The Markovian dynamics is such that the change of the system at a particular time is given as a function of the state of the system at that time. The Schrödinger equation and the von Neumann equation are important examples of this sort of dynamics. In contrast, the non-Markovian evolution involves dynamical equations in which the change of the system at a given time is calculated taking into account not only the present system state, but also past states of the system S. In other words, the system exhibits memory effects. Needless to say, the non-Markovian dynamics is much more complicated to treat mathematically than the Markovian counterpart. As a result, it is extremely helpful to approximate certain system dynamics by means of Markovian-type equations whenever possible. This can be justified in the case that the characteristic timescale over which the reservoir correlation functions decay τ_E is much smaller than the characteristic relaxation time scale of the open system τ_R [61],

$$\tau_R \gg \tau_E. \tag{3.5}$$

Upon condition (3.5), we may neglect memory effects and approximate the exact equation (3.4) by a Markovian-type equation of the form,

$$\frac{d}{dt}\rho_S = \mathcal{L}\rho(t). \tag{3.6}$$

The generator $\mathcal{L}$ (usually called Liouvillian), is a superoperator, i.e., an operator acting on the operator space over the Hilbert space $\mathcal{H}_S$. If the system dimension is $\dim(\mathcal{H}_S) = N$, the corresponding Lioville space on which $\mathcal{L}$ acts is a complex space of dimension N^2. It can be shown that the most general form of $\mathcal{L}$ is given by the so-called *Lindblad master equation* [61],

$$\frac{d}{dt}\rho_S = -i[H, \rho(t)] + \sum_k [2L_k \rho L_k^\dagger - L_k^\dagger L_k \rho - \rho L_k^\dagger L_k], \tag{3.7}$$

where L_k are known as Lindblad operators. The first term on the right-hand side describes a unitary evolution while the second term, also called *dissipator*, accounts for the non-unitary effect of having an environment. In this way, equation (3.7) becomes a convenient description of several quantum dynamics out of equilibrium. In particular, the Markovian approximation is appropriate to study many quantum optical systems in the usual regime of parameters, where the infinite Hilbert space of electromagnetic modes often plays the role of the reservoir.

3.3 Steady states

An important property of any dynamics describing non-equilibrium processes, like the quantum master equation (3.7), is the possibility of finding an *steady state*. The steady state ρ_{ss} refers to the long-term behaviour of the solution of an equation such as (3.7), which is mathematically defined with full generality as,

$$\rho_{\text{ss}} = \lim_{t\to\infty} \rho(t). \tag{3.8}$$

In many cases, the observables measured in the state ρ_{ss} become time independent, which is mathematically expressed as

$$\frac{d}{dt}\rho_{\text{ss}} = 0. \tag{3.9}$$

This occurs as a result of the stabilisation of different competing tendencies given by dissipative fluxes of matter and energy between the system and the environment together with the internal dynamics of the open system, which may reach a compromise equilibrium as time goes by. This eventually leads the system into a steady state far from equilibrium in contrast to a thermal equilibrium reached by an isolated system (known as *thermalization*).

In particular, when the system dynamics is given by a quantum master equation, such as equation (3.6), the steady state ρ_{ss} may be characterised by the eigenoperator of the Liouvillian with zero eigenvalue, i.e.,

$$\mathcal{L}\rho_{ss} = 0, \tag{3.10}$$

as a trivial consequence of equation (3.9). The solution to equation (3.10) is not unique in the most general case, giving rise to *multi-stable solutions*. In some circumstances, there might exist other solutions that approximately satisfy equation (3.10), like in the case of magnetic frustration, which indicates the existence of quasi-degenerate steady states. In the context of magnetism, frustration arises if spins are coupled through competing interactions that cannot be simultaneously satisfied [62].

3.4 A simple example: the damped harmonic oscillator

To understand better the abstract concepts introduced so far, let us consider a specific integrable example by using the well-known harmonic oscillator. As we know, the free evolution is generated by the Hamiltonian

$$H_S = \omega_0 a^\dagger a, \tag{3.11}$$

with ω_0 being the frequency of the oscillator. This could for example represent the electromagnetic field mode inside a cavity, in which case the operators $a^\dagger$and a are the creation and annihilation operators of the mode respectively. The environment of such a cavity can be modeled by infinite modes outside the cavity, with a free Hamiltonian

$$H_E = \sum_{\vec{k}} \sum_{\lambda=1,2} \omega_{\vec{k}} b_\lambda^\dagger(\vec{k}) b_\lambda(\vec{k}). \tag{3.12}$$

The wave vector $\vec{k}$ in (3.12) labels the different modes and λ refers to the two possible polarizations. Let us consider the reservoir of radiation modes to be in an equilibrium state at temperature T, so the environment state is,

$$\rho_E = \frac{1}{Z_E} \exp\left(-\beta H_E\right) = \prod_{\vec{\kappa},\lambda} (1 - \exp\left(-\beta\omega_k\right)) \exp\left[-\beta\omega_{\vec{k}} b_\lambda^\dagger(\vec{k}) b_\lambda(\vec{k})\right]. \tag{3.13}$$

The quantum master equation will adopt the following structure [61],

$$\begin{aligned}\frac{d}{dt}\rho_S &= -i\omega[a^\dagger a, \rho_S] \\ &+ \kappa(N+1)\left(a\rho a^\dagger - \frac{1}{2}a^\dagger a\rho_S - \frac{1}{2}\rho_S a^\dagger a\rho_S\right) \\ &+ \kappa(N)\left(a^\dagger\rho_S a - \frac{1}{2}aa^\dagger\rho_S - \frac{1}{2}\rho_S aa^\dagger\right).\end{aligned} \tag{3.14}$$

We have defined the quantity

$$N = \frac{1}{\exp(\beta\omega_0) - 1}, \tag{3.15}$$

that stands for the average number of quanta in a mode with frequency ω_0 of the thermal bath. The second term in equation (3.14) describes spontaneous emission (at rate κ) as well as thermally induced emission (at rate κN), while the third term accounts for the thermally induced absorption of the cavity (at rate κN). One may obtain a closed equation for $P(n) = \langle n|\rho_S|n\rangle$ when representing equation (3.14) in the basis of the number states $|n\rangle$, which acquires the structure of a classical master equation,

$$\begin{aligned}\frac{d}{dt}P(n,t) &= \kappa(N+1)\left[(n+1)P(n+1,t) - nP(n,t)\right] \\ &\kappa N\left[nP(n-1,t) - (n-1)P(n,t)\right].\end{aligned} \tag{3.16}$$

The steady state solution of this equation can be calculated by, for example, a discrete Fourier transform ($P(k) = \sum_n P(n)e^{(ikn)}$), which gives,

$$P_{\rm ss}(n) = \frac{1}{N+1}\left(\frac{N}{N+1}\right)^n. \tag{3.17}$$

This solution is more recognizable if we re-express it as a thermal state by using equation (3.15) so that,

$$P_{\rm ss}(n) = \left[1 - \exp(-\beta\omega_0)\right]\exp\left[-n\beta\omega_0\right]. \tag{3.18}$$

Additionally, we may also calculate dynamical properties such as the evolution of the average number of photons $\left\langle a^\dagger a(t)\right\rangle$ through the relation,

$$\frac{d}{dt}\left\langle a^\dagger a(t)\right\rangle = tr\{a^\dagger a\frac{d}{dt}\rho\}, \tag{3.19}$$

which by using equation (3.14) becomes a closed equation for $\left\langle a^\dagger a\right\rangle$ with solution,

$$\left\langle a^\dagger a(t)\right\rangle = \left\langle a^\dagger a(0)\right\rangle e^{-\kappa t} + N(1 - e^{-\kappa t}). \tag{3.20}$$

Physically, this process is then correctly describing the relaxation to a thermal equilibrium with the external bath at temperature T.

3.5 Fokker-Planck equations

Phase space representations, introduced briefly in section 2.2.2, turn out to be a helpful tool to study quantum optical master equations. In this thesis we shall focus on the coherent state or P-representation, defined by equation (2.33). In a nutshell, this representation will allow us to transform operator equations such as (3.7) into partial differential equations. To derive an equation of motion for $P(\alpha, \alpha^*, t)$, one has to substitute equation (2.33) into the quantum master equation and use the following equivalences for coherent states,

$$a|\alpha\rangle\langle\alpha| = \alpha|\alpha\rangle\langle\alpha| \tag{3.21}$$

$$|\alpha\rangle\langle\alpha|a^\dagger = \alpha^*|\alpha\rangle\langle\alpha| \tag{3.22}$$

$$a^\dagger|\alpha\rangle\langle\alpha| = \left(\frac{\partial}{\partial\alpha} + \alpha^*\right)|\alpha\rangle\langle\alpha| \tag{3.23}$$

$$|\alpha\rangle\langle\alpha|a = \left(\frac{\partial}{\partial\alpha^*} + \alpha\right)|\alpha\rangle\langle\alpha|. \tag{3.24}$$

After an integration by parts with the assumption of zero boundary conditions at infinity, the operator equation is transformed into a product of $|\alpha\rangle\langle\alpha|$ and a complex function of α, α^*, yielding a differential equation for $P(\alpha, \alpha^*, t)$. Note that this change introduces an extra minus sign for each differential operator ∂_α.

Let us illustrate this procedure with the previous example. The equation (3.14) in the coherent state representation adopts the following form,

$$\begin{aligned}\frac{\partial}{\partial t}P(\alpha,\alpha^*,t) = \kappa N\frac{\partial^2}{\partial\alpha\partial\alpha^*}P(\alpha,\alpha^*,t)\\ -\left[\left(-i\omega_0-\frac{\kappa}{2}\right)\frac{\partial}{\partial\alpha}\alpha+\left(i\omega_0-\frac{\kappa}{2}\right)\frac{\partial}{\partial\alpha^*}\alpha^*\right]P(\alpha,\alpha^*,t).\end{aligned} \tag{3.25}$$

Equation (3.25) has the structure of a Fokker-Planck equation [54], which is indeed a convection-diffusion equation for a probability density $p(\vec{x}, t)$,

$$\frac{\partial p(\vec{x},t)}{\partial t} = -\sum_i \frac{\partial}{\partial x_i}[A_i(\vec{x},t)p(\vec{x},t)] + \frac{1}{2}\sum_{i,j}\frac{\partial^2}{\partial x_i\partial x_j}[g_{i,j}(\vec{x},t)p(\vec{x},t)]. \tag{3.26}$$

The vector field $A_i(\vec{x}, t)$ is known as the *drift vector*, whereas the $g_{i,j}(\vec{x}, t)$ contains the information about the diffusion coefficients. In comparing the general structure (3.26) with equation (3.25), we readily notice that first term on the right hand side accounts for a diffusion process with a coefficient κN, while the second term

represents the drift contribution. Interestingly, the Fokker-Planck equation can be re-expressed as a conservation probability law,

$$\frac{\partial p(\vec{x},t)}{\partial t} + \sum_j \frac{\partial J_i(\vec{x},t)}{\partial x_i} = 0, \tag{3.27}$$

for the probability current density

$$J_i(\vec{x},t) \equiv A_i(\vec{x},t)p(\vec{x},t) - \frac{1}{2}\sum_k \frac{\partial}{\partial x_k}[g_{i,k}(\vec{x},t)p(\vec{x},t)]. \tag{3.28}$$

It follows from (3.27) that the steady state has a vanishing divergence of $\vec{J}$. It is less obvious to state that, in several dimensions, the steady state fulfills

$$\vec{J}_{\text{ss}} = \vec{0}. \tag{3.29}$$

The above condition is correct only for a certain sub-class of Fokker-Planck equations. Let us assume that $g_{i,k}(\vec{x},t)$ is diagonal $g_{i,k}(\vec{x},t) = \delta_{i,j}D(\vec{x})$, then the steady state $p_s(\vec{x})$ satisfies

$$\vec{A}p_s - \frac{1}{2}\nabla(Dp_s) = 0, \tag{3.30}$$

hence

$$\frac{1}{p_s}\nabla p_s = \nabla(\ln p_s) = \frac{2\vec{A}}{D} - \frac{1}{D}\nabla D. \tag{3.31}$$

As the vector field on the right hand side is the gradient of a scalar field, it must be irrotational so

$$\frac{\partial}{\partial x_i}\left(\frac{2A_j}{D}\right) = \frac{\partial}{\partial x_j}\left(\frac{2A_i}{D}\right). \tag{3.32}$$

The vector field $2\vec{A}/D$ may thus be expressed as the gradient of a potential field $U(\vec{x})$, such that $2\vec{A}/D = -\nabla U(\vec{x})$ and

$$U(\vec{x}) = -\int \frac{2\vec{A}}{D}\cdot d\vec{x} + \text{constant}. \tag{3.33}$$

Upon the set of equations 3.32, the expression (3.29) is valid and it can finally be integrated to give

$$p_s(\vec{x}) = \frac{1}{Z}e^{(-U(\vec{x}))}, \tag{3.34}$$

with Z being a normalization constant. This proof will be crucial to derive the analytical steady state solutions in chapters 9 and 10. In our example of the damped harmonic oscillator, the steady state solution can be calculated in this way to obtain,

$$P_{\text{ss}} = \frac{1}{Z}\exp\left[-\frac{|\alpha|}{N}\right], \tag{3.35}$$

which is the P-representation of a thermal state.

Chapter 4

Quantum phase transitions

4.1 Quantum many-body systems and phases

Many interesting systems consist of a collection of quantum degrees of freedom. These could be for example the electrons in the bulk of a solid, the matter in the core of a neutron star or the magnetic moments inside a magnet. Complex phenomena emerge when a number of quantum systems interact with each other, which may give rise to a collective statistical behavior that is fundamentally different from the properties of each single particle alone. The field of quantum many-body physics deals with this problem [52], in which we attempt to describe collective phenomena in terms of the constituting particles of a system along with their interactions. In particular, we are often interested in calculating the ground state or a thermal state of a certain Hamiltonian, or certain properties associated to them. Likewise, one may extend many of the ideas and approaches to the study of dissipative systems described by a Liouvillian.

In this context, it is not alien to find that the same Hamiltonian originates qualitatively distinct collective states depending on certain parameters such as the temperature or the strength of the interactions. These collective states will exhibit fundamentally different properties or *phases*. We encounter these situations in our everyday life, like the solid or liquid phases arising from different organisations of identical molecules of water. Different phases are often associated to different organisations of matter, and the word *order* becomes a synonym of phase.

The mathematical description of phases of matter is highly non-trivial in almost

any case, as the motions of single particles become correlated. The prospects are even worse for indistinguishable degrees of freedom, which are non-locally correlated by principle. Even if a microscopic model is available, an exact analytical solution for the complete model is rarely available. For that reason, one frequently has to resort to several approximations or numerical methods to tackle the problem. Mean-field theory, which will be extensively employed in chapters 9 and 10, is one of the easiest and most common strategies to provide us at least with a qualitative general picture. The essence of this approach is to include correlations only on the average, whereby the effect of the other particles is included only as a mean-field interaction [52]. This transforms the problem into an effective single particle problem. Mathematically, if we have an interaction term H_I involving two operators A and B such that $H_I = AB$, the mean-field approximation is given by coupling A to the mean field of B and vice-versa, concretely

$$H_I^{MF} = A\langle B\rangle + \langle A\rangle B - \langle A\rangle\langle B\rangle. \tag{4.1}$$

Another useful approximation is the adiabatic elimination of certain degrees of freedom. The essence of this approximation relies on the effective separation between fast and slow degrees of freedom in a system. For instance, in atomic and solid state physics this approximation is known as the Born-Oppenheimer approximation [63], which allows us to separate the dynamics of the fast electrons and the slow nuclei. In dissipative systems, this approximation is normally executed by substituting the fast variables by their steady states in the dynamics of the slow degrees of freedom. The adiabatic approximation will be crucial in obtaining analytical results in chapters 9 and 10.

4.2 Quantum phase transitions

Typical examples of a classical phase transition would be given by the transition between solid and liquid states of matter, or the ferromagnetic-paramagnetic transition in a magnet, in which different phases are triggered by thermal fluctuations. In contrast, a *quantum phase transition* (QPT) [64] is a phase transition between quantum phases of matter that is driven by the quantum fluctuations arising from the intrinsic statistical nature of quantum degrees of freedom. Any thermal fluctu-

ation vanishes at $T = 0$, but not the quantum fluctuations in the ground state. Thus, QPT are often studied at zero temperature, where the transition is mathematically represented as a ground state energy that is no longer an analytic function of the Hamiltonian parameters. A famous example is the quantum phase transition from a superfluid to a Mott insulator in a gas of ultracold atoms [65]. Strictly speaking, such non-analytical behavior is accomplished in the so-called *thermodynamic limit*, in which the system size (typically the number of particles) is brought to infinity.

Let us assume a Hamiltonian of the form,

$$H = H_0 + gH_1. \tag{4.2}$$

The Hamiltonians H_0 and H_1 are competing terms which favour different quantum ground states. When $g \ll 1$ the ground state is dominated by H_0, slightly perturbed by H_1. Similarly, when $g \gg 1$ the ground state is essentially that of H_1. As g is tuned between these two extreme limits, the competition between H_0 and H_1 will determine a *critical point* g_c at which the QPT occurs [64]. A classic nomenclature distinguishes between first and *second order* (or *continuous*) quantum phase transitions, that traditionally stemmed from the order of the first derivative of the energy being discontinuous at the critical point. In a first-order phase transition there exists a discontinuity in some observable at the transition, like the discontinuous change in density of various solid/liquid/gas transitions. The correlations around the critical point do not exhibit a qualitative change, showing an exponential decay with distance over the entire phase diagram. Second-order phase transitions, on the contrary, are characterised by a qualitative change in the two-point correlation function $G(|i-j|) = \langle O_i O_j \rangle - \langle O_i \rangle \langle O_j \rangle$, which decays as a power law near the critical point (*long-range order*). This behavior is the result of a divergence in the correlation length of the system, or equivalently, a divergent susceptibility at the critical point [66].

4.3 Spontaneous symmetry breaking

The study of symmetry in a dynamical system is not limited to being a purely static property as it might seem from our discussion in section 2.3. Concretely, unlike energy in a closed system, symmetry is not necessarily conserved: symmetries can

be broken. *Spontaneous Symmetry Breaking* (SSB) refers to the fact that the actual solution to a certain dynamical system has lower symmetry than the dynamical equations governing the evolution [55, 58, 64, 66, 67]. The keys to understanding this phenomenon are found in noticing the multiplicity of solutions to certain dynamical equations as well as their stability. The stability of different solutions are also different in the general case, and it may occur that a solution with greater symmetry becomes less stable than another solution with less symmetry. The system itself then 'picks' a solution that is more stable, and in doing so, the solution breaks a symmetry group of the equations.

The solution after a SSB frequently appears as one among other equally possible solutions, which are related through the symmetry group that has been broken [58]. But how is the choice of the solution made? Indeed, the actual solution is conditioned by some random perturbations not included in the ideal dynamical equations, such as small imperfections or weak external fields. So while the SSB can be associated to a purely mathematical property with regards to the stability of solutions, the specific choice of the actual solution is dictated by the physical system.

SSB may occur in space, time, or both space and time. An example of time symmetry breaking would be given by a certain steady state that becomes periodic for a certain regime of parameters. This is mathematically represented by a Hopf bifurcation [67] (an example is discussed in section 4.6), and it assumes a breaking of the translation group in time.

The phenomenon of SSB, as we have discussed, takes place regardless of the classical or quantum nature of the dynamical equations. To name a few examples in classical physics, we find the splash of a drop of milk (Fig. 4.1), the spiral structure of disk galaxies [68], the Bénard convenction cells [69] or the Couette-Taylor flow experiment in fluid dynamics [70].

Strictly speaking, the SSB will occur only for certain regions of the complete parameter space characterising the dynamical equations. One can therefore identify different symmetry sectors (or phases) in a parameter space and construct the *phase diagram* of the system. In the field of equilibrium statistical mechanics, Landau's phenomenological theory first employed the concept of SSB to understand the emergence of various thermodynamic phases. In this Landau type transitions there exists

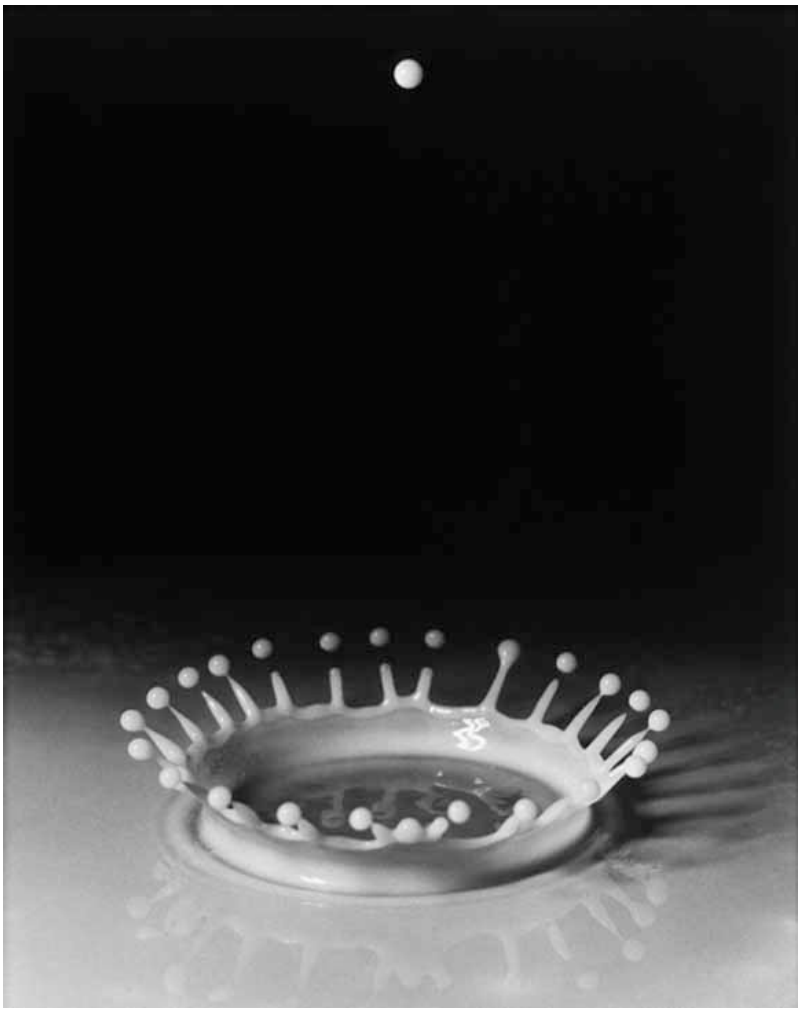

Figure 4.1: The symmetry of a splash. A drop of milk impacts the surface of the same liquid, creating a circular ring that rises and breaks up into 24 peaks, thereby breaking the original $U(1)$ symmetry of the system. [Image reproduced from [71]]

a *local order parameter* that is zero in a disordered phase and becomes different from zero in an ordered phase, indicating a SSB. A canonical example is the Ising model in a tunable external field (analysed in section 4.4), being the magnetization along the field direction a suitable order parameter.

Finally, there is an important theorem to bear in mind relating the dimensionality D of a system and the possible presence of SSB, which will be used in chapter 10.

- **Mermin-Wagner theorem** [72]. There is no spontaneous symmetry breaking in $D = 2$ systems for continuous symmetries. (Discrete $D = 2$ symmetries may be broken (*e.g.* the finite-T transition of the $D = 2$ classical Ising model)).

Intuitively, the physical mechanism behind this theorem is that thermal fluctuations

become much more important in low dimensions and often prevent ordering even at zero temperature.

4.4 A canonical example: the quantum Ising chain

The quantum Ising chain in a transverse field is one of the few examples of an exactly solvable model undergoing a second-order quantum phase transition [64]. Therefore, we shall use it to illustrate some of the concepts introduced before. The model consists of a set interacting spin-1/2 particles, each of them located at one of the N sites of a one-dimensional chain. The Hamiltonian may be parametrised as follows,

$$H_{\mathrm{I}} = -\lambda \sum_{j=1}^{N-1} \sigma_j^z \sigma_{j+1}^z - \sum_{j=1}^{N} \sigma_j^x. \tag{4.3}$$

where σ^x and σ^z are the Pauli matrices defined in equation (2.12). The first term in equation (4.3) accounts for the interaction between neighbouring sites, and it tends to align the spins in the z direction as this configuration posses lower energy. This interaction competes against the presence of a transverse field in the x direction, which induces the flipping of states $|\uparrow\rangle_j$ and $|\downarrow\rangle_j$ through the σ^x operator.

The Hamiltonian (4.3) may be diagonalized by mapping the spin operators onto fermions through the Jordan-Wigner transformation, followed by a canonical transformation (namely a Bogoliouvov transformation) to obtain a diagonal fermionic representation (see [48] for details), yielding

$$H_{\mathrm{I}} = 2 \sum_{q} \omega_q \eta_q^\dagger \eta_q + E_0, \quad E_0 = -\sum_{q} \omega_q. \tag{4.4}$$

where $\omega_q = \sqrt{1 + 2\lambda \cos q + \lambda^2}$ and $\eta, \eta^\dagger$ are fermionic operators.

The diagonalized Hamiltonian (4.4) allows us to compute all the observables of the model. For instance, the energy associated with a single excitation from the ground state is given by the dispersion relation ω_q, which indicates the presence of a finite energy gap excluding the case $\lambda \equiv \lambda_{\mathrm{c}} = 1$ for a wave vector $q = \pi$. In that case the dispersion relation comes down to,

$$\omega_{q \to \pi} = |1 - \lambda|. \tag{4.5}$$

This point at which the energy gap closes locates the critical point of a quantum phase transition. The order parameter in this model is given by the magnetization

perpendicular to the external field, which can be computed from the Hamiltonian (4.4) as [48]

$$\langle \sigma_j^z \rangle = (1 - \lambda^{-2})^{1/8}, \quad \lambda > 1; \quad \langle \sigma_j^z \rangle = 0, \quad \lambda < 1. \tag{4.6}$$

The order parameter takes a non-zero value in an ordered phase for $\lambda > 1$, and

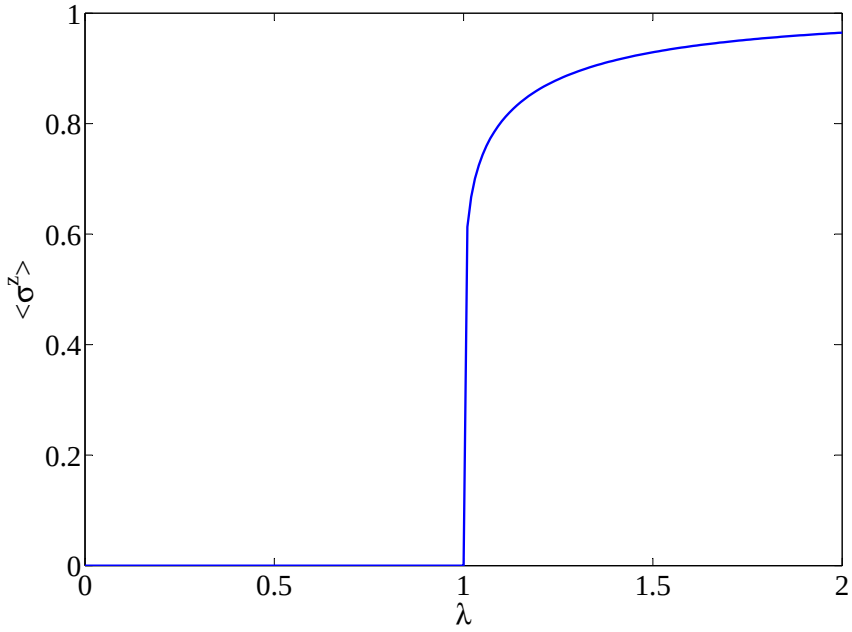

Figure 4.2: Local magnetization $\langle \sigma_j^z \rangle$ in the ground state of the quantum Ising chain.

follows a power-law around the critical point with critical exponent $\beta = 1/8$. Let us stress that the non-analytic features of the observables arise only in the thermodynamic limit. For example, the ground state energy E_0 is a sum of continuous functions, implying it is analytic in the parameter λ. However, by taking the limit $N \to \infty$ the sum is not mathematically guaranteed to satisfy this condition. In our case, the energy can be written in terms of the elliptic integral of the second kind.

$$\mathcal{E}(\phi, \theta) \equiv \int_0^{\phi} dk \sqrt{1 - \theta^2 \sin^2 k}, \tag{4.7}$$

so the energy E_0 can be expressed as,

$$-\frac{E_0}{N} = \frac{2}{\pi}(1+\lambda)\mathcal{E}\left(\frac{\pi}{2}, \theta\right); \quad \theta^2 = \frac{4\lambda}{(1+\lambda)^2}. \tag{4.8}$$

The function (4.8) is no longer an analytic function of λ for $\lambda = 1$ as the *second derivative* is discontinuous at that point. We therefore conclude that the thermodynamic limit is needed to obtain a mathematical description of the phase transition.

Finally, the Ising model allows us to illustrate the concept of SSB regarding quantum phase transitions. According to what we saw in section 2.3, if a Hamiltonian H is invariant under a transformation P, the ground state must be simultaneously an eigenstate of H and P. However, this is strictly true for finite systems. In the case of the Ising model, the Hamiltonian is invariant under the transformation $\sigma_j^z \to -\sigma_j^z$, which can be generated by the parity operator $P \otimes_j^N \sigma_j^x$. It is not difficult to check that $[H_{\text{Ising}}, P]$, so the ground state $|g\rangle$ satisfies $P|g\rangle \propto |g\rangle$. As P is indeed a parity operator (i.e., $P^2 = \mathbb{1}$ and $P^\dagger = P$), the ground state must fulfill the condition $P|g\rangle = \pm|g\rangle$. As a result, the magnetization must be zero for any value of the parameters, as we have

$$\langle g|\sigma_j^z|g\rangle = \langle g|P^2\sigma_j^z P^2|g\rangle = \langle g|P^\dagger \underbrace{P\sigma_j^z P^\dagger}_{-\sigma_j^z} P|g\rangle = -\langle g|\sigma_j^z|g\rangle \Rightarrow \langle g|\sigma_j^z|g\rangle = 0. \quad (4.9)$$

The previous argument is necessarily valid unless we take the thermodynamic limit ($N \to \infty$), where there may be states that do not respect the symmetry P, but still minimize the energy. Indeed, it is possible to prove by perturbation theory [48] that the two ground states with no magnetic field, corresponding to the two possible ferromagnetic orientations of the ground state (all spin pointing upwards or downwards),

$$|\uparrow\rangle \equiv \bigotimes_{j=1}^{N} |\uparrow\rangle_j \,, \quad |\downarrow\rangle \equiv \bigotimes_{j=1}^{N} |\downarrow\rangle_j \,, \quad (4.10)$$

become degenerate in the thermodynamic limit. Consequently, a small perturbation causes the ground state to select one the two. Notice that the previous states break the symmetry P.

4.5 Topological phases and transitions

Although conceptually powerful, the Landau's paradigm of order parameters (local observables) and SSB does not encompass the complete phenomenology concerning quantum phases and transitions. Certain quantum phases are organized in strongly correlated phases in such a way that they are macroscopically different even though they look identical to local observers. In other words, there is no local observable that is capable of distinguishing between a set of ground states, and the underlying order is only revealed when probing nonlocal observables. This phenomenon is known as

topological quantum order (TQO) [73]. This is an obvious contrast with the Ising model previously studied, where the magnetization (a local probe) is enough to distinguish between the two degenerate ground states. Examples of topological order include the quantum compass model defined in section 2.1.3, fractional quantum Hall systems [74], or the toric code model [50].

To formally define TQO we require a set of N orthonormal ground states $|g_\alpha\rangle$, $\alpha = 1, \cdots, N$, with a gap to the excited states. TQO exists if and only if for any local operator L we have,

$$\langle g_\alpha | L | g_\beta \rangle = l\delta_{\alpha,\beta} + c \tag{4.11}$$

where l is a constant and c is a correction that it is either zero or vanishes in the thermodynamic limit [73].

The understanding of these phases is accomplished again by the use of symmetry principles. In particular, a sufficient condition for TQO in connection with the system symmetries is established by the following theorem [73].

- **Theorem**. Let us consider a system satisfying condition (4.11). If all ground states may be linked by discrete $d \leq 1$ or by continuous $d \leq 2$-dimensional Gauge-like symmetries $U \in \mathcal{G}_d$, then the system exhibits finite T-TQO

The symmetry operators U are generically of the form $U^\alpha = \prod_{j \in C_\alpha} g_j^\alpha$, where C_α denotes the spatial subregion in which the Gauge-like symmetry is defined. For example, in the compass model we have two sets of symmetries $O^\alpha = \prod_{j \in C_\alpha} \sigma^\alpha$, with $\alpha = x, y$ and C_α being any line orthogonal to the $\tilde{e}_\alpha$ axis. Hence, for periodic boundary conditions these symmetries are defined along toric cycles, and $d = 1$.

This new order exhibits nonlocal correlations that lead to novel physical consequences, specially fruitful so as to build robust quantum technologies. Namely, there is no SSB of local observables, unlike what happens in the Ising model. In particular, the symmetries of the compass model cannot be spontaneously broken at finite T. For this reason, TQO displays a natural robustness against local perturbations, as they are unable to distinguish between the ground states. Alternatively, we may say that a local noise operator δH_j does not lift the ground-state degeneracy. This property is useful to construct robust quantum memories or to achieve fault tolerant quantum computations. The quantum information is inaccessible (and

hence protected) from any local perturbation, as it is instead spread throughout the whole system.

Another way to understand the absence of SSB in d-dimensional Gauge-like symmetries is through the concept of *topological defect*. These defects could be, for example, solitons or domain walls in systems with $d = 1$ discrete symmetries, or vortices in systems with $d = 2$ and $U(1)$ symmetries. The existence of Gauge-Like symmetries enables free propagation of decoupled topological defects, thereby destroying local order [73].

In spite of the absence of SSB, the presence of topological defects conceals new surprises. In 1972 J. Michael Kosterlitz and David J. Thouless identified a completely new type of phase transition where topological defects play a crucial role [75]. In particular, they studied the classical XY model, defined by the Hamiltonian

$$H_{XY} = -J \sum_{\langle i,j \rangle} \cos(\theta_i - \theta_j). \tag{4.12}$$

This model is simply the classical Heisenberg model in $2D$, expressed in polar coordinates, and so it can be used to describe certain magnets where there exists an easy-plane of magnetization. Furthermore, it gives a valid description of superconducting or superfluid films, where the important thermal fluctuations are only in the phase of the complex order parameter.

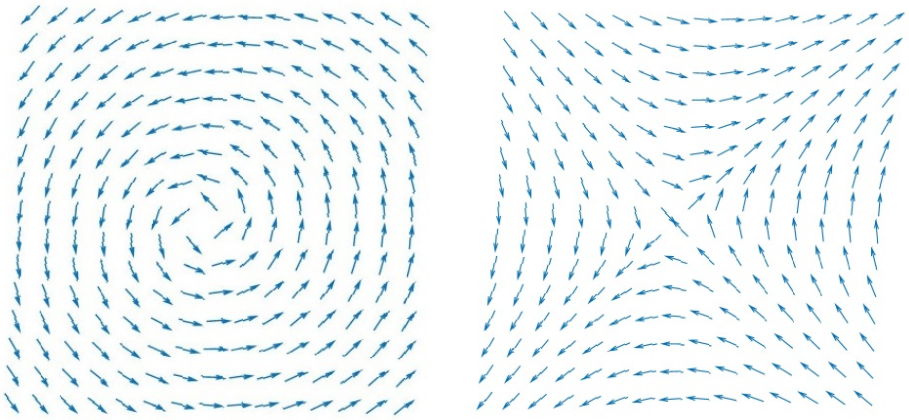

(a) (b)

Figure 4.3: a) Vortex configuration. b) Anti-vortex configuration

As we know, the ground state of the Hamiltonian (4.12) is the ferromagnetic order. More interestingly, there are also spin configurations aligned locally (like

in the ground state) but which cannot be transformed into the ground state by a continuous rotations of the spins. There happens to be two types of these configurations, known as *vortex* and *anti-vortex* (see figure 4.3), which are indeed topological defects. In contrast, a combination of a vortex/anti-vortex configuration can be smoothly transformed into the ground state: vortex and anti-vortex defects cancel each other. In order to classify configurations we need a topological invariant, which in our case is given by the vorticity, defined as

$$v = \frac{1}{2\pi} \oint_C d\vec{r} \cdot \vec{\nabla}\theta(\vec{r}). \tag{4.13}$$

The previous quantity measures the total rotation of the spin vector along the curve, and after dividing with 2π, v becomes the number of turns the spin makes when circling the vortex (winding number). A vortex/anti-vortex is thus characterised by a non-zero value of v (1 and -1 respectively).

A first approximation of the model (4.12) is given after taken the continuum limit, this is, we expand the cosine around zero and extend the range of the angular value to $-\infty$ to ∞,

$$H_{XY} \approx \frac{J}{2} \int_{-\infty}^{\infty} d^2r (\vec{\nabla}\theta(\vec{r}))^2. \tag{4.14}$$

One can readily calculate the correlation function in this simplified model to obtain,

$$\langle \exp\left\{ i(\theta(\vec{r}) - \theta(\vec{0})) \right\} \rangle \propto \left(\frac{a}{r}\right)^{\frac{k_B T}{2\pi J}}. \tag{4.15}$$

This shows a power law even at high temperatures, where an exponential decay would be expected, indicating a possible phase transition. Nonetheless, we know that a Landau-type phase transition is forbidden by the Mermin-Wagner theorem (see section 4.3). Kosterlitz and Thouless identified a new type of phase transition in which topological defects play a crucial role [75]. The problem with the model (4.14) is that it ignores the periodic nature of θ, and ultimately the vortex configurations.

One can easily calculate the energy cost of creating a topological defect, assuming a rotationally symmetrical vortex with $v = 1$ we have,

$$E_v = \frac{1}{2} \int d^2r \left(\frac{1}{r}\right)^2 = J\pi \ln \frac{L}{a}. \tag{4.16}$$

In equation (4.16) L is the system size, and for a large system the energy cost for a single vortex diverges. Even though this result seems to rule out the creation of topological defects by thermal fluctuations, the energy required to create a

vortex/anti-vortex pair (which has zero total vorticity) is only $J2\pi \ln(r/a)$, where r is the separation between the vortices.

One can then understand the topological phase transition as follows. At low temperatures vortex/anti-vortex pairs are thermally excited, and one finds a power law decay for the correlation function (4.15). Then, at certain critical temperature T_c, this gas of pairs will split into individual vortices that will take the system into a new phase with exponentially decaying correlations. The free energy for a single vortex may be approximated as,

$$F = E - TS = J\pi \ln\left(\frac{L}{a}\right) - Tk_B \ln\left(\frac{L^2}{a^2}\right) \tag{4.17}$$

where the entropy is calculated presuming that there are $L^2 = a^2$ possible positions for a vortex with area a^2. Equation (4.17) implies that there exists a critical temperature

$$T_c = \frac{J\pi}{2k_B}, \tag{4.18}$$

where energy balances the entropic contribution. We shall make use of this expression in section 10.6.

4.6 Dissipative quantum phase transitions

The notion of phase transition is not exclusive of closed systems in thermal equilibrium with an environment at a certain temperature T, or quantum systems undergoing a quantum phase transitions at $T = 0$. New interesting phases and transitions arise when we study steady states of open quantum systems. A general feature that distinguishes a non-equilibrium steady state from an equilibrium one is the presence of certain fluxes of energy and excitations between the environment and the system. The competing tendencies between these dissipative fluxes and the internal dynamics of the open system may lead the system to a stationary state far from equilibrium, and moreover, phase transitions between them. This phenomena is already known from classical physics. Some very well-known examples are the transition from laminar to turbulent flow and the Rayleigh-Bénard convection in fluid dynamics [69] .

Let us recall that, in the context of Markovian dissipative dynamics, a steady state ρ_{ss} is characterised by the eigenoperator of the Liouvillian with zero eigenvalue

(3.10). Such steady steady will in general depend on the parameters of the quantum master equation describing the dynamics. As any other many-body problem, qualitatively different steady states may appear in different regions of the parameter space, playing the role of phases of matter as introduced previously. This will happen as a result of the aforementions balances of energy and matter between the system the environment. When there exists a notion of system size in the system (like the number of particles N or the average number of excitations), a phase transition in the steady state may arise when moving throughout the parameter space in the thermodynamic limit. Such type of transition is called *dissipative quantum phase transition* [61].

4.6.1 A simple example: the single qubit laser

A laser is a canonical example of a dissipative quantum phase transition, in which there appears a transition between a thermal state and a lasing phase of coherent photons. It will also serve us to see the mean-field approach in action. In the essential literature concerning the quantum theory of lasers [54, 61, 76–78], it is customary to consider a set of N atoms coupled to a single cavity mode. Here we shall describe a very minimalist model that requires only a single qubit coupled, and it will be the basis for subsequent studies in chapters (9) and (10). Let us consider a two-level system with transition frequency ω. The qubit is coupled to a cavity mode in resonance with the transition frequency. The Jaynes-Cummings model becomes a valid description for the atom-light interaction, and so the Hamiltonian in a picture rotating with ω is

$$H_{AL} = g(a^\dagger \sigma^- + a\sigma^+). \tag{4.19}$$

We shall consider losses of radiation at rate κ and incoherent pumping of the two-level atom at rate γ (see diagram 4.4). These dissipative process arise from the coupling to two different reservoirs that, within the Markovian approximation, result in the following quantum master equation for the total density operator ρ,

$$\begin{aligned}\frac{d}{dt}\rho = &-ig[a^\dagger\sigma^- + a\sigma^+, \rho] \\ &+ \kappa\left(2a\rho a^\dagger - a^\dagger a\rho - \rho a^\dagger a\right) \\ &+ \gamma\left(2\sigma^+\rho\sigma^- - \sigma^-\sigma^+\rho - \rho\sigma^-\sigma^+\right).\end{aligned} \tag{4.20}$$

Despite the simplicity of the model, equation (4.20) is not integrable. In particular,

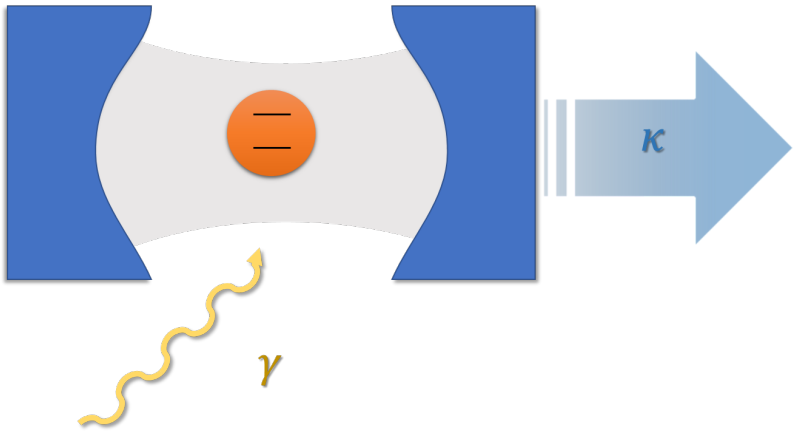

Figure 4.4: A diagram of the single qubit laser: a cavity with radiation losses at rate κ and qubit pumping at rate γ

if we wished to derive the equations of motion for the expected values of the field quadratures or the number of photons, that would result in an infinite hierarchy of differential equations. At this point is where the mean-field theory comes in handy by assuming that the system density operator ρ is separable in the qubit-field subspaces, i.e., $\rho \approx \rho_{\text{field}} \otimes \rho_{\text{qubit}}$. In using this ansatz, we can write expectation values in such a way that $\langle \sigma a \rangle \approx \langle \sigma \rangle \langle a \rangle$, thereby avoiding the infinite hierarchy of equations. Concretely, we can write the following closed system of equations in terms of the variables $A \equiv \langle a \rangle$, $S \equiv -i\langle \sigma^- \rangle$ and $D \equiv \langle \sigma^z \rangle$,

$$\begin{aligned} \dot{A}_j &= -gS - CA, \\ \dot{S}_j &= gDA - \gamma S, \\ \dot{D}_j &= -2g(S^* A + S A^*) - 2\gamma(D-1). \end{aligned} \tag{4.21}$$

The result (4.21) is derived from the Heisenberg equations for such observables as well as using the commutation relations $[a, a^\dagger] = 1$, $\{\sigma^+, \sigma^-\} = 1$ and $[\sigma^z, \sigma^\pm] = \pm 2\sigma^\pm$. The set of nonlinear equations (4.21) are known as the *Maxwell-Bloch equations* [76]. They can be shown to be equivalent to the famous Lorentz equations of fluid dynamics [54], which implies the existence of multiple and chaotic solutions depending on the regime of the parameters. It is customary to assume a regime of strong pumping $\gamma \gg \kappa, g, t$ such that the γ^{-1} is the smallest timescale in the problem. This restriction allows us to employ another useful technique to treat

many-body problems: the adiabatic elimination of the fast variables (as mentioned earlier in section 4.1). This is done simply by taking $\dot{S} = 0$ and $\dot{D} = 0$ and substituting their steady state solutions to obtain a close equation for A. In doing so, we obtain

$$\frac{dA}{dt} = \left(\frac{C_{\mathrm{p}}}{1 + \frac{|A|^2}{n_{\mathrm{mf}}}} - C_{\mathrm{p}} \right) A, \tag{4.22}$$

with $C_{\mathrm{p}} \equiv g^2/\kappa\gamma$ being the so-called *pumping parameter* [61] and $n_{\mathrm{mf}} = 2\gamma^2/g^2$.

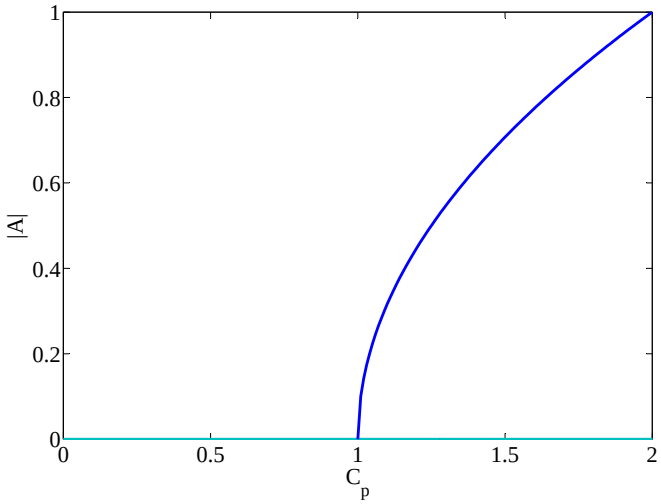

Figure 4.5: The coherent component $|A|$ as a function of the pumping parameter C_p. There exits two branches of solutions. For $C_p > 1$ the upper branch becomes stable and the trivial solution is unstable.

Equation (10.35) exhibits a Hopf bifurcation (see figure 4.5) when

$$C_{\mathrm{p}} = \frac{g}{\gamma\kappa} = 1. \tag{4.23}$$

In the case $C_{\mathrm{p}} < 1$, there is no solution apart from trivial one, defined by $A = 0$. However, if we tune the laser parameters so that $C_{\mathrm{p}} > 1$, there appears another branch of solutions (the upper branch in figure 4.5) fulfilling the following equation,

$$|A|^2 = n_{\mathrm{mf}}(C_p - 1). \tag{4.24}$$

It turns out that the trivial solution now becomes unstable, while the new branch of solutions becomes a stable attractor. Therefore, the point $C_{\mathrm{p}} = 1$ is a critical point that separates a vacuum state of coherent photons from a bright lasing state. One can easily establish a formal analogy between this dissipative phase transition and

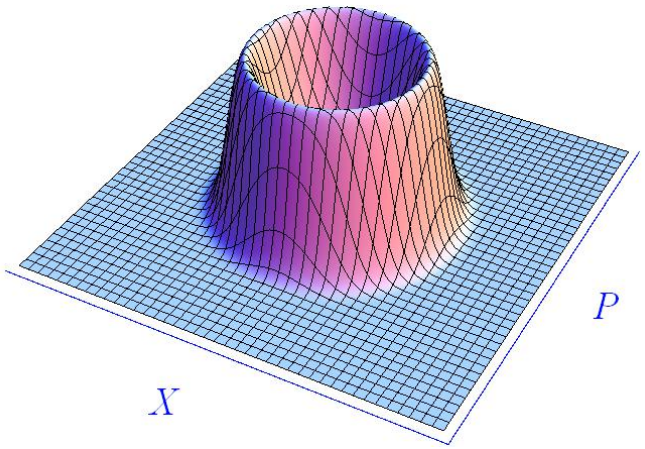

Figure 4.6: The P-representation of a generic lasing steady state of the single qubit laser above threshold $C_{\rm p} > 1$. The solutions shows a $U(1)$ symmetry.

a thermal phase transition [79]. In looking at the graph 4.5, we clearly realise that the coherent component $\langle a \rangle$ (or any field quadrature) is thus an order parameter characterising this transition. What is the broken symmetry in this example? Notice that the master equation is invariant under the global $U(1)$ transformation

$$a \to a e^{i\theta} \quad \sigma^- \to \sigma^- e^{i\theta}, \tag{4.25}$$

so we expect the steady state to possess the same symmetry (there is no thermodynamic limit at this point). In a phase representation of the field mode, the steady state must be symmetrical around the vertical axis, as sketched in figure 4.6. This corresponds to a mixed state of coherent states of phase θ. So why is the mean-field solution breaking the symmetry? The mean-field approximation has artificially selected a particular value (randomly) of θ after introducing the variable $A \equiv \langle a \rangle$. As a result, its predictions become more accurate as we approach the thermodynamic limit. In a typical laser, the limit consists of taking the number of atoms to infinity. For a single qubit laser that is obviously not possible, yet one can define a thermodynamic limit by taking the limit $n_{\rm ss} = \langle a^\dagger a \rangle_{\rm ss} \to \infty$. Essentially, this is translated into rescaling the results with a factor κ/γ.

Chapter 5

Quantum simulation

5.1 Difficulties in classical computation

Exact analytical solutions like the one shown for the quantum Ising chain (section 4.4) are often the rare exception rather than the rule. Furthermore, the analytical tools that we have available are in many cases insufficient to tackle many-body problems, especially those displaying strongly correlated phases, like the quantum compass model (equation (2.15)). Despite the fact that we count with a detailed microscopic description of these models, the diagonalisation of their Hamiltonians turns out to be a highly non-trivial task. Ultimately, one has to rely on numerical simulations to make accurate quantitative predictions, but even in this case there appear new problems for the simulation of a quantum system in a classical computer.

The fundamental problem regarding the simulation of quantum models with classical computers lies in the exponential increase of resources with the system size. Thus, in a general scenario, the simulation of a large number of degrees of freedom becomes intractable. Let us for example assume that we wish to study the ground state of a certain Hamiltonian H of a many-body system arranged on a lattice of dimension D. Let us also assume that the dimension of the Hilbert space in each site is $\dim(\mathcal{H}_j) = N$. For a bosonic system, with an infinite Hilbert space this typically demands a proper truncation of the Hilbert space. All in all, the total Hilbert space will be given by the tensor product $\mathcal{H} = \otimes_j \mathcal{H}_j$, with dimension $\dim(\mathcal{H}) = N^D$. This implies that we need to store N^D numbers to describe the ground state as well as N^{2D} for the Hamiltonian, thereby requiring exponential

memory resources. In practical terms, a system of 50 spins or more goes beyond the capabilities of any classical computer [40].

Some numerical methods were devised to cleverly overcome this challenge, but still they have to face their own limitations. For example, Monte Carlo methods allow the evaluation of integrals for many-body systems in a time that scales polynomially with the number of particles. These stochastic methods are suitable when the functions being integrated vary smoothly and do not change sign so that a relatively small number of points assure a good sampling. Unfortunately for some quantum systems, like fermionic or frustrated systems, the numerical evaluation of the integrals requires the sampling with nonpositive-semidefinite weight functions, which results in an exponential growth of the statistical error with the number of particles. To compensate this effect, the simulation time must also increase exponentially, and hence the advantage of the Monte Carlo method is cancelled, originating the so-called sign problem [80]. The density matrix renormalization group (DMRG) is another technique that offers spectacular results, but it is limited to one dimensional systems.

5.2 Quantum simulators

A conceptually trivial solution to the problem of the exponential increase in the resources was envisaged by Richard Feynman in his seminal lecture 'Simulating Physics with computers' in 1981 [81]. Feynman suggested the possibility of using a controllable quantum system to simulate a less accessible quantum model of interest. In doing so, the problem of the exponential increase in the resources is directly overcome, as the quantum simulator naturally incorporates the resources that we need.

Such a quantum simulator would be restricted to emulate only a limited amount of quantum models, which is to say that they are purpose-oriented quantum computers. In this sense, a quantum computer can be thought of as a universal quantum simulator, capable of emulating any quantum system. Nevertheless, the actual difficulty to achieve a quantum computer that surpasses the computational power of a classical supercomputer forces us to find a compromise solution between compu-

tational power and quantum resources. A quantum simulator, after all, benefits from managing quantum information rather than classical information so that large amounts of information may be handled by using relatively few number of degrees of freedom.

Generically speaking, we may differentiate between digital and analog simulation [40]. In this thesis we shall be solely concerned with the latter. Analog quantum simulators are conceived to mimic the dynamics of a certain model, or at least one may find clever mappings between the simulator and the system. This frequently involves additional external fields or ancillary systems. In particular, periodically driven systems have proved to be a extremely useful tool to simulate a rich variety of phenomena, whether in closed or open systems [82–86]. In chapter 8, periodic driving fields will become an essential tool for quantum simulation purposes.

The result of the simulation is then obtained after measuring proper observables of the system. Whatever the case, there are some generic conditions that any quantum simulator must fulfill [39],

- *Quantum system*: the simulator counts with a system of bosons and/or fermions with or without integral degrees of freedom (spin), which are confined in some region of space.

- *Initialisation*: the simulator can be prepared into a given state, whether pure or mixed, within a certain fidelity.

- *Hamiltonian engineering*: the interactions between the particles of the simulator and the external fields or the environment can be properly adjusted.

- *Detection*: the result of the simulation is obtained through adequate measurements on the simulator, which may be local or collective.

Quantum simulators have already a large number of useful applications [40]. One may study the ground state properties of a certain Hamiltonain, including the experimental observation of quantum phase transitions [65]. Additionally, one may explore the dynamics of excitations or even open system dynamics [47]. An important nest of applications resides in condensed matter physics, where one may explore the physics of Bose-Hubbard models [14, 87]. It is also possible to study

non-equilibrium phenomena like the process towards thermalization or quench dynamics [88]. Quantum simulators have also been used to explore the physics of lattice Gauge theories [84], with applications in high-energy physics. Even classical problems may benefit from the use of quantum simulators [89]. There are already several platforms to implement a quantum simulator, such as atomic quantum gases, ensembles of trapped ions, photonic systems, superconducting circuits, nuclear spins addressed using NMR methodology, or electron spins in quantum dots [90]. Each platform has its own advantages and limitations, and different approaches often tackle complementary aspects of quantum simulation.

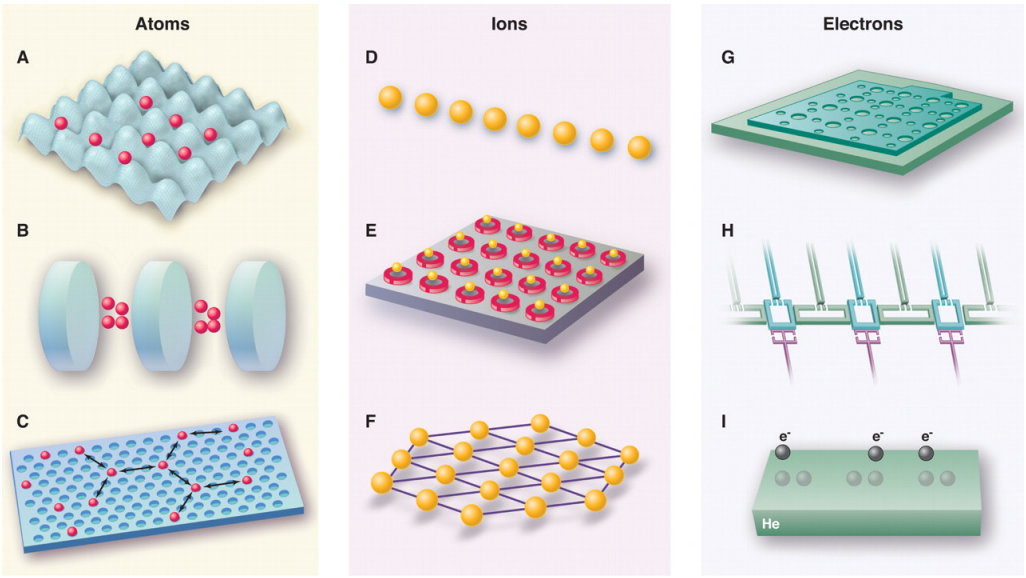

Figure 5.1: Examples of quantum simulators include atoms in optical lattices or arrays of cavities (A,B,C), ions arranged in chains (D), 2D traps or Coulomb crystals (E,F), and electrons in quantum dots (G) or superconducting circuits (H) (Image reproduced from [90]).

For the purposes of this thesis, we shall require the implementation of quantum Ising Hamiltonians (see equation(2.14)). Setups of trapped ions [82, 91] or ultracold atoms in optical lattices [92] are suitable platforms to this end. The dynamics of an interacting gas of bosons loaded in a lattice is well-captured by the Bose-Hubbard Hamiltonian,

$$H_{BH} = -J \sum_{\rangle j,l \langle} a_j \dagger a_l + \sum_j \epsilon_j n_j + \frac{U}{2} \sum_j n_j(n_j - 1), \tag{5.1}$$

where U measures the on-site repulsion, ϵ_j is an offset due to the harmonic trapping

potential and J accounts for the hopping between neighbouring sites. If $U/J \gg 1$, the bosons are delocalized in a superfluid phase; if $U/J \ll 1$, they are localized in a Mott-insulating phase and the hopping terms constitutes a small perturbation. This is the starting point used in section 8.6.1 to implement spin Hamiltonians after mapping internal atomic states onto pesudo-spin degrees of freedom.

Trapped-ion quantum simulators benefit from the natural Coulomb repulsion between ions. The typical distance between them is of the order of microns, which facilitates the manipulation and measurement of each ion state individually. Similarly to the previous atomic setup, internal levels can play the role of pseudospins, although here the interaction is normally long-range. This range can be adjusted through the trapping potential so one may work with effective short-range interactions. The motion of the ions gives rise to collective phononic states, which are not coupled to the internal degrees of freedom. Such coupling is implemented by means of additional laser forces [82, 93], by which we can implement the atom-light interactions considered in this thesis (naturally appearing in lattices of cavity QED [53] and circuit QED systems [47]).

Concerning the readout in trapped-ion setups, state-dependent fluorescence reads the qubit states. This is achieved through a closed cycle of a dipole allowed transition from the ground to the excited state and a forbidden spontaneous decay into the excited state. When the laser –whose frequency is off-resonant for this transition– acts on the ion, the ion will show up bright when it is in the ground state, and dark when it is in the excited state. Additionally, the states of motion can be mapped onto the internal states thanks to the blue and red sideband transitions, and later on read through fluorescence measurements.

Chapter 6

Quantum sensing

6.1 Estimation theory

The central goal of the classical estimation theory is, in a nutshell, to determine the most accurate estimation of a certain parameter φ encoded in a given probability distribution $p_\varphi(\boldsymbol{x})$. More specifically, we look for an optimal estimator $\tilde{\varphi}_N(\boldsymbol{x})$ that outputs the best estimation of φ for a given N-point data set $\boldsymbol{x} = \{x_1, x_2, \cdots, x_N\}$. Hence, the estimator is in turn a random variable itself, whose fluctuations are aimed to be minimised.

In this thesis we shall adopt the so-called frequentist approach, where φ is presumed to be a deterministic parameter with a value that could in principle be given to any precision. The performance of the estimator can be then assessed through the Mean Square Error (MSE) deviation from the true value φ,

$$\Delta^2\tilde{\varphi}_N(\boldsymbol{x}) = \langle(\tilde{\varphi}_N(\boldsymbol{x}) - \varphi)^2\rangle = \int d^N\boldsymbol{x}(\tilde{\varphi}_N(\boldsymbol{x}) - \varphi)^2. \tag{6.1}$$

Additionally, we ideally demand the estimator to be unbiased, such that its average yields the true parameter value,

$$\langle\tilde{\varphi}_N(\boldsymbol{x})\rangle = \int d^N\boldsymbol{x}p_\varphi(\boldsymbol{x})\tilde{\varphi}_N(\boldsymbol{x}) = \varphi. \tag{6.2}$$

The optimal unbiased estimator is achieved after minimising the MSE for all φ. Such optimal estimator will be generally difficult to find, and it may not even be unique for any φ. Yet, the Cramer-Rao bound lower bounds the MSE for any unbiased estimator,

$$\Delta^2\tilde{\varphi}_N(x) \geq \frac{1}{\nu F[p_\varphi]}, \tag{6.3}$$

where ν is the number of independent experiment repetitions and $F[p_\varphi]$ is the well-known *Fisher information*, defined as

$$F[p_\varphi] = \int d^N \boldsymbol{x} \frac{1}{p_\varphi} \left[\frac{\partial p_\varphi(\boldsymbol{x})}{\partial \varphi} \right]^2 . \tag{6.4}$$

The Fisher information is a non-negative function that generically depends on φ, and it is additive for uncorrelated events, i.e., $F[p_\varphi^N] = NF[p_\varphi]$. In essence, the greater the Fisher information is, the higher precision will be accomplished in the parameter estimation. Furthermore, the Fisher information is related to the infinitesimal statistical distance ds^2 between the distributions $p(x|\varphi)$ and $p(x|\varphi)+dp(x)$,

$$\left(\frac{ds}{d\varphi} \right)^2 = F(\varphi). \tag{6.5}$$

In the realm of quantum mechanics, the parameter estimation problem translates into the estimation of a parameter φ encoded in a certain quantum state ρ_φ. In contrast to its classical counterpart, here we rely on a specific measurement scheme $M_{\boldsymbol{x}}$ that yields the probability distribution,

$$p_\varphi(\boldsymbol{x}) = \mathrm{Tr}\left\{ \rho_\varphi M_{\boldsymbol{x}} \right\}. \tag{6.6}$$

In full generality, the measurement scheme is a generalised measurement over the class of Positive Operator Valued Measure (POVM). Once the measurement scheme is determined, we obtain a probability distribution whose quantum mechanical origin no longer plays a significant role. Therefore, the optimal estimation strategy involves a non-trivial search over all POVMs that maximises the Fisher information,

$$\Delta^2 \tilde{\varphi}_N(\boldsymbol{x}) \geq \frac{1}{\nu \max_{M_{\boldsymbol{x}}} F[p_\varphi]} \geq \frac{1}{\nu F_Q[\rho_\varphi]}. \tag{6.7}$$

The last bound in (6.7) defines the *Quantum Cramér-Rao bound* (QCRB), in which we have defined the *Quantum Fisher Information* $F_Q[\rho_\phi]$ (QFI). The QFI can be obtained through the *Symmetric Logarithmic Derivative* (SLD) $L_\varphi[\rho_\varphi]$, which satisfies the following operator equation

$$\partial_\varphi \rho_\varphi = \frac{1}{2}(\rho_\varphi L_\varphi + L_\varphi \rho_\varphi). \tag{6.8}$$

Once the SLD is found, the QFI is given by

$$F_Q[\rho_\varphi] = Tr\left\{ \rho_\varphi L_\varphi^2 \right\}. \tag{6.9}$$

The solution to the operator equation (6.8) will normally imply the diagonalisation of the density operator $\rho_\varphi = \sum_i \lambda_i(\varphi)|e_i(\varphi)\rangle\langle e_i(\varphi)|$, in terms of which we may write,

$$L_\varphi[\rho_\varphi] = \sum_{\substack{i,j \\ \lambda_i+\lambda_j\neq 0}} \frac{2\langle e_i(\varphi)|\dot{\rho}_\varphi|e_j(\varphi)\rangle}{\lambda_i(\varphi)+\lambda_j(\varphi)}|e_i(\varphi)\rangle\langle e_j(\varphi)|. \tag{6.10}$$

Similarly to the Fisher information, the QFI is additive over (uncorrelated) product states, $F_Q[\rho_\varphi^{\otimes N}] = NF_Q[\rho_\varphi]$. This property allows us to interpret the ν factor in the QCRB as the number of independent realizations of an experiment described by the same state ρ_ϕ, or a single experiment with ν uncorrelated copies of the same system $\rho_\varphi = \otimes_j^\nu \rho_\varphi^j$. In this work we shall consider single-shot experiments, so $\nu = 1$, which is to say that the total time does not count as a resource in our analysis.

6.2 Quantum metrology

The field of quantum metrology investigates abstract procedures to accomplish some enhancement (e.g., precision or efficiency) by means of quantum resources [43]. The different implementations of these schemes in physical systems lay the foundation for quantum sensing technologies [94]. In any measurement process one may distinguish between three different processes, (which do not necessarily occur sequentially as we shall see in chapter 10)

- **Preparation of the probes**: the probes are prepared in a certain initial state, which could be uncorrelated $\rho_0 = \otimes_j^N \rho^j$ or entangled $\rho_0 \neq \otimes_j^N \rho^j$.
- **Interaction with the system to be measured**: the probes gain information of the parameter φ to be estimated so $\rho_0 \to \rho_\varphi$
- **Probe readout**: The probes are measured with a certain scheme $M_{\boldsymbol{x}}$ in order to estimate the parameter φ from the probability distribution $p_\varphi(\boldsymbol{x})$.

Regardless of the specific system, any experiment deals with different sources of errors. In particular, there are statistical errors arising from the natural fluctuations occurring in any real experiment. These are accidental (e.g., insufficient control of the probes, random external influences) or fundamental (quantum uncertainty). We may reduce statistical errors by repeating the same experiment

(sequential strategies), or by disposing a certain number of copies of the system (parallel strategies). In this thesis we shall be concerned with the latter approach, which include popular examples like Ramsey interferometers [43] or Mach-Zehnder interferometers [27]. Let us assume that we have a collection of N probes. For a set of N independent random variables, the central limit theorem then states that the precision scales with the inverse square root of N. This is the so-called *shot noise limit*. Nevertheless, additional correlations may enhance this scaling. Quantum correlations between the probes are known to improve the shot noise limit up to the so-called *Heisenberg scaling*, in which the quantum Fisher information scales quadratically with N, leading to a precision that scales with the inverse of N. In figure 6.1 both scenarios are schematically compared.

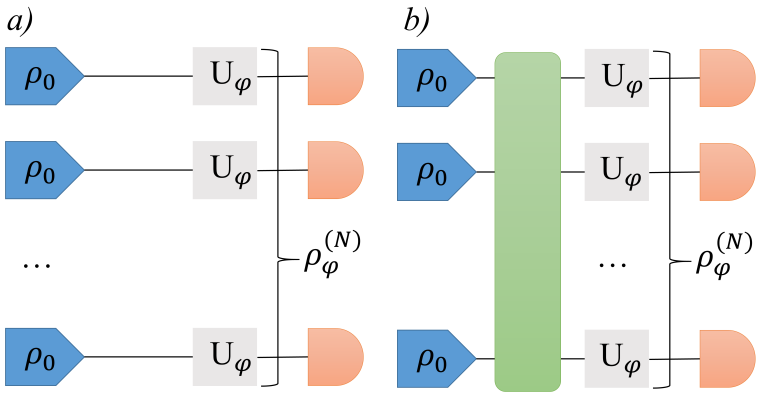

Figure 6.1: Comparison between classical and quantum parallel strategies. In a) the probes are uncorrelated and the shot-noise limit reins. The use of quantum correlations in b) may improve the scaling up to the Heisenberg scaling.

The above definition of Heisenberg scaling must be treated carefully, though. More precisely, the proper scaling will be determined by the *query complexity* of the network of probes [95, 96]. A physical query simply consists of a probe-system interaction, represented by an interaction term $H_I = \sum_{k=1}^{N} \sum_{j=1}^{N} H_j \otimes H_k$. For instance, the query complexity of a chain with long-range two-body interactions is of order $O(N^2)$, while a chain with nearest-neighbour two-body interactions is $O(N)$. The maximal query complexity is obtained in a network of long-range N-body interactions, that gives rise to a query complexity of order $O(2^N)$. To understand the relevance of the query complexity, let us examine a general bound that is indeed

a consequence of the Margolus-Levitin bound on the speed of quantum dynamical evolution [95, 96]. One may define the following distance between pure states,

$$s(\psi, \varphi) = \arccos(|\langle\psi|\varphi\rangle|), \tag{6.11}$$

known as the Wooter's distance. The transformation of a state $|\psi\rangle$ is assumed to be generated by the operator H with a target parameter φ, such that

$$|\psi(\varphi)\rangle = \exp(-i\varphi H)|\psi(0)\rangle. \tag{6.12}$$

If we now evaluate the derivative of the Wooter's distance with respect to φ, we may write the following upper bound by making use of the previous Schrödinger-like equation,

$$\frac{ds}{d\varphi} \leq |\langle H\rangle|. \tag{6.13}$$

Hence, by combining the above inequality with equation (6.5) we obtain the following general expression for the Cramér-Rao bound,

$$\Delta\varphi \geq \frac{1}{|\langle H\rangle|}. \tag{6.14}$$

In conclusion, it is obvious from the above expression that the query complexity of the generator of translations of the parameter to estimate φ is what really determines the actual form of the Heisenberg scaling. This resource counting has the advantage of unifying both interacting and non-interacting (non-linear) systems, and is consistent with those results claiming scalings beyond the Heisenberg scaling [97].

Part III

Research outline

Chapter 7

Overview of the papers

So far I have introduced the context, motivations and background theory necessary to understand the results of this thesis, which will be presented in the form of three papers. This work is a cross-disciplinary effort that applies concepts and methods that arose originally in condensed matter physics, such us spontaneous symmetry breaking or photon-assisted tunneling, into the fields of quantum simulation and quantum sensing. The results may contribute to implement topologically protected quantum qubits and dissipative quantum optical sensing devices robust against decoherence.

In chapter 8 we shall be concerned with the quantum simulation of a spin model that shows topological quantum order, namely the quantum compass model briefly introduced in section 2.1.3. The twofold degenerate topological ground state can be understood in terms of elegant symmetry principles. The type of interactions that naturally appear in quantum simulation setups are isotropic, like in the Ising or Heisenberg model. In this work I show how the implementation of models where the orientation of the spin-spin interactions depend on the spatial orientation of the bonds can be successfully tackled by means of photon-assisted tunneling effects. This tool has been previously exploited in seminal papers to implement synthetic gauge fields [84]. Here I extend this technique and show its potentiality to simulate highly non-trivial models with topological features. To that end, we shall combine two ingredients that are already within the reach of state-of-the-art technologies, concretely the simulation of Ising models along with site-dependent periodically driving fields.

The necessity of addressing single particles make ultracold atoms or trapped ions suitable platforms to test this proposal. In particular, the paper outlines a possible implementation with ultracold atoms in optical lattices and Rydberg atoms, written by Juan José García-Ripoll and Diego Porras respectively. I propose an adiabatic passage as a procedure to prepare one of the twofold degenerate ground states. The use of symmetry principles will be crucial regarding the characterisation of such passage. Concretely, I characterise the final state in terms of an operator named Z, for which I show it is a conserved quantity during the adiabatic evolution in appendix 8.9.

In chapter 9 we move on to the study of quantum optical systems for sensing purposes where dissipative interactions, far from being an obstacle, become a key ingredient to increase the precision in measurements. I introduce two general principles that are illustrated with a minimal probe: a single qubit laser (introduced in section 4.6).

The first working principle relies on the breaking of the underlying $U(1)$ symmetry of the lasing steady state when an external field is applied, being its amplitude and phase the parameters to be estimated. The potential benefit for sensing can be well understood in terms of the spontaneous symmetry breaking occurring in the thermodynamic limit of the system. Suitable order parameters (light quadratures) exhibit a sensitivity that improves with the system size, which in this case corresponds to the number of photons in the steady state. I apply the theory of quantum Fisher information to prove the optimality of this measurement scheme concerning the saturation of the quantum Cramér-Rao bound. In this way, I use symmetry principles as powerful conceptual tools to understand the enhancement in the precision from an abstract point of view. At a physical level, the understanding is rooted in the amplification effect caused by an active medium, the qubit laser, in which nonlinear interactions magnifies the influence of a target external field. The precision in the estimation of amplitude and phase of the field is shown to be enhanced when one increases the incoherent pumping acting on the qubit.

The second working principle is to take advantage of dissipative phase transitions, and more specifically, the special sensitivity of the system at the critical point. Analytical and numerical studies show that the critical point is optimal to

make parameter estimation, which is valid for both optimal and non-optimal measurement schemes. This fact may be exploited when certain measurement schemes, without being optimal, may be more accessible from an experimental point of view. Specifically, I present analytical and numerical results for the number of photons, which is non-optimal in our set-up. Throughout this work we restrict ourselves to parameter regimes close to the critical point, which luckily allows us to give accurate analytical results in terms of integrable Fokker-Planck equations. An implementation with trapped ions by D. Porras is sketched at the end.

In chapter 10 I build on the previous ideas and extend the setup to networks of single qubit lasers close to the lasing critical point. From the experience gathered in chapter 9, strong pumping regimes and proximity to the critical point are again the starting point for a sensing scheme. In contrast to the previous paper, where we only counted with a single probe, here I explore how the correlations between the probes may enhance the overall sensitivity of the network.

In the context of quantum metrology or quantum interferometry, it is accepted that quantum correlations between the probes may lead a Heisenberg scaling with the number of probes. In this final paper I investigate the effect of classical correlations between the probes, which are later shown to provide us with analytical expressions for the steady state. To introduce such classical correlations, the interaction between the probes will be mediated solely by dissipation, which will require some reservoir engineering. In particular, I use a coherent hopping with intermediate lossy cavities that can be adiabatically eliminated, resulting in an effective incoherent coupling between the probes. Remarkably, the systems allows an analytical treatment thanks to a phase space representation that gives rise to an integrable Fokker-Planck equation. The steady state of the system turns out to be formally equivalent to a thermal state of the classical compass model described in section 4.5. This will allow us to derive analytical expressions for the quantum Fisher information in the steady state. Finally, I show how the presence of long-range correlations turns out to be crucial to accomplish a Heisenberg scaling with the number of probes. Such correlations may occur naturally in systems where there exists spontaneous symmetry breaking, or may be induced in finite systems with strong pumping regimes.

Part IV

Results

Chapter 8

Topological phases of shaken quantum Ising lattices

8.1 Abstract

The quantum compass model consists of a two-dimensional square spin lattice where the orientation of the spin-spin interactions depends on the spatial direction of the bonds. It has remarkable symmetry properties and the ground state shows topological degeneracy. The implementation of the quantum compass model in quantum simulation setups like ultracold atoms and trapped ions is far from trivial, since spin interactions in those systems typically are independent of the spatial direction. Ising spin interactions, on the contrary, can be induced and controlled in atomic setups with state-of-the art experimental techniques. In this work, we show how the quantum compass model on a rectangular lattice can be simulated by the use of the photon-assisted tunneling induced by periodic drivings on a quantum Ising spin model. We describe a procedure to adiabatically prepare one of the doubly-degenerate ground states of this model by adiabatically ramping down a transverse magnetic field, with surprising differences depending on the parity of the lattice size. Exact diagonalizations confirm the validity of this approach for small lattices. Specific implementations of this scheme are presented with ultracold atoms in optical lattices in the Mott insulator regime, as well as with Rydberg atoms.

8.2 Introduction

In the pursuit of the quantum computer, the problem of decoherence arises as the main obstacle to preserve coherent linear superpositions as to take advantage of the computational power they can provide us with. In principle, quantum error correction codes offer a solution to achieve a fault-tolerant quantum computation [98]. An alternative route consists of using topologically protected Hilbert spaces [99, 100]. In this context, a two dimensional quantum compass model on a square lattice was proposed by Douçot *et al.* [101] as a simple model to implement a protected qubit. Generally speaking, 'compass models' refer to a broad type of lattice Hamiltonians in which the couplings between sites depend on the orientation of the bonds in the lattice. A thorough review of these Hamiltonians and their properties can be found in Ref. [49].

The quantum compass model was originally introduced in 1982 as a toy model to gain insight in the context of Mott insulating transition metal compounds, for which one finds anisotropy of the exchange for different pairs of ions. The name 'compass model' arises by analogy with the dipolar coupling in a classical model of magnetic needles arranged in a lattice [51]. The 2D-version of this model on a $n \times m$ lattice is defined by the following spin Hamiltonian ($S = 1/2$),

$$H_{\mathrm{C}} = -J_x \sum_{\boldsymbol{j}} \sigma^x_{\boldsymbol{j}} \sigma^x_{\boldsymbol{j}+\boldsymbol{e}_x} - J_y \sum_{\boldsymbol{j}} \sigma^y_{\boldsymbol{j}} \sigma^y_{\boldsymbol{j}+\boldsymbol{e}_y}, \tag{8.1}$$

where $\sigma^{x,y}_{\boldsymbol{j}}$ are the usual Pauli matrices and $\boldsymbol{j} = (j_x, j_y)$ is a vector that runs over the lattice sites. We shall assume free boundary conditions in the following. We can choose ferromagnetic couplings ($J_x, J_y > 0$) without loss of generality, since ferromagnetic and antiferromagnetic quantum compass models are related by unitary transformations. One observes in Hamiltonian (8.1) that there are two competing tendencies owing to two types of Ising-like interactions: bonds along the y axis induce spin alignment along y ($\langle \sigma^y_{\boldsymbol{j}} \rangle \neq 0$), while bonds along the x axis induce spin alignment along x ($\langle \sigma^x_{\boldsymbol{j}} \rangle \neq 0$); the resulting ground state is therefore a highly entangled state without an obvious order parameter. Many recent numerical studies have examined the quantum phase transition of the anisotropic model on a square lattice through the isotropic point ($J_x = J_y$), pointing to the existence of a first

order quantum phase transition [102–104]. It has been theoretically shown that this model arises as an effective description of the low-energy physics in systems of magnetically frustrated Josephson junction arrays [100, 101], and experiments have shown signatures of the physics of this model in few qubit setups [105].

The physical implementation of the quantum compass model (8.1) in atomic systems would represent a significant breakthrough in research on topologically protected qubits. However, experimental techniques for analogue quantum simulation [39] typically provide us with effective spin-spin interactions that are independent of the spatial direction of the bonds. For instance, Ising interactions, with couplings of the form $\sigma_{\boldsymbol{i}}^{x}\sigma_{\boldsymbol{j}}^{x}$ along every spatial direction, can be readily induced and controlled in systems like trapped ions [82, 87, 91], ultracold atoms in optical lattices [92, 106–108] and Rydberg atoms [109–111]. Two notable exceptions are polar molecules and Rydberg atoms in p- or d-states, where for example a variety of compass models can be realized using Rydberg p-states [112]. In this work, we surpass this limitation by showing that the quantum compass interactions can be implemented by dressing Ising spin-spin interactions with periodic driving fields.

The basic idea of our work is the dressing of Ising interactions by the *photon-assisted tunneling* induced by periodic drivings with a site-dependent phase over a square spin lattice . A judicious choice of the site-dependence of the driving phase leads to the spatial dependence of interactions in the quantum compass model. (see Fig. 8.1). The necessary periodic drivings can be implemented with running spin-dependent optical potentials such as those demonstrated in [113]. Our ideas have a direct application in the implementation of topological models with ultracold atoms and Rydberg atoms with realistic techniques, since basically we only request an additional spin-dependent moving lattice to the trapping optical lattice potential. Indeed, periodically driven atomic lattices with site dependent phases have brought a lot of attention in recent years, as they can be used in the simulation of synthetic gauge fields [84, 85, 114–120]. The dressing of one-dimensional quantum Ising systems by periodic drivings with a gradient in intensity has been considered recently in [121]. Even though there are problems that may hinder the simulation of the ground state physics as proposed in our implementation, such as heating problems in state-dependent optical lattices, or short lifetimes in Rydberg atoms, we expect

our proposal to be achievable in the long run.

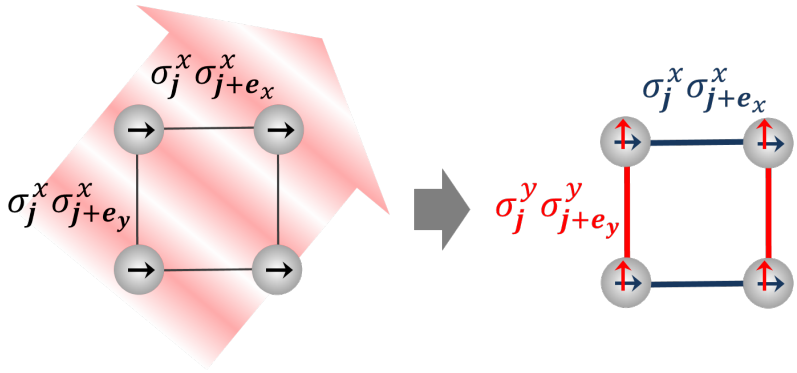

Figure 8.1: General scheme: Our model assumes an initial quantum Ising lattice as a starting point. Periodic drivings with a site-dependent phase allow us to dress the original Ising interaction to obtain the quantum compass model, in which sites interact through spin-components depending on the orientation of the bond.

This article is organized as follows. In section 8.3 we review some general symmetry properties of the quantum compass model that will be necessary to understand the adiabatic preparation of the ground state. In Sec. 8.4 the photon-assisted tunneling scheme is applied to engineer the quantum compass model using a 2D Ising model together with a convenient periodic driving. In Sec. 8.5 we discuss an adiabatic preparation of the ground state of this model; the corresponding implementation of this procedure using ultracold atoms or Rydberg atoms in optical lattices is presented in Sec. 8.6. Finally, Sec. 8.7 summarizes the main results obtained in this work.

8.3 Symmetry properties of the compass model

Let us now look over the main symmetry properties of the quantum compass model that we shall use throughout this work [101]. Generally speaking, a symmetry operation represented by certain operator P commuting with the Hamiltonian H may lead to the presence of degenerate states. This means that P acting on a state $|\psi\rangle$ results in another state $|\varphi\rangle$ with the same energy, although this argument fails in the case we get the same state, $|\psi\rangle = |\varphi\rangle$. Nonetheless, if we find another symmetry operation Q such that $[P, Q] \neq 0$ for any state $|\psi\rangle$, one can be sure that all states are at least doubly degenerate. To see how this works, let us suppose that acting

on the state $|\psi\rangle$ with P and Q we obtain the same state $|\psi\rangle$. This implies that $PQ|\psi\rangle = QP|\psi\rangle = |\psi\rangle$, hence $[P, Q] = 0$, which is contrary to our initial statement. We have therefore proved that the resulting states are necessarily different. Leaving aside accidental degeneracy, another condition must be imposed if we wish to get doubly degenerate states avoiding further degeneracy. This condition turns out to be $[P^2, Q] = [P, Q^2] = 0$ [101]. The reason for this is that if one starts with an eigenstate of $Q(P)$ and then acting on it with $P(Q)$, the resulting state has to be different from the original one as we just proved, but acting again on this state with $P(Q)$, one should come back to the initial state. Having two sets of non-commuting operators $\{P_i\}$ and $\{Q_j\}$, the previous conditions are generalized as $[P_i, Q_j] \neq 0$ $\forall i, j$ and $[P_i P_j, Q_k] = [P_i, Q_j Q_k] = 0$ $\forall i, j, k$ [101].

The Hamiltonian (8.1) has two sets of discrete symmetries satisfying the above conditions, namely

$$P_{j_y} = \prod_{j_x}^{n} \sigma^y_{(j_x, j_y)} \quad j_y = 1, 2, \ldots, m \tag{8.2}$$

$$Q_{j_x} = \prod_{j_y}^{m} \sigma^x_{(j_x, j_y)} \quad j_x = 1, 2, \ldots, n \tag{8.3}$$

i.e, each P_{j_y} is the row product of σ^y in that row while Q_{j_x} is the column product of σ^x in the column. Physically, Q_{j_x} corresponds to a rotation by an angle π around the x axis of all the spins of the column labeled by j_x, while P_{j_y} corresponds to a rotation by an angle π around the y axis of all the spins of the row labeled by j_y. In particular, they satisfy $\{P_{j_y}, Q_{j_x}\} = 0$ $\forall j_x, j_y$ and $[P_i P_j, Q_k] = [P_i, Q_j Q_k] = 0$ $\forall i, j, k$. Thus, aside from accidental degeneracies, one expects every state to be doubly and only doubly degenerate. We shall then assume that the ground state of the quantum compass model is effectively a two level system satisfying the conditions of a protected qubit. Local noise acting on a single lattice site may not commute with the symmetry operators P_{j_y} and Q_{j_x} corresponding to the row and column of such site, but the remaining symmetries ensures the system to remain doubly degenerate. This is the case unless at least $\min(m, n)$ of these perturbations act simultaneously over the whole lattice. While the presence of degeneracy is not a sign of topological order, the robustness against local perturbations is a clear signature of the topological nature of the compass model.

The set of integrals of motion P_{j_y} (or alternatively Q_{j_x}) can be used to distin-

guish between the two degenerate states of the ground state since they have different quantum numbers, namely either $(p_1, \ldots, p_m) = (1, \ldots, 1)$ or $(p_1, \ldots, p_m) = (-1, \ldots, -1)$. This result was proved in Ref. [122] for a square lattice, and it can be straightforwardly generalized for a rectangular lattice. Heuristically, one may expect this result by exploring the trivial case for which $J_x = 0$. In such a case the model is simplified to a set of Ising columns with ferromagnetic coupling. For simplicity, taking the square lattice lxl, the ground state consists of 2^l states defined by $m_{j_y,1} = \ldots = m_{j_y,l} = \pm 1$ with $j_y = 1, \ldots, l$, where $m_{\boldsymbol{j}}$ is the eigenvalue of $\sigma^y_{\boldsymbol{j}}$. As all the rows are identical, all the $p'_{j_y}s$ are equal as well for all j_y, thus we conclude the value of p_{j_y} is either $+1$ or -1 for every row.

The non-local operators P_{j_y} and Q_{j_x} represent a sufficient condition for topological quantum order in this model [73]. Effectively, unlike Landau type systems, no local operator can be found to distinguish between the ground states in the quantum compass model. In comparison, in a Landau type system like the Ising model (8.4), the local spin operator σ^z_j may distinguish between the two possible Ising ground states. Physically this corresponds to the fact that there is no way to differentiate the states by means of local measurements, and the nontrivial information of the state is revealed when performing an adequate non-local measurement. In our case, notice that such non-local measurement can be performed after measuring each σ^y_j (or σ^x_j) sequentially, and then compose the information obtained to calculate the observable P_{j_y} (or Q_{j_x}).

Mathematically this is represented by a d-dimensional Gauge-like symmetry operation localized on a d-dimensional region of the complete D-dimensional lattice ($d \leq D$). A local Gauge symmetry corresponds to $d = 0$ whereas a global symmetry operation is given when $d = D$. A group symmetry operator U can be expressed in terms of unitary operators in the way of an Aharonov-Bohm phase or a Wilson loop. In the case of the quantum compass model ($D = 2$), U can be written as $U = \prod_{j \in l_\alpha} \sigma^\alpha_j$ for $\alpha = x, y$, where l_α denotes any line orthogonal to the $\boldsymbol{e}_\alpha$ axis.

Notice that our previous definitions of P_{j_y} and Q_{j_x} are recovered when substituting $\alpha = y$ and x respectively. Thus, these operators are defined along cycles on a torus when we assume periodic boundary conditions, constituting $d = 1$ symmetries. No change in the degeneracy of the ground state is expected when changing between

open and periodic boundary conditions as the construction of these symmetry operators is identical in both cases. Therefore, we suggest that the target observables to demonstrate the topological order in this system may be the operators P_{j_y} and Q_{j_x} and their resilience.

8.4 Photon-assisted tunneling

In this section we shall use the photon-assisted tunneling toolbox [85] to implement the quantum compass model. To understand how to achieve this goal, let us first have a look at the quantum Ising model,

$$H_0 = -J_x \sum_{\boldsymbol{j}} \sigma^x_{\boldsymbol{j}} \sigma^x_{\boldsymbol{j}+\boldsymbol{e}_x} - J_y \sum_{\boldsymbol{j}} \sigma^x_{\boldsymbol{j}} \sigma^x_{\boldsymbol{j}+\boldsymbol{e}_y}. \tag{8.4}$$

Expressing the spin operators in terms of the raising and lowering operators, i.e. $\sigma^x = (\sigma^+ + \sigma^-)$ and $\sigma^y = -i(\sigma^+ - \sigma^-)$, equation (8.4) turns out to be,

$$H_0 = -J_x \sum_{\boldsymbol{j}} \left(\sigma^+_{\boldsymbol{j}} \sigma^+_{\boldsymbol{j}+\boldsymbol{e}_x} + \sigma^+_{\boldsymbol{j}} \sigma^-_{\boldsymbol{j}+\boldsymbol{e}_x}\right) - J_y \sum_{\boldsymbol{j}} \left(\sigma^+_{\boldsymbol{j}} \sigma^+_{\boldsymbol{j}+\boldsymbol{e}_y} + \sigma^+_{\boldsymbol{j}} \sigma^-_{\boldsymbol{j}+\boldsymbol{e}_y}\right) + \text{H.c.} \tag{8.5}$$

In contrast, rewriting the quantum compass model (8.1) in a similar way, we obtain a slightly different expression

$$H_C = -\sum_{\boldsymbol{j}} \left(J_x^{++} \sigma^+_{\boldsymbol{j}} \sigma^+_{\boldsymbol{j}+\boldsymbol{e}_x} + J_x^{+-} \sigma^+_{\boldsymbol{j}} \sigma^-_{\boldsymbol{j}+\boldsymbol{e}_x}\right) - \sum_{\boldsymbol{j}} \left(-J_y^{++} \sigma^+_{\boldsymbol{j}} \sigma^+_{\boldsymbol{j}+\boldsymbol{e}_y} + J_y^{+-} \sigma^+_{\boldsymbol{j}} \sigma^-_{\boldsymbol{j}+\boldsymbol{e}_y}\right) + \text{H.c.}, \tag{8.6}$$

where we have defined $J^{++}_{x,y} = J^{+-}_{x,y} = J_{x,y}$. By the use of the photon assisted tunneling in the original Hamiltonian (8.4), we aim for finding a set of effective coupling constants such that equation (8.5) equals equation (8.6), which in turn implies

$$\begin{aligned} (J_x^{++})_{\text{eff}} &= (J_x^{+-})_{\text{eff}}, \\ (J_y^{++})_{\text{eff}} &= -(J_y^{+-})_{\text{eff}}. \end{aligned} \tag{8.7}$$

Now that our goal is clear, let us use the ingredients of the photon-assisted tunneling toolbox to find how to satisfy the conditions (8.7). In doing so, the Hamiltonian of the system can be written as,

$$H = H_0 + H_d(\tau), \tag{8.8}$$

where we define,

$$H_{\rm d}(\tau) = \sum_{\boldsymbol{j}} \frac{\Omega_{\boldsymbol{j}}}{2}\sigma^z_{\boldsymbol{j}} + \sum_{\boldsymbol{j}} \frac{\eta}{2}\omega_d \cos(\omega_{\rm d}\tau + \phi_{\boldsymbol{j}})\sigma^z_{\boldsymbol{j}}. \tag{8.9}$$

The second term in (8.9) represents a periodic energy driving of the qubit, while $\Omega_{\boldsymbol{j}}$ is typically chosen such that the first term in equation (8.9) represents a gradient of the individual frequencies [84], i.e., $\Omega_j = \Omega_0 + \Delta\Omega \cdot j$, although it will be taken as a constant for the purpose of this work, $\Omega_{\boldsymbol{j}} = \Omega$. These two elements are all that we need to take advantage of the photon-assisted tunneling toolbox [85]. Notice that there is a freedom in choosing the spatial dependence in $\phi_{\boldsymbol{j}}$, and we shall assume a linear dependence in both x and y axis,

$$\phi_{\boldsymbol{j}} = \Delta\phi_x j_x + \Delta\phi_y j_y, \tag{8.10}$$

where $\Delta\phi_{x,y}$ are given constants, and $j_{x,y}$ are positions in the lattice.

Let us now express the Hamiltonian H_0 in the interaction picture with respect to H_d, namely $H_0(t) = U(t)^\dagger H_0 U(t)$ where $U(t) = e^{-i\int_0^t d\tau H_d(\tau)}$. In this picture, the raising and lowering operators evolve like,

$$\sigma^\pm_{\boldsymbol{j}}(t) = e^{\pm i\Omega t} e^{\pm i\eta \sin(\omega_{\rm d}t + \phi_{\boldsymbol{j}})} e^{\mp i\eta \sin\phi_{\boldsymbol{j}}} \sigma^\pm_{\boldsymbol{j}}. \tag{8.11}$$

Notice that the last term in equation (8.11) can be gauged away using the unitary transformation $\sigma^\pm_{\boldsymbol{j}} \to e^{\pm i\eta\sin\phi_{\boldsymbol{j}}}\sigma^\pm_{\boldsymbol{j}}$. Hence one obtains a Hamiltonian having the same structure as equation (8.6), in which we replace the bare couplings by their corresponding time-dependent dressed couplings

$$(J^{++}_{x,y})_{\rm eff} = J_{x,y} e^{i2\Omega\tau} e^{i\eta\sin(\omega_d\tau+\phi_{\boldsymbol{j}})} e^{i\eta\sin(\omega_d\tau+\phi_{\boldsymbol{j}+\boldsymbol{e}_{x,y}})}, \tag{8.12}$$

$$(J^{+-}_{x,y})_{\rm eff} = J_{x,y} e^{i\eta\sin(\omega_d\tau+\phi_{\boldsymbol{j}})} e^{-i\eta\sin(\omega_d\tau+\phi_{\boldsymbol{j}+\boldsymbol{e}_{x,y}})}. \tag{8.13}$$

To help in the analytical treatment, we make use of the trigonometric relation $\sin(A)+\sin(B) = 2\sin(\frac{A+B}{2})\cos(\frac{A-B}{2})$ and the Jacobi-Anger expansion,

$$e^{(iz\sin\phi)} = \sum_{n=-\infty}^{\infty} \mathcal{J}_n(z) e^{(in\phi)}, \tag{8.14}$$

where $\mathcal{J}_n$ are Bessel functions of the first kind, yielding

$$(J^{++}_{x,y})_{\rm eff} = J_{x,y} e^{i2\Omega\tau} \sum_s \mathcal{J}_s\left(2\eta\cos\frac{\Delta\phi_{x,y}}{2}\right) e^{is(\omega_d\tau + \frac{\phi_{\boldsymbol{j}}+\phi_{\boldsymbol{j}+\boldsymbol{e}_{x,y}}}{2})}, \tag{8.15}$$

$$(J^{+-}_{x,y})_{\rm eff} = J_{x,y} \sum_s i^s \mathcal{J}_s\left(2\eta\sin\frac{\Delta\phi_{x,y}}{2}\right) e^{is(\omega_d\tau + \frac{\phi_{\boldsymbol{j}}+\phi_{\boldsymbol{j}+\boldsymbol{e}_{x,y}}}{2})}. \tag{8.16}$$

Assuming $J_{x,y} \ll \Omega$ and tuning the driving frequency to $\omega_d = 2\Omega$, the rotating-wave approximation (RWA) allows us to neglect the fast-oscillating terms and to keep those terms fulfilling the resonance condition $s = -1$ in equation (8.15) and $s = 0$ in equation (8.16). Having done this, we obtain the following dressed couplings,

$$(J^{++}_{x,y})_{\text{eff}} = J_{x,y}\mathcal{F}^{++}_{x,y}(\eta, \Delta\phi_{x,y})e^{-i\left(\frac{\phi_{\boldsymbol{j}}+\phi_{\boldsymbol{j}+\boldsymbol{e}_{x,y}}}{2}\right)} \tag{8.17}$$

$$(J^{+-}_{x,y})_{\text{eff}} = J_{x,y}\mathcal{F}^{+-}_{x,y}(\eta, \Delta\phi_{x,y}), \tag{8.18}$$

where we define a set of complex amplitudes,

$$\mathcal{F}^{++}_{x,y}(\eta, \Delta\phi_{x,y}) = \mathcal{J}_{-1}\left(2\eta\cos\frac{\Delta\phi_{x,y}}{2}\right) \tag{8.19}$$

$$\mathcal{F}^{+-}_{x,y}(\eta, \Delta\phi_{x,y}) = \mathcal{J}_{0}\left(2\eta\sin\frac{\Delta\phi_{x,y}}{2}\right). \tag{8.20}$$

Finally, rewriting the term $\frac{\phi_{\boldsymbol{j}}+\phi_{\boldsymbol{j}+\boldsymbol{e}_{x,y}}}{2} = \phi_{\boldsymbol{j}} + \frac{\Delta\phi_{x,y}}{2}$ we may use the following unitary transformation: $\sigma^{+}_{\boldsymbol{j}} \longmapsto \sigma^{+}_{\boldsymbol{j}}e^{i\phi_{\boldsymbol{j}}/2}$, resulting in the effective Hamiltonian we were looking for,

$$\begin{aligned} H_{\text{eff}} = -J_x\sum_{\boldsymbol{j}}\left(\mathcal{F}^{++}_{x}\sigma^{+}_{\boldsymbol{j}}\sigma^{+}_{\boldsymbol{j}+\boldsymbol{e}_x} + \mathcal{F}^{+-}_{x}\sigma^{+}_{\boldsymbol{j}}\sigma^{-}_{\boldsymbol{j}+\boldsymbol{e}_x}\right) \\ - J_y\sum_{\boldsymbol{j}}\left(\mathcal{F}^{++}_{y}\sigma^{+}_{\boldsymbol{j}}\sigma^{+}_{\boldsymbol{j}+\boldsymbol{e}_y} + \mathcal{F}^{+-}_{y}\sigma^{+}_{\boldsymbol{j}}\sigma^{-}_{\boldsymbol{j}+\boldsymbol{e}_y}\right) + \text{H.c.} \end{aligned} \tag{8.21}$$

Following the idea given in equation (8.7), we notice that the quantum compass model can be implemented if we manage to find a set of parameters, $(\eta, \Delta\phi_x, \Delta\phi_y)$, such that

$$\begin{aligned} \mathcal{F}^{++}_{x}(\eta, \Delta\phi_x) &= \mathcal{F}^{+-}_{x}(\eta, \Delta\phi_x,), \\ \mathcal{F}^{++}_{y}(\eta, \Delta\phi_y) &= -\mathcal{F}^{+-}_{y}(\eta, \Delta\phi_y). \end{aligned} \tag{8.22}$$

Is there any solution to the system of equations (8.22)? We will show numerically that there are actually an infinite number of solutions. First, note that equation (8.22) can be expressed as,

$$\left|\mathcal{F}^{++}_{x,y}(\eta, \Delta\phi_{x,y})\right| = \left|\mathcal{F}^{+-}_{x,y}(\eta, \Delta\phi_{x,y})\right|, \tag{8.23}$$

$$\arg(\mathcal{F}^{++}_{x}(\eta, \Delta\phi_x)) = \arg(\mathcal{F}^{+-}_{x}(\eta, \Delta\phi_x)) + 2k\pi, \tag{8.24}$$

$$\arg(\mathcal{F}^{++}_{y}(\eta, \Delta\phi_y)) = \arg(\mathcal{F}^{+-}_{y}(\eta, \Delta\phi_y)) + k\pi, \tag{8.25}$$

where k is an integer. To solve this system of equations, let us define the functions $f(\eta, \Delta\phi_{x,y}) = \left|\mathcal{F}^{++}_{x,y}(\eta, \Delta\phi_x)\right| / \left|\mathcal{F}^{+-}_{x,y}(\eta, \Delta\phi_{x,y})\right| - 1$ and $g(\eta, \Delta\phi_{x,y}) = \arg(\mathcal{F}^{++}_{x,y}(\eta, \Delta\phi_y)) - \arg(\mathcal{F}^{+-}_{x,y}(\eta, \Delta\phi_y))$. Trivially, we see that equation (8.23) is equivalent to find the zeros of the function f, while the solutions to equation (8.24) and equation (8.25) are equivalent to the function g taking the values $2k\pi$ and $k\pi$ respectively. The jellyfish-like pattern showed in figure 8.2(a) represents the function f, for which we have limited the range of the function to the interval $[-0.1, 0.1]$ so that the graph clearly shows the region in which the function becomes zero. On the other hand, the function g is shown in Fig. 8.2(b), limited to the range $[0, 2\pi]$. In looking at the graphs, it is straightforward to confirm that there are an infinite number of solutions. The isotropic point, $(J_x = J_y)$ is reached when the solutions are taken symmetrically with respect to the symmetry axis of the jellyfish-like pattern; an example could be $\{\eta = 1, \Delta\phi_x = 4.6539, \Delta\phi_y = 1.6293\}$, which gives the value $\mathcal{F}^{++}_x = \mathcal{F}^{+-}_y = 0.5368$.

In the following, we discuss the effect of possible fluctuations/inaccuracies in $(\eta, \Delta\phi_{x,y})$. In looking at Fig. 8.2, it is clear that the condition over the phase, given by the function $g(\eta, \Delta\phi_{x,y})$, remains generally stable when considering small deviations with respect to the exact solutions. In contrast, the main source of error would be caused by the condition over the amplitude (8.23), especially in the case $f(\eta, \Delta\phi_{x,y})$ could vary rapidly close to the compass solutions. One can estimate this error by assuming a linear approximation around the optimal solutions, $(\eta^*, \Delta\phi^*_{x,y})$, as

$$\Delta f(\eta, \Delta\phi_{x,y}) = \eta^*(\Delta\eta/\eta^*)\partial_\eta f + \Delta\phi^*_{x,y}(\Delta(\Delta\phi_{x,y})/\Delta\phi^*_{x,y})\partial_{\Delta\phi} f. \tag{8.26}$$

The previous derivatives can be computed and expressed in terms of Bessel functions. For example, using the above values and nearby solutions, we find that the order of magnitude of the error in Δf is 10^{-2} or even 10^{-3} when 1% of relative error is assumed for both η and $\Delta\phi_{x,y}$. This represents a small perturbation to the compass model that in principle should not spoil the quantum simulation. Nonetheless, there are some regions which are more sensitive to small perturbations, namely those close to the singular points observed in the jellyfish pattern 8.2(a). Those points correspond to singular solutions where the function f goes to infinity (which is the reason why the function is shown in a limited range). Although theoretically pos-

sible, these regions would not be appropriate for a realistic experiment. Depending of the main source of error in an experimental setup, one could choose a particular solution that minimizes the error in Δf. Typically, it is more difficult to control the $\Delta\phi_{x,y}$ parameter, in which case solutions with, for instance $\eta \approx 0.95$, would improve the error in $\Delta\phi_{x,y}$ as there exist solutions in the $\Delta\phi$ direction as shown Fig. 8.2(a).

8.5 Adiabatic passage

Now that we have shown how the quantum compass model can be implemented using periodic drivings, we aim for preparing the ground state of this model. One way to do so is by finding an adequate adiabatic passage starting from the ground state of certain initial Hamiltonian for which the ground state is known and can be prepared, and then slowly changing this Hamiltonian until the quantum compass model is eventually reached. One possible option using a transverse magnetic field will be discussed in this section.

Let us then consider an additional transverse magnetic field along z in our original Hamiltonian (8.8) as follows,

$$H = H_0 + H_d(\tau) + \sum_{\boldsymbol{j}} \frac{\delta(t)}{2}\sigma^z_{\boldsymbol{j}}, \tag{8.27}$$

where δ is a time-dependent parameter that measures the strength of the field. Notice that we had already introduced a transverse field along z in equation (8.8), so the overall transverse field depends on the sum of both terms, $\epsilon/2 = (\Omega + \delta)/2$. One may also express $H_0 + \sum_{\boldsymbol{j}} \delta\sigma^z_{\boldsymbol{j}}$ in the interaction picture with respect H_d; it is then straightforward to check that, following the same procedure used in Sec. 8.4 and setting the same resonance condition $\omega_d = 2\Omega$, we arrive at the following effective Hamiltonian,

$$H'_{\text{eff}}(t) = H_{\text{eff}} + \sum_{\boldsymbol{j}} \frac{\delta(t)}{2}\sigma^z_{\boldsymbol{j}}, \tag{8.28}$$

where H_{eff} was given in equation (8.21). Therefore, ensuring the magnetic field is strong enough so that $\delta \gg \Omega, \eta \gg J_x, J_y$, one can safely assume that the magnetic field is the dominant term in (8.28), being the ground state $|0\rangle = \prod_{\boldsymbol{j}} |\uparrow\rangle_{\boldsymbol{j}}$ in terms of eigenstates of $\sigma^z_{\boldsymbol{j}}$. Finally, a feasible adiabatic passage to reach the compass model consists of decreasing ϵ from $\epsilon \gg \Omega, \eta$ slowly enough until reaching the compass

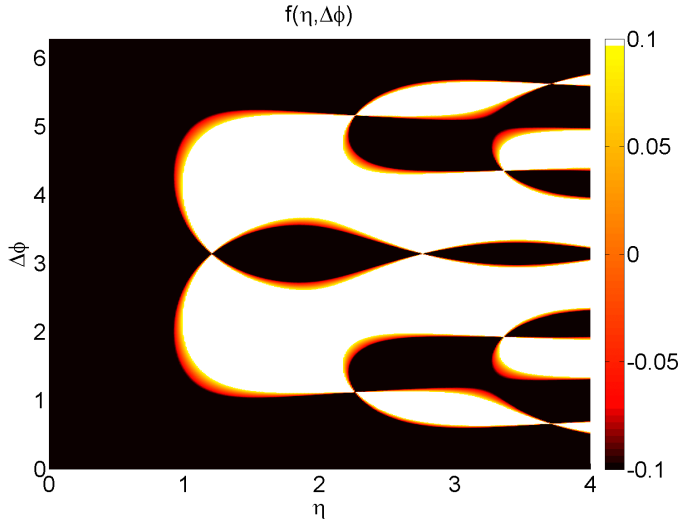

(a)

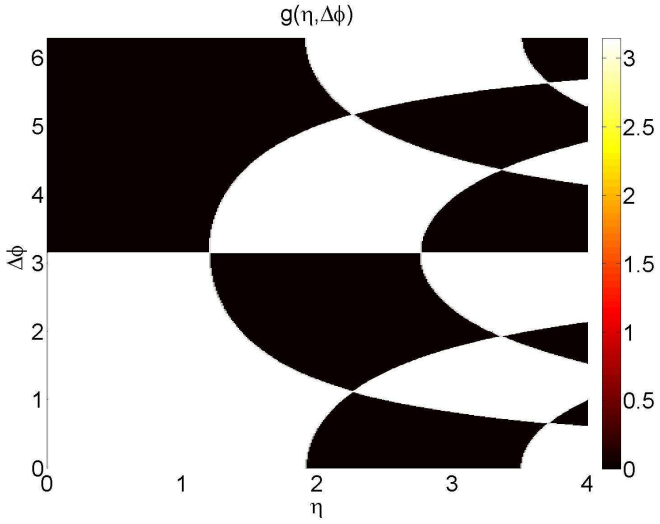

(b)

Figure 8.2: In this figure we plot the functions that govern the spin-spin interactions as a function of the periodic driving parameters. **(a)** Function $f(\eta, \Delta\phi_{x,y}) = \left|\mathcal{F}^{++}_{x,y}(\eta, \Delta\phi_x)\right| / \left|\mathcal{F}^{+-}_{x,y}(\eta, \Delta\phi_{x,y})\right| - 1$. The values $f(\eta, \Delta\phi_{x,y}) = 0$ represents the solutions to equation (8.23). The range of the function is limited to the interval $[-0.1, 0.1]$ to show clearly the points at which the function is zero. **(b)** Function $g(\eta, \Delta\phi_{x,y}) = \arg(\mathcal{F}^{++}_{x,y}(\eta, \Delta\phi_y)) - \arg(\mathcal{F}^{+-}_{x,y}(\eta, \Delta\phi_y))$, limited to the range $[0, 2\pi]$. The regions with $g(\eta, \Delta\phi_{x,y}) = 0$ and π correspond to the solutions to equation (8.24) and equation (8.25) respectively.

condition $\epsilon = \Omega = \omega_d/2$ ($\delta = 0$). One expects this system to undergo a quantum phase transition as the magnetic order of the transverse magnetic field and the quantum compass model are different.

The adiabatic approximation describes, upon certain conditions, how slowly we need to vary $\delta(t)$ to ensure the system remains in the ground state through the evolution. According to this approximation, the instantaneous eigenstates of the time-dependent Hamiltonian $H(t)$ at a given time evolve continuously to the corresponding eigenstates at later times, provided that the eigenenergies do not cross and the evolution is slow enough. The intrinsic time scale used to determine what slow and fast mean is usually provided by the gaps in the spectrum. This also provides a general validity condition for adiabatic behavior that corresponds to the probability that the final state of the system is different from the initial state [123],

$$\max_{0\leq t\leq T}\left|\frac{\langle k|\dot{H}(t)|n\rangle}{\Delta_{nk}}\right| << \min_{0\leq t\leq T}|\Delta_{nk}| \tag{8.29}$$

where T is the total evolution time, and Δ_{nk} the energy gap between level n and k. Note that the ground state of the transverse field Hamiltonian is unique, while the compass ground state is doubly-degenerate, thus we expect crossing of levels at the end of the adiabatic preparation; moreover, the natural question arises about what state is eventually reached.

A simple possible way to overcome the issues above is by finding an integral of motion conserved through the evolution that we may use to tell the twofold ground state apart. Under this assumption, the adiabatic approximation would still be valid if there is no crossing of levels with the same conserved quantum number. As it was shown above, the set of integrals of motion $P_{j_y}(Q_{j_x})$ can be used to distinguish between the two degenerate states, since they have different quantum numbers, namely either $(p_1,\ldots,p_M) = (1,\ldots,1)$ or $(p_1,\ldots,p_M) = (-1,\ldots,-1)$ (similarly for the quantum numbers $(q_1,\ldots,q_N)$) ; however these are not good quantum numbers when the magnetic field term is included in the Hamiltonian. The operator $Z \equiv \prod_{\boldsymbol{j}} \sigma^z_{\boldsymbol{j}}$ is fortunately an integral of motion of the whole Hamiltonian (8.28) as it is straightforward to check, and so it can be used in principle to determine the actual ground state reached at the end of the adiabatic passage. Surprisingly, the parity operator Z can distinguish between the twofold ground state only in those cases such that we have an odd-odd or odd-even lattice size. In Appendix I, it is proved that for

both odd-odd and odd-even cases the eigenvalues of Z are either $z = +1$ or $z = -1$, while in the even-even case the eigenvalue is always $z = +1$. This is another sign of the topological order appearing in the compass model. Hence we expect two different kinds of behaviour in the adiabatic passage depending on the parity of the lattice size. In the first case, the two ground states of the compass model are not connected, thereby the only relevant gap to be considered is between the ground and first even excited state. Recall that the ground state of the transverse field Hamiltonian has eigenvalue $z = +1$, so we expect to prepare the ground state of the compass model corresponding to this eigenvalue; however we would be unable to prepare the ground state corresponding to the eigenvalue $z = -1$ using this approach. In the second case, with an even-even lattice size, any superposition of the ground states are eigenstates of the operator Z with eigenvalue $z = +1$, and for that reason, in this case we could only assume that the final state is a superposition state given by the specific adiabatic evolution performed on the system. The adiabaticity of this case would be given by the gap between the first and and second even excited states.

Exact diagonalizations for small systems (up to a 5×4 lattice) were performed to observe the evolution of the relevant gaps involved in the quantum phase transition so as to examine the validity of the adiabatic approximation. Additionally, the magnetization along z was found to be an order parameter of the quantum phase transition, where the ground state of the transverse magnetic field is magnetically ordered, $M_z \neq 0$, and the compass ground state is disordered, $M_z = 0$. In order to simplify the analysis, the following parametrization was introduced,

$$\begin{aligned} H &= (1-\lambda)H_C + \lambda H_m \\ H_C &= -\sum_{\boldsymbol{j}} \sigma^x_{\boldsymbol{j}} \sigma^x_{\boldsymbol{j}+\boldsymbol{e}_x} - \sum_{\boldsymbol{j}} \sigma^y_{\boldsymbol{j}} \sigma^y_{\boldsymbol{j}+\boldsymbol{e}_y} \\ H_m &= \sum_{\boldsymbol{j}} \sigma^z_{\boldsymbol{j}}, \end{aligned} \tag{8.30}$$

therefore $\lambda = 1$ corresponds to the initial transverse field and $\lambda = 0$ represents the isotropic quantum compass model. Recall that no periodic boundary conditions are assumed here so as to better describe a realistic experimental setup.

Keeping in mind the results for the integral of motion Z, the relevant gap in an odd-odd and odd-even lattice is the one given by the first even excited state of the system, Δ. In contrast, this gap goes to zero in an even-even lattice, so the relevant

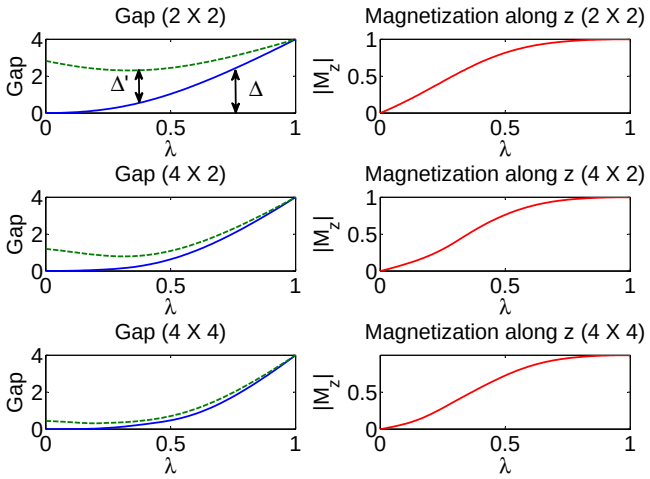

Figure 8.3: Quantum phase transition from transverse field to compass model for an even-even lattice size. We show the gaps together with the absolute value of the normalized magnetization along z of the model (8.30) for different values of the lattice size. The solid and dashed lines corresponds, respectively, to the gap between the first and second even excited states with respect to the ground state. The value $\lambda = 1$ corresponds to the initial transverse field Hamiltonian and $\lambda = 0$ represents the isotropic quantum compass model.

gap in this case, Δ', is given by the energy difference with the second even excited state. Note that those levels with odd parity ($z = -1$) do not play any role in any case as the Hamiltonian does not connect states with different parities. Fig. 8.3 shows the evolution of these gaps for different sizes together with the magnetization $|M_z|$ as the parameter λ changes from $\lambda = 1$ to $\lambda = 0$. For the odd-odd and odd-even cases we confirm that there exists a finite gap along the adiabatic passage between the ground state and the first even excited state that narrows as the lattice size becomes larger. As expected, this gap goes to zero in the even-even case when the two degenerate even ground states collide in the compass model as shown in Fig. 8.4. Therefore, the relevant gap when we approach $\lambda = 0$ is given by the energy difference between the first and second even excited states Δ'. In conclusion, these results show that the even ground state of the compass model can be prepared using this adiabatic passage in the odd-odd and odd-even cases , whereas for the even-even case we expect the system to be in a superposition of the ground states given by the

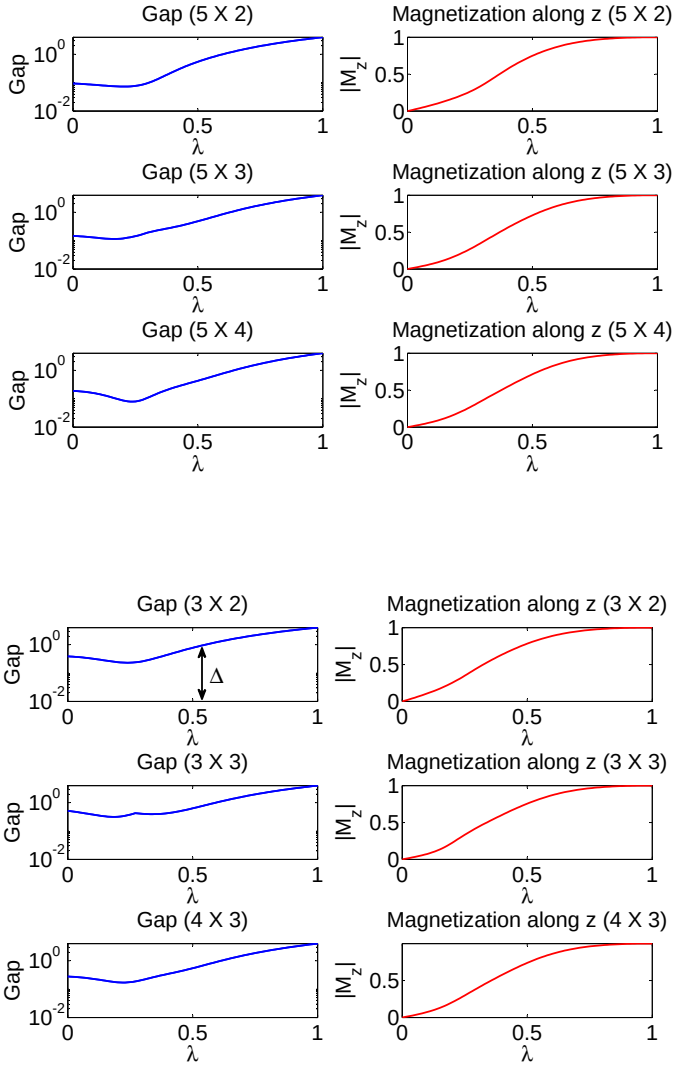

Figure 8.4: Quantum phase transition from transverse field to compass model for an odd-even/odd-odd lattice size. We show the gaps together with the absolute value of the normalized magnetization along z of the model (8.30) for different values of the lattice size. The gaps are represented in a semi-log plot. The value $\lambda = 1$ corresponds to the initial transverse field Hamiltonian and $\lambda = 0$ represents the isotropic quantum compass model.

specific evolution of $\delta(t)$.

Lastly, given the energy gaps shown in figures (8.3, 8.4), one may estimate the condition under which the adiabaticity is fulfilled using equation (8.29). For simplicity, we shall assume a linear evolution in time, $\delta(t) = \delta_0(1 - t/\tau_{ev})$, where τ_{ev} is the total evolution time. In such a case, the matrix elements we need to calculate

are of the form $\langle k|\sum\sigma_j^z|n\rangle$. As a crude estimation, these matrix elements are of the order of the number of sites N at worst. Furthermore, to maximize the first term in (8.29), we could use the gap at $\lambda = 0$ as this is a good estimation of the minimum gap. Thus, a rough condition for adiabaticity would be given by,

$$\frac{N\delta_0}{\Delta_{\lambda=0}} \ll \tau_{ev}\Delta_{\lambda=0}. \tag{8.31}$$

8.6 Physical implementations

In this section we show how our ideas can be implemented using specific atomic experimental setups. One possible implementation of the quantum compass model using Josephson junctions arrays was proposed by Douçot.et.al [101]. A close related model was actually implemented in a proof-of-principle experiment using superconducting nanocircuits.

A scalable and efficient implementation of the quantum compass model in atomic experimental setups would be very useful as atomic systems present many advantages for quantum state preparation and measurement. Furthermore, implementing a controllable longitudinal magnetic field like in equation (8.29) may allow experimentalist to adiabatically create the topologically degenerate ground state. Periodic drivings like those required for our proposal can be implemented in atomic systems by means of lasers, with a site dependent phase that corresponds to the laser optical phase. Ions trapped in two-dimensional arrays of microtraps or Coulomb crystals could be considered here, because optical forces can be used to induce Ising interactions [82, 87]. However, the dipolar decay of trapped ion spin-spin interactions would lead to long-range quantum compass models, with properties that may depart from the original Hamiltonian (8.1).

In the following we focus on proposals for atomic setups that may provide us with short-range Ising interactions, namely, neutral bosonic ultracold atoms and Rydberg atoms in optical lattices.

8.6.1 Ultracold bosons in optical lattices

We need first to understand how the following effective quantum Ising Hamiltonian can be implemented with ultracold bosons. For this we rely on a quantum simulation

proposal which relies on the internal state of atoms that are frozen in a Mott insulator state in an optical lattice [92, 106]. Under appropriate circumstances, hopping can only be a virtual process that enables superexchange interactions, as explained in [92] through perturbative calculations. These interactions have been demonstrated experimentally, both in superlattices [124, 125], as well as in longer tubes with a few quasiparticle excitations [126].

We consider an optical lattice in the Mott-insulator regime with one atom per site (unity filling) and each atom having two accessible internal states, playing the role of a pseudo-spin $S = 1/2$. The atoms may be formally identified with two types of bosons, '$\uparrow$', and '$\downarrow$', and one may denote the bosonic operators $a_{\boldsymbol{i}}$ and $b_{\boldsymbol{i}}$ as the destruction operators of each internal state at the site $\boldsymbol{i}$. Such a system is well described with the Bose-Hubbard Hamiltonian when the energies involved are small enough so that the second Bloch band never gets populated,

$$\begin{aligned} H &= \sum_{\langle \boldsymbol{i},\boldsymbol{j}\rangle} H^{\rm hop}_{\boldsymbol{i},\boldsymbol{j}} + \sum_{\boldsymbol{j}} H^{\rm int}_{\boldsymbol{j}} \qquad (8.32)\\ H^{\rm hop}_{\boldsymbol{i},\boldsymbol{j}} &= -J_a(a^\dagger_{\boldsymbol{i}} a_{\boldsymbol{j}} + h.c.) + J_b(b^\dagger_{\boldsymbol{i}} b_{\boldsymbol{j}} + h.c.)\\ H^{\rm int}_{\boldsymbol{j}} &= \frac{1}{2}U_{aa} a^\dagger_{\boldsymbol{j}} a^\dagger_{\boldsymbol{j}} a_{\boldsymbol{j}} a_{\boldsymbol{j}} + \frac{1}{2}U_{bb} b^\dagger_{\boldsymbol{j}} b^\dagger_{\boldsymbol{j}} b_{\boldsymbol{j}} b_{\boldsymbol{j}} + U_{ab} a^\dagger_{\boldsymbol{j}} b^\dagger_{\boldsymbol{j}} b_{\boldsymbol{j}} a_{\boldsymbol{j}}, \end{aligned}$$

The Hamiltonians $H^{\rm hop}$ and $H^{\rm int}$ represent, respectively, the probability of atoms hopping to neighbouring sites and their effective on-site interaction. Assuming we are in the Mott-insulator regime, $J \ll U$, the hopping Hamiltonian can be considered as a small perturbation with respect to all other terms. We project our problem into the subspace of single atomic occupation and use quasi-degenerate second-order perturbation theory to obtain an effective spin Hamiltonian. The corresponding operators of the effective spin system are $\sigma^+_{\boldsymbol{j}} = a^\dagger_{\boldsymbol{j}} b_{\boldsymbol{j}}$, $\sigma^-_{\boldsymbol{j}} = a_{\boldsymbol{j}} b^\dagger_{\boldsymbol{j}}$ and $\sigma^z_{\boldsymbol{j}} = a^\dagger_{\boldsymbol{j}} a_{\boldsymbol{j}} - b^\dagger_{\boldsymbol{j}} b_{\boldsymbol{j}}$. The effective spin Hamiltonian reads

$$H_{\rm S} = \sum_{\langle \boldsymbol{i},\boldsymbol{j}\rangle} \left(\lambda^z \sigma^z_{\boldsymbol{i}} \sigma^z_{\boldsymbol{j}} + \lambda^\perp (\sigma^x_{\boldsymbol{i}} \sigma^x_{\boldsymbol{j}} + \sigma^y_{\boldsymbol{i}} \sigma^y_{\boldsymbol{j}})\right) + \sum_{\boldsymbol{i}} h^z \sigma^z_{\boldsymbol{j}} \qquad (8.33)$$

with constants given by [92]

$$\begin{aligned} \lambda^z &= \frac{J_a^2 + J_b^2}{2U_{ab}} - \frac{J_a^2}{U_{aa}} - \frac{J_b^2}{U_{bb}}, \quad \lambda^\perp = -2\frac{J_a J_b}{U_{ab}},\\ h^z &= \frac{J_a^2}{U_{aa}} - \frac{J_b^2}{U_{bb}}. \qquad (8.34) \end{aligned}$$

For details on the range of validity and the derivation of those equations we refer the reader to Ref. [92]. We notice that if the term $\lambda^{\perp} = 0$, then we can use the remaining Ising interaction as a starting point to derive the quantum compass model. To be in a regime such $\lambda^{\perp} = 0$, one could suppress the tunneling of b-atoms by choosing a spin-dependent lattice with $J_b \ll J_a$. If we neglect J_b we get

$$H_{\mathrm{S}} = -J \sum_{\langle \boldsymbol{i},\boldsymbol{j} \rangle} \sigma^z_{\boldsymbol{i}} \sigma^z_{\boldsymbol{j}} + \sum_{\boldsymbol{i}} h^z \sigma^z_{\boldsymbol{j}}, \tag{8.35}$$

with $J = J_a^2 \left(1/U_{aa} - 1/(2U_{ab})\right)$, and $h^z = -J_a^2/U_{aa}$.

To implement periodic drivings, we consider additional lasers inducing Raman transitions between levels $\uparrow$ and $\downarrow$. Here, the spatial dependence of the phase will appear naturally, since the optical phase of the lasers vary linearly from site to site. We need to implement the driving and longitudinal field in equation (8.9). Note that, since we obtained an Ising interaction in the z-basis, the longitudinal fields required in equation (8.9) must be expressed in terms of σ^x operators. A constant field is implemented by a two-photon Raman transition or microwave field inducing transitions between the two atomic levels,

$$H_{\mathrm{mw}} = \frac{\Omega}{2} \sum_{\boldsymbol{i}} \sigma^x_{\boldsymbol{i}}. \tag{8.36}$$

The periodic driving fields are then implemented by a running-wave potential induced by pairs of lasers with effective wavevector $\Delta\mathbf{k}$, and relative detuning within each pair ω_{d},

$$H_{\mathrm{las}}(t) = \frac{\Omega_{\mathrm{las}}}{2} \sum_{\boldsymbol{i}} \cos(\Delta\mathbf{k} \cdot \mathbf{r}_{\boldsymbol{i}} - \omega_{\mathrm{d}} t) \sigma^x_{\boldsymbol{i}}. \tag{8.37}$$

Note that time-dependent optical lattice potentials have been implemented for spin-dependent transport of ultracold bosons in optical lattices (see for example [113]). We notice that the laser optical phase is translated into a site-dependent optical phase with a linear dependence on the site position [84, 85],

$$\phi_{\boldsymbol{i}} = d_0(\Delta\mathbf{k} \cdot \boldsymbol{i}), \tag{8.38}$$

where we have used that $\mathbf{r}_{\boldsymbol{i}} = d_0 \boldsymbol{i}$, with d_0 the distance between sites in the lattice. After implementing a rotation of the spin basis ($\bar{\sigma}^z = \sigma^x$, $\bar{\sigma}^x = -\sigma^z$) in Hamiltonians (8.35, 8.36, 8.37), we obtain the driving term in equation (8.9), with $\eta\omega_{\mathrm{d}} = \Omega_{\mathrm{las}}$,

and the phase gradient $\Delta\phi_{x,y} = (\Delta\mathbf{k})_{x,y} d_0$. Our final Hamiltonian is

$$\begin{aligned} H &= H_{\rm S} + H_{\rm mw} + H_{\rm las}(t) = \\ &- J\sum_{\langle \boldsymbol{i},\boldsymbol{j}\rangle} \bar{\sigma}^x_{\boldsymbol{i}} \bar{\sigma}^x_{\boldsymbol{j}} + \sum_{\boldsymbol{i}} h^x \bar{\sigma}^x_{\boldsymbol{j}} + \frac{\Omega}{2}\sum_{\boldsymbol{i}} \bar{\sigma^z}_{\boldsymbol{i}} + \\ &\qquad \frac{\eta\omega_{\rm d}}{2}\sum_{\boldsymbol{i}} \cos(\Delta\mathbf{k}\cdot\mathbf{r}_{\boldsymbol{i}} - \omega_{\rm d} t)\bar{\sigma}^z_{\boldsymbol{i}}. \end{aligned} \tag{8.39}$$

We get our target Hamiltonian plus an additional magnetic field term, $h^x \sum_{\boldsymbol{i}} \bar{\sigma}^x_{\boldsymbol{i}} = h^x \sum_{\boldsymbol{i}} (\bar{\sigma}^+_{\boldsymbol{i}} + \bar{\sigma}^-_{\boldsymbol{i}})$. Under the resonance condition $\omega_{\rm d} = 2\Omega$ raising and lowering operators rotate with frequency Ω (see equation (8.11)). Thus, the h^x term can be neglected in a rotating wave approximation in the limit $\Omega \gg J, h^x$.

8.6.2 Rydberg atoms in optical lattices

Rydberg atoms offer us another physical setup with Ising interactions that can be controlled by periodic driving fields. We consider a square lattice with one single Rydberg atom per site. An effective spin is formed with the states $|-\rangle_{\mathbf{j}} = |g\rangle_{\mathbf{j}}$, and $|+\rangle_{\mathbf{j}} = |r\rangle_{\mathbf{j}}$, corresponding to the ground and excited Rydberg state, respectively. The Hamiltonian describing this system is given by [109]

$$H_{\rm Ry} = \frac{U}{2}\sum_{<\mathbf{i},\mathbf{j}>} \frac{\sigma^z_{\mathbf{i}}+1}{2}\frac{\sigma^z_{\mathbf{j}}+1}{2} + \frac{\Delta}{2}\sum_{\mathbf{j}} \sigma^z_{\mathbf{j}}. \tag{8.40}$$

We have assumed fast decaying interactions between Rydberg states, such that the effective spin-spin interaction runs over first neighbours only. To obtain the compass model we need a periodic driving in the x-basis, since Ising interactions appear in the z-basis. Furthermore, we need to counteract the local longitudinal field given by $h^z = \Delta + U/2$. For this, we consider two counter-propagating driving fields inducing a Raman transition with wavevectors $\mathbf{k}$ and $-\mathbf{k}$, and detunings $\omega_0 + \omega_{\rm d}$ and $\omega_0 - \omega_{\rm d}$, respectively.

$$\begin{aligned} H_{\rm las}(t) = &\sum_{\boldsymbol{i}} \frac{\Omega_{\rm las}}{2}\left(e^{i\mathbf{k}\cdot\mathbf{r}_{\boldsymbol{i}} - i(\omega_0+\omega_{\rm d})t}\sigma^+ + \text{H.c.}\right) + \\ &\sum_{\boldsymbol{i}} \frac{\Omega_{\rm las}}{2}\left(e^{-i\mathbf{k}\cdot\mathbf{r}_{\boldsymbol{i}} - i(\omega_0-\omega_{\rm d})t}\sigma^+ + \text{H.c.}\right). \end{aligned} \tag{8.41}$$

We choose $\omega_0 = \Delta + U/2$ to counteract the effect of the longitudinal field. An additional coupling with vanishing effective wavevector is required to implement

the term proportional to Ω in equation (8.9). Note that transitions between atomic ground and Rydberg states usually required two-photon Raman processes, such that the effective wavevector can vanish with a suitable orientation of the individual laser beams. We choose a term of the form,

$$H_{\Omega}(t) = \frac{\Omega}{2} \sum_{\boldsymbol{i}} \left(e^{-i\omega_0 t} \sigma^{+} + \text{H.c.} \right). \tag{8.42}$$

If we express the sum of contributions (8.40,8.41,8.42) in a frame rotating with the frequency ω), we get

$$H_{\text{Ry}} + H_{\text{las}} + H_{\Omega} \rightarrow \frac{U}{8} \sum_{<\boldsymbol{i},\boldsymbol{j}>} \sigma_{\boldsymbol{i}}^{z} \sigma_{\boldsymbol{j}}^{z} + \frac{\Omega}{2} \sum_{\boldsymbol{i}} \sigma_{\boldsymbol{i}}^{x} + \frac{\Omega_{\text{las}}}{2} \sum_{\boldsymbol{i}} \cos(\mathbf{k} \cdot \mathbf{r}_{\boldsymbol{i}} - \omega_{\text{d}} t) \sigma_{\boldsymbol{i}}^{x}. \tag{8.43}$$

After a rotation of the spin basis we obtain our targeted driven Ising model, with $J = -U/4$, and the phase gradient given by the laser optical phases, $\phi_{\boldsymbol{i}} = d_0(\mathbf{k}\, \boldsymbol{i})$.

8.7 Conclusions

We have shown that Ising interactions in a square lattice can be dressed by a periodic driving field and transformed into a quantum compass model. The key idea is to use site-dependent driving phases such that the dressed spin-spin interactions depend on the orientation of the bonds connecting lattice sites. We have also show that the ground state of the quantum compass model can be reached by adiabatically ramping down a field in the spin z-direction. By using symmetry arguments, we have found conditions under which one of the degenerate ground states can be reached, depending on the initial quantum state, and the number of sites in the lattice.

We have discussed two possible implementations with ultracold bosonic atoms and Rydberg atoms in optical lattices. However, our ideas can be used in other experimental setups, for example in two-dimensional arrays of trapped ions. The latter system requires further investigation, since Ising interactions in trapped ion setups are long-ranged [82], something that would lead to the implementation of long-range quantum compass models. Implementations in atomic setups constitute appropriate candidates to build robust quantum memories, where the naturally longer coherence time is more relevant than the operation time and the possibility of addressing individual sites facilitates the measurement of P_{j_y} or Q_{j_y} ; yet, a realistic implementation

still faces technical challenges like the heating problem in state-dependent optical lattices.

Any experimental setup with spin interactions where couplings can be dressed by periodic fields is also amenable for the implementations of our ideas, like for example, arrays of superconducting qubits interacting with classical fields in transmission lines [127, 128].

8.8 Acknowlegments

The research leading to these results has received funding from the People Programme (Marie Curie Actions) of the European Union's Seventh Framework Programme (FP7/2007-2013) under REA grant agreement no: PCIG14-GA-2013-630955. J.J. García-Ripoll acknowledges funding by Mineco Project FIS2012-33022 and CAM Research Network QUITEMAD+.

8.9 Appendix A: Eigenvalues and eigenstates of the operator Z

In this section we find the eigenvalues and eigenstates of the operator $Z \equiv \prod_{\boldsymbol{j}} \sigma^z_{\boldsymbol{j}}$ corresponding to the Hilbert subspace spanned by the doubly-degenerate ground state of the quantum compass model. First, recall that the set of integrals of motion $\{P_{j_y}\}$ defined in equation (8.2) can be used to characterize the twofold ground state since they have different quantum numbers, namely either $(p_1, \ldots, p_{j_y}, \ldots, p_m) = (1, \ldots, 1, \ldots, 1)$ or $(p_1, \ldots, p_{j_y}, \ldots, p_m) = (-1, \ldots, -1, \ldots, -1)$. If we define the states corresponding to the previous eigenvalues as $|\pm\rangle_p$, this result can be written as $P_{j_y}|\pm\rangle_p = \pm|\pm\rangle_p \ \forall j_y$. Alternatively, the set $\{Q_{j_x}\}$ can also be used for this purpose, giving the quantum numbers q_{j_x}. The corresponding eigenstates satisfy $Q_{j_x}|\pm\rangle_q = \pm|\pm\rangle_q \ \forall j_x$, where the states $|\pm\rangle_q$ are in general different from $|\pm\rangle_p$. This result was proved in Ref.[122] for a square lattice $l \times l$, and it can be straightforwardly generalized for a $n \times m$ lattice.

Let us define the operators $X \equiv \prod_{\boldsymbol{j}} \sigma^x_{\boldsymbol{j}}$ and $Y \equiv \prod_{\boldsymbol{j}} \sigma^y_{\boldsymbol{j}}$. We can express X and Y in terms of the sets of operators $\{P_{j_y}\}$ and $\{Q_{j_x}\}$ as $X = \prod_{j_x}^n Q_{j_x}$ and $Y = \prod_{j_y}^m P_{j_y}$.

Thus the states $|\pm\rangle_q$ and $|\pm\rangle_p$ are also eigenstates of X and Y respectively, leading to the eigenequations

$$X|\pm\rangle_q = (\pm 1)^n |\pm\rangle_q, \tag{8.44}$$

$$Y|\pm\rangle_p = (\pm)^m |\pm\rangle_p. \tag{8.45}$$

Notice, though, that the action of X on the basis $|\pm\rangle_p$ is unknown, and similarly for Y on the basis $|\pm\rangle_q$. Bearing in mind the relation $\sigma^a\sigma^b = \mathbb{1}\delta^{ab} + i\sum \epsilon^{abc}\sigma^c$ $(a = 1, 2, 3)$ for the Pauli matrices, we find a useful equation to relate the previous operators, $XY = (i)^{m\times n} Z$. This allows us to calculate the commutators and anti-commutators for these operators, namely

$$\{X, Y\} = 2Re(i^{m\times n})Z, \tag{8.46}$$

$$[X, Y] = 2Im(i^{m\times n})Z. \tag{8.47}$$

We will show in the following how the above equations enable us to determine the eigenstates and eigenvalues of the operator Z in three different cases, depending on the parity of the lattice size, i.e., the parity of n and m. Before doing so, let us prove a result that we shall require later. We would like to relate the basis $|\pm\rangle_p$ and $|\pm\rangle_q$, and this can be done by the fact that $\{P_{j_y}, Q_{j_x}\} = 0\ \forall j_x, j_y$. Effectively, as $P_{j_y}|\pm\rangle_p = \pm|\pm\rangle_p\ \forall j_y$, this implies $P_{j_y}(Q_{j_x}|\pm\rangle_p) = \mp(Q_{j_x}|\pm\rangle_p)$. Hence we infer that the state $Q_{j_x}|\pm\rangle_p$ has to be proportional to one of the eigenstates of P_{j_y}. The only possible solution in this particular case is $Q_{j_x}|\pm\rangle_p \propto |\mp\rangle_p$, since the choice $Q_{j_x}|\pm\rangle_p \propto |\pm\rangle_p$ leads to contradiction $P_{j_y}|\pm\rangle_p = \mp|\pm\rangle_p$. Using an analogous argument for P_{j_y}, one can show that $P_{j_y}|\pm\rangle_q \propto |\mp\rangle_q$.

8.9.1 Case 1: even n-even m

In this case the previous relations take the following form,

$$\{X, Y\} = 2Z, \tag{8.48}$$

$$[X, Z] = [Y, Z] = 0, \tag{8.49}$$

$$X|\pm\rangle_q = |\pm\rangle_q, \tag{8.50}$$

$$Y|\pm\rangle_p = |\pm\rangle_p. \tag{8.51}$$

equation (8.49) and equation (8.51) imply $Y(Z|\pm\rangle_p) = Z|\pm\rangle_p$. Hence the states $Z|\pm\rangle_p$ have to be proportional to the eigenstates of Y, either $Z|\pm\rangle_p \propto |\pm\rangle_p$ or $Z|\pm\rangle_p \propto |\mp\rangle_p$. The proper option can be inferred from the anti-commutator relation (8.48), which states that $Z = XY$. Effectively, introducing the state $|\pm\rangle_p$ to both sides of $Z = XY$, we find that $Z|\pm\rangle_p = X|\pm\rangle_p$. For even n, the operator X can be expressed as an even product of $Q'_{j_y}s$ since $X = \prod_{j_x}^{n} Q_{j_x}$, each of these terms acting in a way that $Q_{j_x}|\pm\rangle_p \propto |\mp\rangle_p$ as proved before. Therefore, the only possibility is that $Z|\pm\rangle_p \propto |\pm\rangle_p$. The eigenvalues $z_\pm$ can also be calculated using equation (8.48), since we have ${}_p\langle\pm|Z|\pm\rangle_p =_q \langle\pm|XY|\pm\rangle_p$, which leads to ${}_q\langle\pm|\pm\rangle_p z_\pm =_q \langle\pm|\pm\rangle_p$. Finally, we conclude that the states $|\pm\rangle_p$ are degenerate eigenstates of the operator Z with eigenvalues $z_\pm = 1$. Similarly, the same result holds for the states $|\pm\rangle_q$, i.e., $Z|\pm\rangle_p = |\pm\rangle_p$.

8.9.2 Case 2: even n-odd m

The basic equations for this case can be written as follows,

$$\{X, Y\} = 2Z(-1)^{(n/2\times m)}, \tag{8.52}$$

$$[X, Z] = [Y, Z] = 0, \tag{8.53}$$

$$X|\pm\rangle_q = |\pm\rangle_q, \tag{8.54}$$

$$Y|\pm\rangle_p = \pm|\pm\rangle_p. \tag{8.55}$$

Equivalently to the previous case, as we have an even product of $Q'_{j_y}s$ we infer that $Z|\pm\rangle_p \propto |\pm\rangle_p$. Now using equation (8.52) the eigenvalues $z_\pm$ can be computed as ${}_q\langle\pm|\pm\rangle_p(-1)^{(n/2\times m)}z_\pm = (\pm 1)_q\langle\pm|\pm\rangle_p$. Therefore, the operator Z satisfies the relation $Z|\pm\rangle_p = \pm(-1)^{(n/2\times m)}|\pm\rangle_p$. This case is trivially equivalent to the odd-even case by a proper rotation, and in such a case the operator Z fulfills an analogous relation for the states $|\pm\rangle_q$.

8.9.3 Case 3: odd n-odd m

Finally, in this case our initial relations lead to a familiar set of equations,

$$\{X, Y\} = \{Y, Z\} = \{Z, X\} = 0, \tag{8.56}$$

$$[X, Y] = 2i^{m\times n} Z, \tag{8.57}$$

$$[Y, Z] = 2i^{m\times n} X, \tag{8.58}$$

$$[Z, X] = 2i^{m\times n} Y, \tag{8.59}$$

$$X|\pm\rangle_q = \pm|\pm\rangle_q, \tag{8.60}$$

$$Y|\pm\rangle_p = \pm|\pm\rangle_p. \tag{8.61}$$

Notice that these are essentially the same commutation and anti-commutation relations as the ones for the Pauli matrices, so we can use the well-known results of this representation to assure that the eigenvalues Z in this subspace are $z_\pm = \pm 1$. One can also take advantange of the results for the Pauli matrices to express the eigenvectors of Z, $|\pm\rangle_z$ in terms of the eigenvectors of X or Y. In particular, in term of the basis $|\pm\rangle_q$ we have $|\pm\rangle_z = 1/\sqrt{2}(|+\rangle_q + |-\rangle_q)$.

Chapter 9

Quantum sensing close to a dissipative phase transition: Symmetry breaking and criticality as metrological resources

9.1 Abstract

We study the performance of a single qubit laser as a quantum sensor to measure the amplitude and phase of a driving field. By using parameter estimation theory we show that certain suitable field quadratures are optimal observables in the lasing phase. The quantum Fisher information scales linearly with the number of bosons and thus the precision can be enhanced by increasing the incoherent pumping acting on the qubit. If we restrict ourselves to measurements of the boson number observable, then the optimal operating point is the critical point of the lasing phase transition. Our results point to an intimate connection between symmetry breaking, dissipative phase transitions and efficient parameter estimation.

9.2 Introduction

Quantum sensing and metrology is likely to be a key practical application of quantum technologies. It has been established both by theory and experiments that quantum

effects can be exploited to increase the accuracy of measurement devices [43, 129–132]. Practical applications, however, face significant challenges. In an ideal scenario quantum metrology requires the preparation of many-particle entangled states by quantum operations that so far are only possible with a few degrees of freedom. Dissipation and noise pose severe limitations which often hinder the metrological advantages of entangled states [133–137]. Quantum setups such as superconducting circuits [47, 138, 139] and trapped ions [13, 87] offer us the opportunity to engineer quantum states of matter with a high degree of control over interactions and dissipation. It has been shown that dissipation may be actually exploited as an effective tool in quantum state engineering [140, 141]. The question naturally arises, whether we can use dissipation to design metrological protocols and sensors [142, 143]. We propose two working principles for such quantum sensors. First, one could exploit the sensitivity of a dissipative steady state to an external field which explicitly breaks some suitable underlying symmetry. The second route could take advantage of the sensitivity at the critical point of a dissipative phase transition [144–147]. Such a sensor would have the advantage that state preparation is not required and, furthermore, dissipation is a control parameter of the sensor dynamics, rather than an error source.

In this chapter, we show that a single qubit laser is a minimalist model where both ideas can be tested. A macroscopic laser with n photons can be described by a coherent state of the light field with a mean value $\langle a\rangle = \sqrt{n}e^{i\theta}$, which assumes the spontaneous breaking of the underlying lasing phase symmetry by choosing an arbitrary value of θ [148]. This approach can be justified by assuming an infinitesimal field (e.g., an environmental fluctuation) that fixes the laser phase [149]. However, in a finite-size system (e.g., a single qubit laser) an external field with finite amplitude, ϵ, is required to explicitly break the phase symmetry (see Fig. 9.1). Here the thermodynamic limit is found when $n \to \infty$ [150], at which the system undergoes a spontaneous symmetry breaking (SSB), i.e., $\lim_{\epsilon\to 0}\lim_{n\to\infty}\langle a\rangle \neq 0$. This relation implies that the order parameter $\langle a\rangle$ must increase with the system size n with an scaling yet to be determined, leading to a high sensitivity to ϵ.

The chapter is structured as follows. Firstly, we present a semiclassical description in phase space of a single qubit laser in the presence of a weak symmetry

breaking driving field. This allows us to estimate analytically the quantum Fisher information (QFI) related to the amplitude $|\epsilon|$ and phase ϕ of the driving, which further shows the connection between symmetry breaking and efficient parameter estimation. We identify the optimal observables that fully exploit the system's metrological capacity. Non-equilibrium criticality is then examined as an alternative metrological resource with nonoptimal protocols using the average number of bosons. We conclude with a discussion of possible error sources as well as applications.

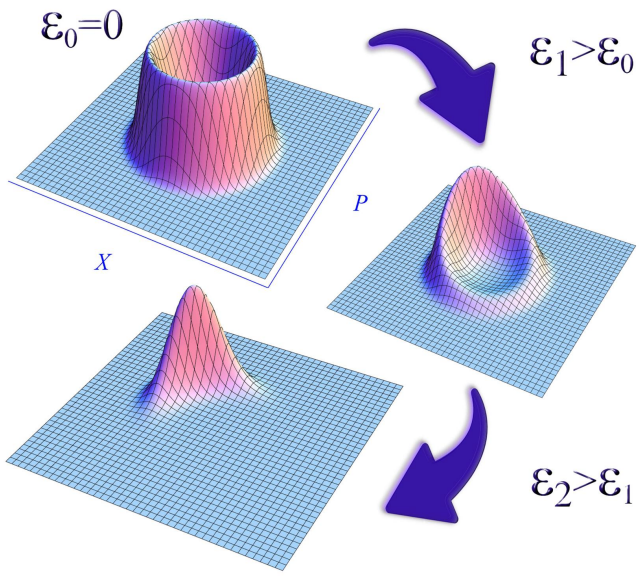

Figure 9.1: Sketch of a explicit symmetry breaking in the *Glauber-Sudarshan P* representation of the lasing steady state (9.9) when an external periodic driving field $\epsilon \neq 0$ is introduced.

9.3 Single qubit laser

In this section we consider a bosonic mode coupled by a Jaynes-Cummings interaction to a two-level system (qubit) with levels $|g\rangle$ and $|e\rangle$. Additionally, we introduce a periodic driving which becomes the target weak field. Both the qubit and driving frequencies are assumed to be resonant with the bosonic mode. In an interaction picture rotating at the mode frequency, the coherent dynamics is described by the

Hamiltonian

$$\begin{aligned} H &= H_{\rm JC} + H_{\rm d}, \\ H_{\rm JC} &= g(\sigma^+ a + a^\dagger \sigma^-), \quad H_{\rm d} = \epsilon^* a + \epsilon a^\dagger, \end{aligned} \tag{9.1}$$

where $\epsilon = |\epsilon| e^{i\phi}$, with $|\epsilon|$ and ϕ being the driving amplitude and phase, respectively. $\sigma^\pm$ are the ladder operators of the two-level system, $\sigma^+ = |e\rangle\langle g|$ and $\sigma^- = |g\rangle\langle e|$. In addition to this coherent dynamics, the system is subjected to incoherent pumping of the qubit and losses of the bosonic mode with rates γ and κ, respectively (see diagram 9.2. The resulting dissipative process is well captured by the following

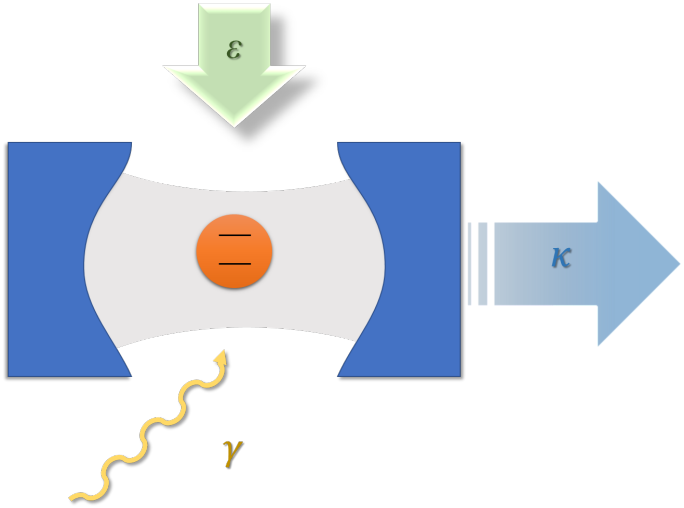

Figure 9.2: A diagram of a single qubit laser used as a probe for the weak field ϵ.

master equation for the system density matrix ρ,

$$\dot{\rho} = -i[H, \rho] + \mathcal{L}_{\{\sigma^+, \gamma\}}(\rho) + \mathcal{L}_{\{a, \kappa\}}(\rho), \tag{9.2}$$

where Lindblad super-operators are defined as $\mathcal{L}_{\{O,\Gamma\}}(\rho) = \Gamma(2O\rho O^\dagger - O^\dagger O\rho - \rho O^\dagger O)$. In a mean field approximation to the case without driving ($\epsilon = 0$) the steady-state is determined by the *pump parameter*, $C_{\rm p} \equiv g^2/\gamma\kappa$. This sets a dissipative phase transition into a lasing phase when $C_{\rm p} > 1$ [61], $\langle a \rangle$ being the order parameter. To evaluate the response of the single qubit laser to an external driving, we need to go beyond mean-field theory. Since we are only interested in the output laser field, we start by finding an effective Liouvillian able to describe the reduced dynamics of the bosonic mode. This can be accomplished in a strong pumping regime [54, 76], i.e., $\gamma \gg \kappa, g, |\epsilon|$, in which the qubit can be adiabatically eliminated, leading to

an effective quartic master equation for the bosonic mode (see Appendix 9.10 for a detailed derivation),

$$\dot{\rho}_f = -i[\epsilon^* a + \epsilon a^\dagger, \rho_f] + \mathcal{L}_{\{a^\dagger, A\}}(\rho_f) + \mathcal{L}_{\{a, C\}}(\rho_f) + \mathcal{L}_{\{aa^\dagger, B\}}(\rho_f) - \mathcal{L}_{\{a^{\dagger 2}, B\}}(\rho_f). \quad (9.3)$$

We have defined the coefficients $A = g^2/\gamma$, $B = 2g^4/\gamma^3$, $C = \kappa$, and $\rho_f = \mathrm{Tr}_{\mathrm{quibt}}\{\mathcal{L}(\rho)\}$ is the reduced density matrix of the bosonic field. Our expression is valid in a regime of strong incoherent pumping, such that the probability of occupation of the ground state can be neglected. This condition is justified both below the lasing phase transition, $C_\mathrm{p} < 1$, and slightly above the threshold, $C_\mathrm{p} \gtrsim 1$ (see Appendix 9.10).

9.4 Semi-classical limit

The master equation obtained in equation (9.3) is still challenging to tackle analytically. By using phase space methods we shall obtain a Fokker-Planck equation valid in a regime with high number of bosons [151, 152]. This will allow us to get analytical results that will be assessed below by comparing to exact numerical calculations. We start by introducing the *coherent state* or *Glauber-Sudarshan P representation* of the effective master equation [54, 56], defined as

$$\rho(t) = \int d^2\alpha P(\alpha, \alpha^*, t)|\alpha\rangle\langle\alpha|, \quad (9.4)$$

where $|\alpha\rangle$ is the coherent state $|\alpha\rangle = \exp(\alpha a^\dagger - \alpha^* a)|0\rangle$. The function $P(\alpha, \alpha^*)$ plays a role analogous to that of a classical probability distribution over $|\alpha\rangle\langle\alpha|$, with the normalization condition $\int d^2\alpha P(\alpha, \alpha^*, t) = 1$, and expectation values of normal ordered operators, $\langle (a^\dagger)^p a^q\rangle = \int d^2\alpha (\alpha^*)^p \alpha^q P(\alpha, \alpha^*)$. Note that P is actually a quasi-probability distribution, since it is in general not a positive distribution function.

By substituting the representation (9.4) of ρ into equation (9.3), one may convert the operator master equation into an equation of motion for $P(\alpha, \alpha^*, t)$. This can be accomplished by using the equivalences 3.23,3.24. An integration by parts with the assumption of zero boundary conditions at infinity, which introduces an extra minus sign for each differential operator, converts the integrand of equation (9.4) into a product of $|\alpha\rangle\langle\alpha|$ and a c-number function of α, α^*. This leads to a differential

equation for $P(\alpha, \alpha^*, t)$. When the laser is operating near the steady state and above threshold, $|\alpha|^2$ is a large number of the order of the average number of photons. Notice also that B is a very small coefficient compared to A, such that $B/A \propto (g/\gamma)^2 \ll 1$. Consequently, we shall retain only the most important terms in B. This corresponds to dropping any contribution smaller than $B|\alpha|^2\alpha$. In doing so, we end up with the following Fokker-Planck equation for P,

$$\frac{\partial P}{\partial t} = -\frac{\partial}{\partial \alpha}[(A - C - B|\alpha|^2)\alpha - \epsilon']P + c.c. + 2A\frac{\partial^2 P}{\partial \alpha \partial \alpha^*} \tag{9.5}$$

where $\epsilon' \equiv i\epsilon$. Let us write this equation in Cartesian coordinates, with $\alpha = x_1 + ix_2$ and $\partial/\partial\alpha = 1/2(\partial/\partial x_1 - i\partial/\partial x_2)$, then

$$\frac{\partial P}{\partial t} = -\sum_{i=1}^{2} \frac{\partial}{\partial x_i}[(A - C - B\vec{x}^2)x_i - \epsilon_i']P + \frac{A}{2}\sum_{i=1}^{2}\frac{\partial^2 P}{\partial x_i^2}, \tag{9.6}$$

where we introduce the two-dimensional vectors $\vec{x} = (x_1, x_2)$ and $\vec{\epsilon'} = (\Re(\epsilon'), \Im(\epsilon'))$. In the stationary state $\partial P/\partial t = 0$, equation (9.6) may be rewritten as $\sum_i \partial J_i/\partial x_i = 0$, where the current $\vec{J}$ is defined by

$$J_i = [(A - C - B\vec{x}^2)x_i - \epsilon_i'] - \frac{A}{2}\frac{\partial P}{\partial x_i}. \tag{9.7}$$

When the drift vector $A_i \equiv [(A - C - B\vec{x}^2)x_i - \epsilon_i']$ satisfies the potential condition $\partial A_i/\partial x_j = \partial A_j/\partial x_i$, as it does in our case, the solution to the Fokker-Planck equation is derived by imposing $\vec{J} = 0$ [54]. This leads to a differential equation for P that can be directly integrated to give

$$P(\vec{x}) = \frac{1}{N}\exp\left\{\frac{1}{A}\left[\left(A - C - \frac{B}{2}\vec{x}^2\right)\vec{x}^2 - 2\vec{\epsilon'}\cdot\vec{x}\right]\right\}, \tag{9.8}$$

where N is a normalization constant. The steady-state solution (9.8) can be conveniently expressed in polar coordinates $\alpha = re^{i\theta}$ as follows,

$$P(r, \theta) = \frac{1}{N}\exp\left(-\lambda r^4 + \mu r^2 - 2\nu r \sin(\theta - \phi)\right), \tag{9.9}$$

where we have introduced the parameters $\lambda = B/2A$, $\mu = (A-C)/A$, and $\nu = |\epsilon|/A$. Note that the probability distribution (9.9) is positive, which indicates that the steady-state admits a classical description. Equation (9.9) can be used to calculate expectation values in the steady state through parametric derivatives of the normalization constant, N. In the appendix 9.11, it is detailed how to approximately

calculate N using Laplace's method together with explicit expressions of useful observables. In the absence of driving ($\epsilon = 0$), the laser phase is uniformly distributed in $[0, 2\pi]$, implying that any average field quadrature vanishes. In contrast, when $\epsilon \neq 0$, the driving field explicitly breaks the phase symmetry and the state adopts a preferred phase with exponential sensitivity as illustrated in Fig. 9.1. According to equation (9.9) we expect the output laser field to have a phase delay of $\pi/2$ with respect to the input driving.

Not any explicit symmetry breaking may lead to an advantageous sensing scheme. However, when this is associated to a SSB in the thermodynamic limit, the corresponding order parameter is expected to be very sensitive to such symmetry breaking field. Such subclass of nontrivial explicit symmetry breaking process is henceforth referred to *induced symmetry breaking*. In our case, this general symmetry argument is translated as a high sensitivity of the coherent component $\langle a \rangle$ to ϵ, which implies that the single qubit laser may be used as a probe to estimate the amplitude of extremely weak forces. The average field quadrature $\langle \hat{P}_\phi \rangle = \langle i(ae^{-i\phi} - a^\dagger e^{i\phi}) \rangle$ will be shown to be particularly sensitive to the external driving, and it follows the following analytical expression,

$$\langle \hat{P}_\phi \rangle = 2r_0 \frac{I_1(2\nu r_0)}{I_0(2\nu r_0)} \underset{\nu r_0 \ll 1}{\approx} \frac{2r_0^2}{A}|\epsilon|, \tag{9.10}$$

where $I_n(z)$ are the modified Bessel functions of the first kind, and r_0^2 stands for steady average number of bosons with no driving (see appendix 9.11 for detailed derivation),

$$\langle n \rangle_{\epsilon \approx 0} = r_0^2 = (A - C)/B. \tag{9.11}$$

The SSB of the lasing phase transition here implies $\lim_{\epsilon \to 0} \lim_{r_0^2 \to \infty} \langle \hat{P}_\phi \rangle \neq 0$. This entails a certain scaling of $\langle \hat{P}_\phi \rangle$ with the system size, here r_0^2, now explicitly given by equation (9.10). Figure 9.3 shows the comparison of these results with numerical calculations of the exact and the adiabatic equation, Eqs. (9.2) and (9.3) respectively. From Fig. 9.3 we differentiate two distinct regimes. First, we have a linear regime $\langle \hat{P}_\phi \rangle \propto |\epsilon|$ if $|\epsilon|$ is small enough, where $\langle \hat{P}_\phi \rangle$ scales linearly with the number of bosons. Essentially, the more pronounced the slope is, the higher the sensor sensitivity will be. Second, we have a saturation regime where $\langle \hat{P}_\phi \rangle^2 \approx \langle a^\dagger a \rangle$ and the laser admits a fully classical description [54].

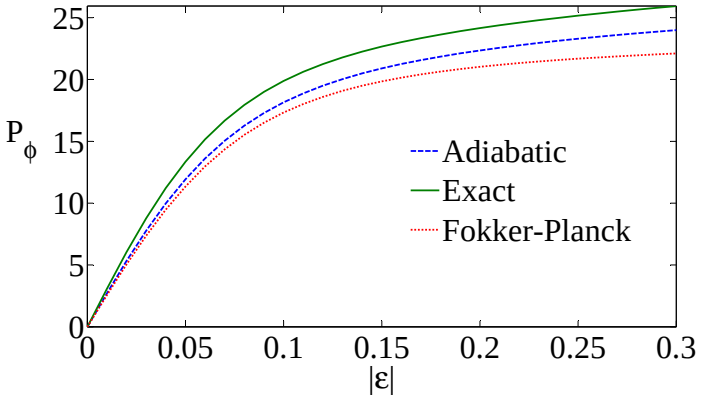

Figure 9.3: Plot of the averaged field quadrature $\langle \hat{P}_\phi \rangle$ as a function of the amplitude $|\epsilon|$, showing the comparison of exact calculations of equation (9.2) (solid line), the adiabatic equation (9.3) (dashed line) and analytical result by the Fokker-Planck equation (dotted line). Parameters: $g = 58, \gamma = 3000, \kappa = 1$.

9.5 Quantum Fisher information and optimal measurements

Equation (9.10) suggests that the induced symmetry breaking allows us to measure weak field amplitudes $|\epsilon| \ll 1$. The capability of this sensing scheme will be mainly determined by its resolution. The theory of quantum Fisher information [27, 153] provides us with an ultimate lower bound on the precision of parameter estimation that is possible in a quantum model, which will be used the single qubit laser as a probe.

Assume that a target parameter φ is encoded in a certain density matrix ρ_φ. The quantum *Cramer-Rao bound* establishes a lower bound to the error in the estimation of φ,

$$\Delta^2 \varphi \geq \frac{1}{N_{\text{exp}} F_Q[\rho_\varphi]} \tag{9.12}$$

where $F_Q[\rho_\varphi]$ is the QFI and N_{exp} is the number of experiment repetitions. The QFI can be viewed as a quantitative measure of distinguishability of a state ρ_φ from its neighbours $\rho_{\varphi+\delta\varphi}$. Thus it can be used as a quantitative characterization of the maximal sensor resolution. A measurement scheme that saturates the bound equation (9.12) is called optimal. The *symmetric logarithmic derivative* operation (SLD) is known to be optimal for all quantum states [154]. It is defined by the

Hermitian operator L_φ satisfying the relation

$$\partial_\varphi \rho_\varphi = \frac{1}{2}(\rho_\varphi L_\varphi + L_\varphi \rho_\varphi). \tag{9.13}$$

The QFI is then given by $F_Q[\rho_\varphi] = Tr\left\{\rho_\varphi L_\varphi^2\right\}$. In the eigenbasis of ρ_φ, i.e., $\rho_\varphi = \sum_i \lambda_i(\varphi)|e_i(\varphi)\rangle\langle e_i(\varphi)|$, the SLD is written as

$$L_\varphi[\rho_\varphi] = \sum_{\substack{i,j \\ \lambda_i+\lambda_j\neq 0}} \frac{2\langle e_i(\varphi)|\dot{\rho}_\varphi|e_j(\varphi)\rangle}{\lambda_i(\varphi)+\lambda_j(\varphi)}|e_i(\varphi)\rangle\langle e_j(\varphi)|, \tag{9.14}$$

First we shall focus on the estimation of the field amplitude $|\epsilon|$ for a given known phase ϕ. By using the analytical result for the steady state equation (9.9), we aim for deriving theoretical results for the SLD as well as the QFI. To do so, it is necessary to solve the operator equation (9.13) for $L_{|\epsilon|}$. In this context, a comprehensive solution of equation (9.13) is already known for Gaussian states in phase space, i.e., quadratic in α, α^* [155]. Assuming the adiabatic elimination regime, i.e, $\gamma \gg \kappa, g, |\epsilon|$, the coefficients A, B satisfy $A/B \propto (\gamma/g)^2 \gg 1$. Hence the P function (9.9) can be well approximated by the following Gaussian-like approximation,

$$P(r,\theta) = N^{-1}\exp\left(-\frac{(r-r_0)^2}{2\sigma^2} - \nu r\sin(\theta-\phi)\right) \tag{9.15}$$

where $r_0^2 = \mu/(2\lambda)$ and $\sigma^2 = 1/(4\mu)$. Even though this represents a simplification with respect to the original P function (9.9), the state is still not Gaussian in the variables α, α^*, for which exact solutions are known for the SLD and QFI [155]. Even so, let us try to solve equation (9.13) in the coherent-state representation. Using equation (9.15), the left-hand side of equation (9.13) gives

$$\partial_{|\epsilon|}P(r,\theta) = \left(-N^{-1}\partial_{|\epsilon|}N + \frac{i}{A}(\alpha e^{-i\phi} - \alpha^* e^{i\phi})\right)P. \tag{9.16}$$

It turns out that $N^{-1}\partial_{|\epsilon|}N$ is equivalent to the average of the field quadrature $\langle\hat{P}_\phi\rangle = \langle i(ae^{-i\phi} - a^\dagger e^{i\phi})\rangle$. This result induces us to introduce the ansatz $L_{|\epsilon|} = S_0 + Sa + S^* a^\dagger$, with S_0, S proper coefficients, which corresponds essentially to the measurement of a suitable field quadrature. Inserting this ansatz in the right-hand side of equation (9.13) and bearing in mind the equivalences (3.23) and (3.24), we have

$$L_{|\epsilon|}\rho = \int_0^\infty \int_0^{2\pi} r d\theta dr (S_0 + S\alpha + S^*(\alpha^* - \partial_\alpha))P, \tag{9.17}$$

with analogous result for $\rho L_{|\epsilon|}$. In a deep lasing regime (well above threshold but still within the validity regime of equation (9.3)) where $r_0 \gg \sigma$, the derivative ∂_α in equation (9.17) can be simplified assuming that $\alpha = re^{i\theta} \approx r_0 e^{i\theta}$, yielding

$$\partial_\alpha P = \frac{e^{-i\theta}}{2}(\frac{\partial}{\partial r} - \frac{i}{r}\frac{\partial}{\partial \theta})P = (-\frac{\alpha^*}{2\sigma^2} + \frac{r_0}{2\sigma^2}e^{-i\theta} + \frac{i|\epsilon|}{A}e^{-i\phi})P \approx \frac{i|\epsilon|}{A}e^{-i\phi}P. \quad (9.18)$$

Identifying now terms from both sides of equation (9.13), the SLD reads

$$L_\epsilon[\rho_{|\epsilon|}] = \frac{1}{A}\left(-\langle \hat{P}_\phi \rangle + \frac{|\epsilon|}{A} + \hat{P}_\phi\right). \quad (9.19)$$

The contribution $|\epsilon|/A^2$ can be neglected in comparison with the contribution given by $\hat{P}_\phi$, leading to the SLD $L_\epsilon[\rho_{|\epsilon|}] = \left(-\langle \hat{P}_\phi \rangle + \hat{P}_\phi\right)/A$. Happily, this in turn implies that $\langle L_{|\epsilon|} \rangle = 0$, a property that any SLD must fulfill according to its own definition (9.13). The QFI may now be calculated as $F_Q[\rho_\varphi] = Tr\left\{\rho_\varphi L_\varphi^2\right\}$ in terms of a parametric derivative of the normalization constant N introduced in equation (9.9), specifically as the fluctuations of $\hat{P}_\phi$ (see Appendix 9.11),

$$F_Q[\rho_{|\epsilon|}] = \frac{2r_0^2}{A^2}\left(1 + \frac{I_2(2\nu r_0)}{I_0(2\nu r_0)} - 2\left(\frac{I_1(2\nu r_0)}{I_0(2\nu r_0)}\right)^2\right) \underset{\nu r_0 \ll 1}{\approx} \frac{2r_0^2}{A^2}. \quad (9.20)$$

In Fig. 9.4 we show a comparison between the analytical result (9.20) and an exact numerical calculation of equation (9.2) by using equation (9.14). There are two important conclusions that are drawn from equation (9.20). Firstly, it shows that the metrological capacity for estimating $|\epsilon|$ is maximal when the induced symmetry breaking occurs, and decreases as the symmetry is already broken. This is intuitively natural since the parameter $|\epsilon|$ is directly associated with the symmetry breaking, and the gain of information is maximal at that point. This feature can be reasonably expected in any sensing scheme relying on spontaneous symmetry breaking as this one. Consequently, this type of sensing is advantageous when measuring extremely weak fields as the precision naturally increases in such domain. The parameters of the laser can be adjusted so that the amplitude remains in the first-order approximation, where the precision remains constant for a fixed amplitude as equation (9.20) indicates. Secondly, the QFI scales linearly with the steady average number of bosons n as $|\epsilon| \to 0$. In the macroscopic limit, defined here as $r_0^2 \to \infty$, F_Q diverges as a result of the sensitivity of the steady state to an infinitesimal perturbation, giving rise to a spontaneous symmetry breaking. These

results show a useful connection between symmetry breaking and efficient parameter estimation. The prior knowledge of ϕ in estimating $|\epsilon|$ may be eluded by performing an average of different quadratures over the range $[0, 2\pi]$, decreasing the QFI by a $1/2$ factor but still conserving the same scaling.

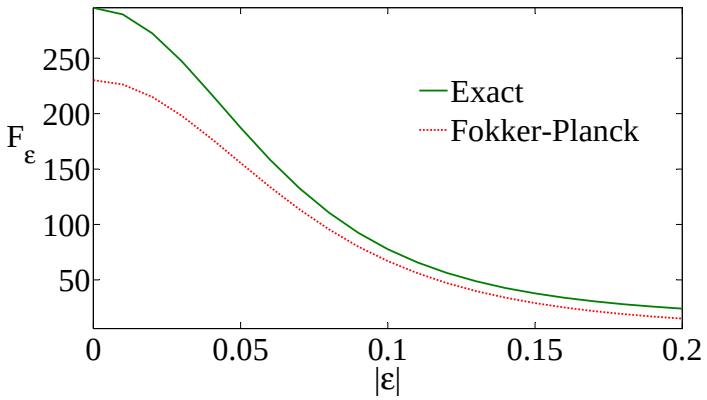

Figure 9.4: Plot of the quantum Fisher information $F_{|\epsilon|}$ as a function of the amplitude $|\epsilon|$ that shows the comparison between an exact calculation given by equation (9.2) and the analytical result (9.20). Parameters: $g = 58, \gamma = 3000, \kappa = 1$.

In the light of these results, we examine whether a similar approach can be used for measuring the phase ϕ for a given amplitude. A completely analogous procedure can now be used to solve again the operator equation (9.13). Now the left-hand side of equation (9.13) gives

$$\partial_\phi P(r,\theta) = \left(-N^{-1}\partial_\phi N + 2\nu(\alpha e^{-i\phi} + \alpha^* e^{i\phi})\right) P. \tag{9.21}$$

The term $N^{-1}\partial_\phi N = \langle 2\nu r \cos(\theta - \phi)\rangle$ is easily shown to be zero. Using then a linear ansatz $L_\phi = S_0 + Sa + S^* a^\dagger$, the right-hand side of equation (9.13) is analogous to equation (9.17). The comparison between both sides of the equation yields the SLD,

$$L_\phi[\rho_\phi] = \nu\left(\hat{X}_\phi\right). \tag{9.22}$$

where $\hat{X}_\phi$ is the field quadrature $\hat{X}_\phi = (ae^{-i\phi} + a^\dagger e^{i\phi})$. The operator $L_\phi[\rho_\phi]$ also satisfies $\langle L_\phi\rangle = 0$ as required by the definition (9.13) . The QFI is then $F_Q[\rho_\phi] = Tr\left\{\rho_\phi L_\phi^2\right\} = \nu^2\langle \hat{X}_\phi^2\rangle$, which turns out to be equivalent to

$$F_Q[\rho_\phi] = \nu\langle \hat{P}_\phi\rangle \underset{\nu r_0 \ll 1}{\approx} \frac{2r_0^2|\epsilon|^2}{A^2}, \tag{9.23}$$

where we have used equation (9.10). This result predicts that the QFI scales linearly with n and quadratically with the field amplitude as $|\epsilon| \to 0$. Graphically, the behavior of the QFI in this case is indirectly given in Fig. 9.3. In contrast to equation (9.20) for estimating the amplitude, here the QFI increases with $|\epsilon|$ since naturally a nonzero signal is required to have a localized phase. Note that the optimal observable $\hat{X}_\phi$ depends itself on the target parameter, ϕ. To operate in the optimal measurement regime we need a first estimation of the observable, ϕ_0. If such estimation satisfies the condition $\delta\phi = (\phi - \phi_0) \ll 1$, the quadrature $\hat{X}_{\phi_0}$ leads to an optimal protocol for estimating ϕ, with a precision determined by equation (9.23). This requirement is analogous to the optimal free precession time in Ramsey spectroscopy [156].

In summary, our optimal scheme makes use of the coherent component $\langle a \rangle$ to estimate $|\epsilon|$ within the linear regime of induced symmetry breaking, $\hat{P}_\phi$ and $\hat{X}_\phi$ being the optimal observables for estimating the amplitude $|\epsilon|$ and phase ϕ respectively. We stress the fact that the quantity r_0^2 appearing in Eqs. (9.20) and (9.23) refers to the number of bosons in the steady state, the main contribution of which comes from the incoherent pumping but *not* the target field, concretely $r_0^2 \approx \gamma/\kappa$ in the lowest order. This implies that one can increase the precision in parameter estimation for a fixed driving intensity ϵ solely by increasing the laser pumping γ. Additionally, recall that none of the results presented in this chapter depend on the initial quantum state of the bosonic field, as the system steady state is unique for all of them.

9.6 Criticality as a metrological resource

The results obtained in Eqs. (9.20) and (9.23) constitute the maximal metrological capacity of the single qubit laser for estimating $|\epsilon|$ and ϕ respectively, as they saturate the Cramer-Rao bound (9.12). However, estimation by nonoptimal observables may be experimentally more accessible depending on the particular platform used. Here we shall study number of bosons in the steady state n, which is nonoptimal for this model. Using the analytical results for n and Δn (see Appendix 9.11), the expected relative error above threshold for estimating $|\epsilon|$ by means of n is

$$\frac{\Delta|\epsilon|}{|\epsilon|} = \frac{1}{|\epsilon|}\frac{\Delta n}{\frac{\partial n}{\partial|\epsilon|}} = \frac{C_p\kappa}{g\nu^2} + \frac{g}{2\gamma}\left(\frac{C_p - 1}{C_p}\right) + O(|\nu|^2). \tag{9.24}$$

equation (9.24) indicates that the precision increases as we approach the critical point $C_p = 1$, at which the precision scales as $\Delta|\epsilon|/|\epsilon| \propto \kappa^{5/2}/(|\epsilon|^2\gamma^{1/2})$[1]. The ratio between the optimal and nonoptimal protocols, $(\Delta|\epsilon|)_{\text{non}}/(\Delta|\epsilon|)_{\text{op}} \propto \kappa/|\epsilon|$ suggests that both methods give comparable resolutions when $\epsilon \approx \kappa$. Figure 9.5 depicts exact numerical results for $\Delta|\epsilon|/|\epsilon|$, confirming maximal precision around the critical point as the thermodynamic limit is approached. Such limit is reached when $n \to \infty$ [150], or equivalently $\gamma/\kappa \to \infty$.

The maximal precision given by the critical point manifests a connection between nonequilibrium criticality in dissipative systems and efficient parameter estimation. An analogous result has been already explored for closed systems [144]. Physically, it is intuitive to think that the system at the critical point becomes more sensitive to any perturbation, leading to a greater sensor resolution. The potential of criticality for sensing can be exploited in setups where the qubit-boson coupling, g, can be controlled with the necessary accuracy to ensure that the system stays at the critical point. This is actually the case in, e.g., single trapped ion phonon lasers [157], where this coupling is implemented by a laser and its strength modulated by its intensity. Also, in superconducting qubits, qubit-photon coupling terms can be induced and controlled with periodic driving fields [86].

A phase estimation by measuring the number of bosons is also possible if we extend the previous setup to arrange an adequate interferometric scheme (see diagram 9.6). Concretely, we add a new reference field term $H_{\text{ref}} = |\epsilon_0|(ae^{-i\phi_0} + a^\dagger e^{i\phi_0})$ to equation (9.1), where we assume that $|\epsilon_0|$, ϕ_0 are known parameters. Both the probe field and the reference field must be comparable to observe interference effects, so we shall assume for simplicity that they both have the same amplitude, $|\epsilon_0| = |\epsilon|$. One may treat this new input field as we did in the previous sections, in which case the P function for the steady state will be

$$P(r,\theta) = \frac{1}{N}\exp\left(-\lambda r^4 + \mu r^2 - 2\nu' r\sin\left(\theta - \phi'\right)\right) \tag{9.25}$$

with $\nu' = 2\nu\cos[(\phi - \phi_0)/2]$ and $\phi' = (\phi + \phi_0)/2$. Comparing equation (9.25) with equation (9.9), we note that the addition of the reference field to the probe field leads to a total driving field with phase ϕ' and amplitude $|\epsilon'| = 2|\epsilon|\cos((\phi - \phi_0)/2)$.

[1] An exact calculation at the critical point shows that the precise scaling is $\Delta|\epsilon|/|\epsilon| = (\pi/(-4+2\pi))^{1/2}\kappa^{5/2}/(|\epsilon|^2\gamma^{1/2})$

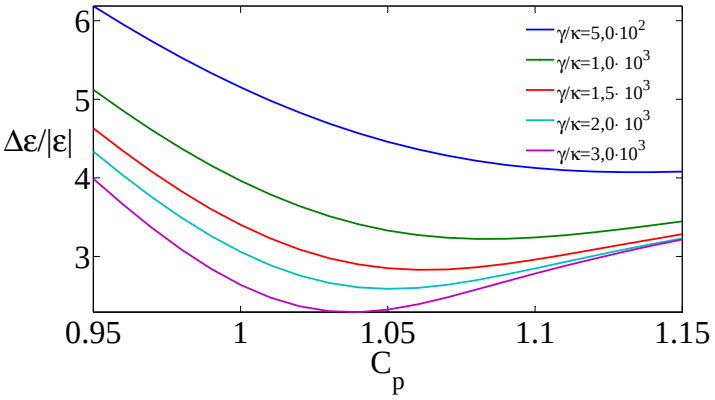

Figure 9.5: Plot of the relative error $\Delta|\epsilon|/|\epsilon|$ by using the average number of bosons as a function of the pump parameter $C_\mathrm{p} = g^2/\gamma\kappa$ as the thermodynamic limit is approached, $\gamma/\kappa \to \infty$ ($|\epsilon| = 0.1$); ranging consecutively from $\gamma/\kappa = 5,0 \cdot 10^2$ at the top line up to $\gamma/\kappa = 3,0 \cdot 10^3$ at the bottom line.

Interference has thus translated the information of ϕ into a new phase-dependent amplitude ϵ', which can be now estimated through measurements of the average boson number with the precision shown in equation (9.24). In the lowest order this leads to a precision $\Delta\phi \approx C_\mathrm{p}\kappa/(g\nu^2 \sin(\phi - \phi_0))$, showing that the optimal operating condition is $\phi - \phi_0 = \pi/2$.

9.7 Possible sources of errors

One may wonder whether potential sources of error in real experiments could jeopardize our previous results. In the appendix 9.12 we consider three possible sources of error: dephasing of the qubit, heating of the bosonic mode, and detuning Δ between the qubit and the mode. Our calculations show that the detuning is expected to be negligible as long as $\gamma \gg \Delta$, while the dephasing and heating result in a renormalization of the constants A and B.

Additionaly, in the case that we are dealing with cavity modes, we must note that the observables calculated throughout this work refer to measurements of the field inside the cavity. It would be possible to use the same observables for the field outside the cavity, resulting in a renormalization of the parameters. Such renormalization would not alter the fundamental scalings found in our study, as

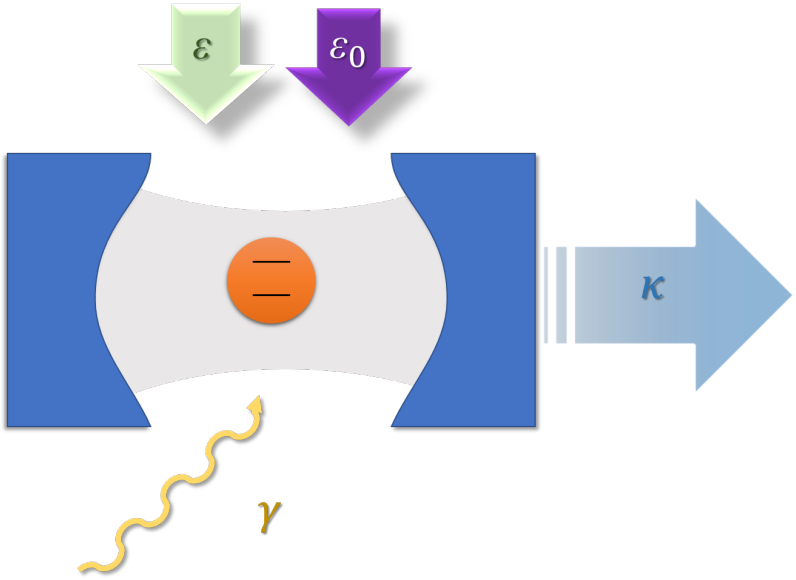

Figure 9.6: A diagram of the interferometer: a new reference field $\epsilon_0 = |\epsilon|e^{\phi_0}$ with known phase ϕ_0 is applied into the cavity.

they rely on general symmetry properties of the model. In essence, we conclude that our results are robust to any perturbation that respects the symmetry of the model and the universal scalings of the lasing phase transition.

9.8 Physical Implementations

Single qubit photon lasers can be implemented with single atoms [158] or superconducting qubits [86, 159, 160]. Furthermore, our ideas can be also applied to single qubit phonon lasers [157, 161]. Here, the quantized excitations (phonons) of a trapped ion play the role of the photons in an optical laser, whereas internal electronic levels provide us with a qubit. Our scheme would lead to a precise measurement of internal ultra-weak forces of the form $H_f = Fx_0(a+a^\dagger)$ resonant with the trapping frequency [162–165]. Phonon lasing has actually been already observed in a single trapped ion experiment [157]. All the interactions and techniques required to implement this idea are routinely used in trapped ion experiments, see, for example, [11] for an excellent review on the topic.

To have full control of the parameters involved in our model we will consider a two-ion crystal in which one of the ions acts as a single-atom phonon laser, whereas a second auxiliary ion is used to provide us with a sympathetic cooling mechanism

[166]. To avoid the requirement of individual addressing of each of the two ions, different species could be used. We assume that ions are weakly coupled by the Coulomb interaction. We introduce phonon annihilation operators a_1 and a_2 associated to quantized vibrations of ions 1 and 2, respectively. The coupling term between the ions takes the form [167, 168],

$$H_{\mathrm{c}} = t_{\mathrm{C}} \left(a_1^\dagger a_2 + a_1 a_2^\dagger \right). \tag{9.26}$$

If we consider radial vibrations, then $t_{\mathrm{C}} = 2e^2/(md^3\omega_{\mathrm{T}}^2)$, where d_0 is the distance between ions, m refers to the ion's mass and ω_{T} is the trapping frequency.

Let us consider now the first ion's quantum dynamics. To make the connection with trapped ion physics clearer, we will work in a spin basis where the role of states $|e\rangle$ and $|g\rangle$ is interchanged with respect to the discussion in the main text. In our trapped-ion scheme, spin pumping will be induced by the radiative decay from an excited state $|e\rangle$ to the ground state $|g\rangle$, whereas a spin-phonon coupling of the form $(\sigma^+ a^\dagger + \sigma^- a)$ will be induced. This is described by the following Liouvillian,

$$\mathcal{L}_1(\rho) = -i[H_1, \rho] + \mathcal{L}_{\{\sigma_1^-, \gamma\}}(\rho). \tag{9.27}$$

The Hamiltonian acting on ion 1 includes a blue-sideband coupling between the internal state of the ion and the local vibrational mode as well as the coupling to the external force that we aim to measure,

$$H_1 = g(\sigma_1^+ a_1^\dagger + \sigma_1^- a_1) + \epsilon(a_1^\dagger + a_1). \tag{9.28}$$

We have introduced ladder operators, σ_1^+, σ_1^-, associated to the internal state of ion 1. The blue side-band term can be induced by lasers with frequency $\omega_{\mathrm{L}} = \omega_0 + \omega_{\mathrm{T}}$, where ω_0 is the frequency of the internal state transition [11]. Finally, the last term of Eq (9.27) is simply the radiative decay of the excited state [11]. To ensure that the dynamics of the ion is constrained to only two levels, one could simply choose $|g\rangle$ and $|e\rangle$ as the two levels of a cycling transition.

The only missing element is a cooling mechanism acting on ion 1. For this we will use ion 2 to provide us with a cooling medium by an effect known as sympathetic cooling. For this we assume that ion 2 is being continuously laser cooled with a rate κ_2,

$$\mathcal{L}_2 = \mathcal{L}_{\{a_2, \kappa\}}(\rho). \tag{9.29}$$

If the Coulomb coupling is small relative to the cooling rate ($t_{\rm C} \ll \kappa_2$), we can adiabatically eliminate ion 2 and obtain an effective cooling term for ion 1, with cooling rate $\kappa_{\rm eff} = t_{\rm C}^2/\kappa_2$. The reduced density matrix for ion 1, ρ_1, is thus subjected to the following quantum dynamics,

$$\dot{\rho}_1 = \mathcal{L}_1(\rho_1) + \mathcal{L}_{\{\kappa_{\rm eff}, a_1\}}(\rho_1). \tag{9.30}$$

Our scheme is a phononic version of the single qubit laser described in the main text. To assess the sensitivity of such a device in the measurement of external forces, we consider now some typical values for cooling rates and vibrational couplings. We focus on the optimal measurement protocol, which would imply measuring the quadrature, $\hat{P}_\phi$, defined in the main text. Quadratures of vibrational operators can be efficiently measured by coupling phonon observables to the ion's internal state and detecting the emitted fluorescence (see for example [11]). By using our calculation of the error as estimated from the QFI we get

$$\Delta\epsilon = \frac{1}{\sqrt{F_Q[\rho_{|\epsilon|}]}} = \frac{A}{\sqrt{2}r_0}. \tag{9.31}$$

To estimate A, we express it like $A = g^2/\gamma = C_{\rm p}\kappa_{\rm eff} \approx \kappa_{\rm eff}$, where we have assumed that we work in a regime with cooperativity parameter $C_{\rm p} \approx 1$.

Our scheme can be applied to measure ultra-weak forces. The relation between the driving strength $|\epsilon|$ and the applied external force, F, is $|\epsilon| = Fx_0$, where

$$x_0 = \frac{1}{\sqrt{2m\omega_{\rm T}}}, \tag{9.32}$$

is the size of the vibrational ground state. Our final expression for the force sensitivity reads (in standard units including $\hbar$),

$$\Delta F \approx \frac{\hbar\kappa_{\rm eff}}{\sqrt{2n_{\rm ph}}x_0}, \tag{9.33}$$

where we have used the fact that the number of phonons, $n_{\rm ph} \approx r_0^2$. To get an estimate of the precision with which an ultra-weak force could be measured, we consider that ion 1 is $^{40}Ca^+$ and $\omega_{\rm T}/(2\pi) = 10$ MHz, which yields $x_0 = 3.5$ nm. Other typical values are $t_{\rm C}/(2\pi) = 4$ kHz [168] and $k_2/(2\pi) = 40$ kHz, leading to $\kappa_{\rm eff}/(2\pi) = 0.4$ kHz. With those values we get

$$\Delta F \approx 53 \text{ yN}/\sqrt{n_{\rm ph}}. \tag{9.34}$$

By increasing the number of phonons in the lasing regime to values such as $n_{\rm ph} = 2 \times 10^3$, one could obtain precisions $\Delta F \approx 1.2$ yN, well within the yocto-Newton regime and beyond the precision of results reported in experiments [162].

Large phonon numbers are in principle not difficult to get in a trapped-ion phonon laser. For example, taking into account typical values of $\gamma/(2\pi) = 20$ MHz our equation (9.11) yields the value $n_{\rm ph} = 2 \times 10^3$ with a side-band coupling $g/(2\pi) = 66.5$ kHz, well within the state of the art [11].

A limiting factor could be the presence of motional heating, $\kappa_{\rm h}$. However, heating rates in linear Paul traps can be as low as 0.1 vibrational quanta per ms, which translates into $\kappa_{\rm h}/(2\pi) = 0.008$ kHz [169]. Under those conditions, $\kappa_{\rm eff} \gg \kappa_{\rm h}$ and the effect of heating could be neglected or incorporated into minor corrections to the trapped-ion sensor (see Sec. 9.7).

9.9 Acknowledgments

This paper was funded by the People Programme (Marie Curie Actions) of the European Union Seventh Framework Programme under REA Grant no: PCIG14-GA-2013-630955. We thank Jacob Dunningham and Pedro Nevado for fruitful discussions.

9.10 Appendix A: Adiabatic elimination

Here we shall derive the effective quartic master equation claimed in equation (9.3), as a result of the adiabatic elimination of the fast spin variable. Firstly, we shall trace over the spin degree of freedom from the master equation for the single qubit laser,

$$\dot{\rho} = -i[H, \rho] + \mathcal{L}_{\{\sigma^+,\gamma\}}(\rho) + \mathcal{L}_{\{a,\kappa\}}(\rho), \tag{9.35}$$

thereby obtaining an equation for the reduced density matrix of the bosonic field $\dot{\rho_f} = {\rm Tr}_{\rm qubit}\{\mathcal{L}(\rho)\}$. Namely, this equation reads

$$\begin{aligned}\dot{\rho}_f = &-ig(a\rho_{ge} + a^\dagger\rho_{eg} - \rho_{ge}a - \rho_{eg}a^\dagger)- \\ &- i(\epsilon a^\dagger\rho_f + \epsilon^* a\rho_f - \epsilon\rho_f a^\dagger - \epsilon^*\rho_f a^\dagger)+ \\ &+ \kappa(2a\rho_f a^\dagger - a^\dagger a\rho_f - \rho_f a^\dagger a),\end{aligned} \tag{9.36}$$

where we introduced the notation $\rho_{ge} = \langle g|\rho|e\rangle = \rho_{eg}^{\dagger}$ and $\epsilon = |\epsilon|e^{i\phi}$. To obtain a closed equation for the reduced density matrix ρ_f, we have to eliminate the operators ρ_{ge}, ρ_{eg} from equation (9.36). We obtain the corresponding equations of motion for these operators using the original master equation,

$$\dot{\rho}_{ge} = -ig(a^{\dagger}\rho_{ee} - \rho_{gg}a^{\dagger}) - \gamma\rho_{ge}, \tag{9.37}$$

where we have neglected the contributions from κ and ϵ in comparison with γ. In the limit $\gamma \gg \kappa, g, |\epsilon|$, we can adiabatically eliminate the operators ρ_{ge} and ρ_{eg} from equation (9.36) by taking $\dot{\rho}_{ge} \approx 0$ in equation (9.37) and substituting their steady-state solutions,

$$\rho_{ge} = -i\frac{g}{\gamma}(a^{\dagger}\rho_{ee} - \rho_{gg}a^{\dagger}). \tag{9.38}$$

As the resulting equation still depends on the operators ρ_{gg} and ρ_{ee}, we make use of the single qubit master equation to obtain the equations of motions of these operators,

$$\dot{\rho}_{ee} = -ig(a\rho_{ge} - \rho_{eg}a^{\dagger}) + 2\gamma\rho_{gg} \tag{9.39}$$

$$\dot{\rho}_{gg} = -ig(a^{\dagger}\rho_{eg} - \rho_{ge}a) - 2\gamma\rho_{gg} \tag{9.40}$$

where we again neglect terms with κ and ϵ. One may now obtain a perturbative solution to the steady states of Eqs. (9.39) and (9.40) in terms of the field density matrix ρ_f. To do so, let us adiabatically eliminate ρ_{gg} by taking $\dot{\rho}_{gg} \approx 0$ in equation (9.40), yielding

$$\rho_{gg} = -\frac{ig}{2\gamma}(a^{\dagger}\rho_{eg} - \rho_{ge}a) = \frac{g^2}{2\gamma^2}(2a^{\dagger}\rho_{ee}a - a^{\dagger}a\rho_{gg} - \rho_{gg}a^{\dagger}a). \tag{9.41}$$

In a first-order approximation, the ground-state population is negligible due to the fast pumping of the atoms ($\gamma \gg 1$). Therefore, we expect to find $\rho_{gg} \approx 0$ and $\rho_{ee} = \rho - \rho_{gg} \approx \rho_f$ in first order. A second-order correction is achieved by inserting this first-order approximation into equation(9.41), hence

$$\rho_{gg} = \frac{g^2}{\gamma^2}a^{\dagger}\rho_f a \tag{9.42}$$

$$\rho_{ee} = \rho_f - \rho_{gg} = \rho_f - \frac{g^2}{\gamma^2}a^{\dagger}\rho_f a. \tag{9.43}$$

One can finally insert Eqs. (9.42) and (9.43) into equation (9.36) to arrive at the desired closed equation for ρ_f,

$$\begin{aligned}\dot{\rho}_f = &-i(\epsilon a^\dagger \rho_f + \epsilon^* a \rho_f - \epsilon \rho_f a^\dagger - \epsilon^* \rho_f a) + \\ &+ \frac{g^2}{\gamma}(2a^\dagger \rho_f a - a a^\dagger \rho_f - \rho_f a a^\dagger) + \\ &+ \frac{2g^4}{\gamma^3}(a a^\dagger \rho_f a a^\dagger - a^{\dagger 2} \rho_f a^2) + \\ &+ \kappa(2a\rho_f a^\dagger - a^\dagger a \rho_f - \rho_f a^\dagger a). \end{aligned} \tag{9.44}$$

The second term in the right-hand side of equation (9.44) accounts for the single photon emission by the excited qubit (linear gain), while the third represents the contribution of two cycles of emission and re-excitation (gain saturation). equation (9.44) can be cast in Lindblad form as presented in equation (9.3). A few brief remarks are worth mentioning about the single qubit laser physics. Using equation (9.44) and setting $\epsilon = 0$, we can easily derive an equation for the diagonal elements ρ_{nn}, namely

$$\begin{aligned}\dot{\rho}_{nn} = &-(2A - B(n+1))(n+1)\rho_{nn} \\ &+ 2An\rho_{n-1,n-1} - Bn(n-1)\rho_{n-2,n-2} \\ &- 2Cn\rho_{nn} + 2C(n+1)\rho_{n+1,n+1}, \end{aligned} \tag{9.45}$$

where we defined the coefficients $A = g^2/\gamma$, $B = 2g^4/\gamma^3$ and $C = \kappa$. In contrast to the classic *Scully-Lamb* treatment of the four-level laser [76], no detailed balance solution can be found to equation (9.45). The rate equation for the average photon number $\langle n \rangle = \sum n\rho_{nn}$ can be also derived from (9.45),

$$\langle \dot{n} \rangle = 2(A - C)\langle n \rangle + 2A - B(2\langle n^2 \rangle + 5\langle n \rangle + 5). \tag{9.46}$$

According to equation (9.46), there will be an initial exponential increase in the mean photon number if $A > C$, hence $A = C$ is the threshold condition for the laser phase. This agrees with the prediction of a mean field treatment to this problem, in which the lasing phase is found when the pump parameter $C_{\mathrm{p}} \equiv g^2/\gamma\kappa$ satisfies $C_{\mathrm{p}} > 1$ [61].

We now address the conditions of validity of the adiabatic elimination. Using equation (9.42), the condition $\rho_{gg} \approx 0$ is translated into

$$\langle \sigma^+ \sigma^- \rangle = \mathrm{Tr}\{\rho_{\mathrm{gg}}\} = \left(\frac{\mathrm{g}}{\gamma}\right)^2 (1 + \mathrm{n}) \ll 1. \tag{9.47}$$

Below threshold ($C_\mathrm{p} < 1$), this is satisfied as long as $g/\gamma \ll 1$. Above threshold ($C_\mathrm{p} > 1$), we can estimate $n = (A - C)/B$ (see App. 9.11), which leads to

$$\langle \sigma^+ \sigma^- \rangle \approx \frac{1}{2} \frac{C_\mathrm{p} - 1}{C_\mathrm{p}} \ll 1. \tag{9.48}$$

Consequently, for the adiabatic elimination to be self-consistent above threshold we must require $C_\mathrm{p} \gtrsim 1$.

9.11 Appendix B: Laplace's method

We shall calculate different observables associated to the $P(\alpha, \alpha^*)$ function obtained in equation (9.9), corresponding to the steady-state solution of the Fokker-Planck equation (9.5). To do so, it is first necessary to compute the normalization constant N given in (9.9). This can be approximately integrated using Laplace's method, which is helpful for integrals of the form

$$I(s) = \int_{-\infty}^{\infty} f(x) e^{sg(x)} dx \approx \sqrt{\frac{2\pi}{s g''(x_0)}} f(x_0) e^{sg(x_0)}, \tag{9.49}$$

in which x_0 stands for the global maximum of $g(x)$, $g''(x_0)$ represents its second derivative evaluated at x_0, and $f(x)$ varies slowly around x_0 and is independent of the parameter s. In our case, N has the form

$$N = \int_0^{\infty} \int_0^{2\pi} r d\theta dr e^{(-\lambda r^4 + \mu r^2 - 2\nu r \sin(\theta - \phi))}. \tag{9.50}$$

Integrating over θ gives

$$N = 2\pi \int_0^{\infty} r dr I_0(2\nu r) e^{(-\lambda r^4 + \mu r^2)}, \tag{9.51}$$

where I_n are the modified Bessel functions of the first kind. Above threshold, where $\mu \gg \lambda$, the normalization constant N is approximated by equation (9.49) as

$$N \approx \sqrt{\frac{\pi^3}{\lambda}} I_0(2\nu r_0) \exp\left(\frac{\mu^2}{4\lambda}\right), \tag{9.52}$$

where $r_0 = \sqrt{\mu/2\lambda}$. The laser field quadrature $\langle \hat{P}_\phi \rangle = \langle i(a e^{-i\phi} - a^\dagger e^{i\phi}) \rangle$ may now be computed by taking the parametric derivative $\langle \hat{P}_\phi \rangle = N^{-1}(\partial N / \partial \nu)$, which gives

$$\langle \hat{P}_\phi \rangle = 2 r_0 \frac{I_1(2\nu r_0)}{I_0(2\nu r_0)}. \tag{9.53}$$

Assuming that $|\epsilon| \ll 1$, one may expand equation (9.53) in a Taylor series as

$$\langle \hat{P}_\phi \rangle \approx 2\nu r_0^2 - \nu^3 r_0^4 + O(\nu^4), \tag{9.54}$$

which in first order indicates a linear dependence in $|\epsilon|$ as claimed in equation (9.10). To compute the uncertainty of $\langle \hat{P}_\phi \rangle$ a second derivative is required, specifically $\Delta^2 \hat{P}_\phi = \langle \hat{P}_\phi^2 \rangle - (\langle \hat{P}_\phi \rangle)^2 = (\partial^2 N/\partial \nu^2)/N - ((\partial N/\partial \nu)/N)^2$, the result of which reads

$$\Delta^2 \hat{P}_\phi = 2r_0^2 \left(1 + \frac{I_2(2\nu r_0)}{I_0(2\nu r_0)} - 2 \left(\frac{I_1(2\nu r_0)}{I_0(2\nu r_0)} \right)^2 \right). \tag{9.55}$$

When $|\epsilon| \ll 1$, a Taylor expansion of (9.55) gives

$$\Delta^2 \hat{P}_\phi = 2r_0^2 \left(1 - \frac{3\nu^2 r_0^2}{2} + O(\nu^4) \right). \tag{9.56}$$

On the other hand, the parametric derivatives with respect to μ can be related to the average number of bosons and its uncertainty. First, the average number of bosons $\langle n \rangle = \langle r^2 \rangle$ is given by $\langle n \rangle = N^{-1}(\partial N/\partial \mu)$, yielding

$$\langle n \rangle = r_0^2 + \frac{\nu r_0}{\mu} \frac{I_1(2\nu r_0)}{I_0(2\nu r_0)} = r_0^2 + \frac{\nu}{2\mu} \langle \hat{P}_\phi \rangle. \tag{9.57}$$

If $|\epsilon| \ll 1$, equation (9.57) is approximated by

$$\langle n \rangle = r_0^2 + \frac{r_0^2 \nu^2}{\mu} - O(\nu^4). \tag{9.58}$$

See Fig. 9.7. The corresponding uncertainty can be computed as $\Delta^2 n = \langle n^2 \rangle - (\langle n \rangle)^2 = (\partial^2 N/\partial \mu^2)/N - ((\partial N/\partial \mu)/N)^2$. The final result of such calculation gives

$$\Delta^2 n = \frac{2\mu + \nu^2}{4\lambda\mu} - \frac{\nu^2}{2\lambda\mu} \left(\frac{I_1(2\nu r_0)}{I_0(2\nu r_0)} \right)^2 - \frac{r_0 \nu}{2\mu^2} \frac{I_1(2\nu r_0)}{I_0(2\nu r_0)} + \frac{\nu^2}{4\lambda\mu} \frac{I_2(2\nu r_0)}{I_0(2\nu r_0)}. \tag{9.59}$$

If $|\epsilon| \ll 1$, $\Delta^2 n$ is approximated by

$$\Delta^2 n = \frac{1}{2\lambda} - \frac{\nu^4}{8\lambda^2} + O(\nu^8). \tag{9.60}$$

Finally, the averaged field quadrature $\langle \hat{X}_\phi \rangle = \langle (a e^{-i\phi} + a^\dagger e^{i\phi}) \rangle$ and its uncertainty are needed to compute the quantum Fisher information. The former is directly given by the parametric derivative $\langle \hat{X}_\phi \rangle = (\partial N/\partial \phi)/N = 0$. From equation (9.9) one can show that the relation $(\partial^2 N/\partial \phi^2)/N = -\nu \langle \hat{P}_\phi \rangle + \nu^2 \langle \hat{X}_\phi^2 \rangle$ holds, allowing us to compute the field uncertainty $\Delta^2 \hat{X}_\phi$ analytically as

$$\Delta^2 \hat{X}_\phi = \langle \hat{X}_\phi^2 \rangle = \nu^{-1} \langle \hat{P}_\phi \rangle, \tag{9.61}$$

since $\partial N/\partial \phi = 0$.

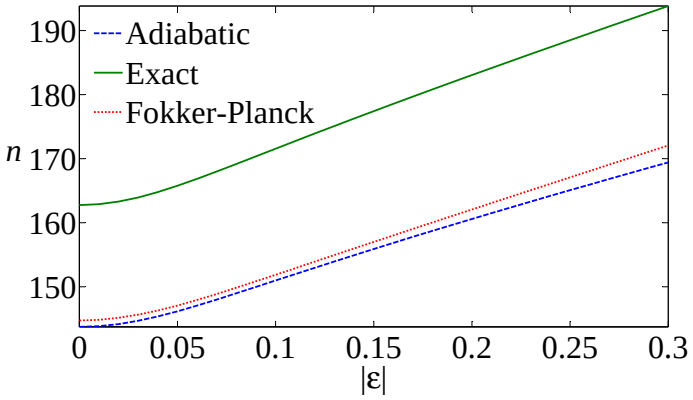

Figure 9.7: Plot of the averaged number of bosons as a function of the amplitude $|\epsilon|$, showing the comparison of exact calculations (solid line), the adiabatic equation (9.44) (dashed line) and analytical results by Laplace's method (dotted line). Parameters: $g = 58, \gamma = 3000, \kappa = 1$

9.12 Appendix C: Sources of error

In this section we discuss in more detail how possible sources of error could affect the ideal dynamics as presented in equation (9.35). On the one hand, we consider two possible noise terms for the dissipation: a nonradiative dephasing process of the qubit at rate $\gamma_{\rm dep}$ plus heating of the bosonic mode at rate $\kappa_{\rm h}$. These terms can be modeled as

$$(\dot{\rho})_{\rm err} = -\frac{\gamma_{\rm dep}}{2}(\sigma^z \rho \sigma^z - \rho) + \kappa_{\rm h}(2a^\dagger \rho_f a - a a^\dagger \rho_f - \rho_f a a^\dagger), \tag{9.62}$$

which have to be added to the general master equation (9.35). The dephasing term changes equation (9.37) for ρ_{eg} just by a renormalization of the pumping $\gamma' = \gamma + \gamma_{\rm dep}/2$ whereas leaving the equations (9.40) and (9.39) intact. Hence, Eqs. (9.38) and (9.42) are modified as

$$\rho_{ge} = -i\frac{g}{\gamma'}(a^\dagger \rho_{ee} - \rho_{gg} a^\dagger) \tag{9.63}$$

$$\rho_{gg} = \frac{g^2}{\gamma\gamma'} a^\dagger \rho_f a. \tag{9.64}$$

The heating term has the same form as the second term in equation (9.36). As a result, the effect of this process turns out to be a renormalization of the coefficients

A, B, such that

$$A' = \frac{g^2}{\gamma'} + \kappa_{\rm h}, \quad B' = \frac{g^4}{(\gamma')^2\gamma} \approx \frac{g^4}{\gamma^3 + \gamma^2\gamma_{\rm dep}}. \tag{9.65}$$

On the other hand, we also consider a possible detuning between the mode frequency ω and the qubit frequency δ. In an interaction picture rotation at the mode frequency, this effect is included as a new term in the Hamiltonian as follows

$$H = H_{\rm JC} + H_{\rm d} + \frac{\Delta}{2}\sigma^z, \tag{9.66}$$

where $\Delta = \delta - \omega$ is the detuning. This term alters equations (9.38) and (9.42) as follows

$$\rho_{ge} = -i\frac{g}{\gamma - i\Delta}(a^\dagger\rho_{ee} - \rho_{gg}a^\dagger) \tag{9.67}$$

$$\rho_{gg} = \frac{g^2}{\gamma^2 + \Delta^2}a^\dagger\rho_f a. \tag{9.68}$$

Consequently, equation (9.44) is modified by adding a new term with a prefactor $g^2\Delta/(\gamma^2 + \Delta)$ that can be safely neglected, and a renormalization of the coefficients A, B, such that

$$A' = \frac{g^2}{\gamma(1 + (\frac{\Delta}{\gamma})^2)}, \quad B' = \frac{g^4}{\gamma^3(1 + (\frac{\Delta}{\gamma})^2)}. \tag{9.69}$$

As we are in the strong pumping regime $\gamma \gg \Delta$, the effect of a possible small detuning is expected to be negligible. In conclusion, we observe that the possible sources of error considered, i.e., dephasing, heating and detuning, result in a renormalization of the constants defined in the ideal case, but they are not expected to jeopardize the sensing process or the performance in a significant way.

Chapter 10

Heisenberg scaling with classical long-range correlations

10.1 Abstract

The Heisenberg scaling is typically associated with nonclassicality and entanglement. In this work, however, we discuss how classical long-range correlations between lattice sites in many-body systems may lead to a $1/N$ scaling in precision with the number of probes. In particular, we show that networks of coupled single qubit lasers can be mapped onto a classical XY model, and a Heisenberg scaling with the number of sites appears when estimating the amplitude and phase of a weak periodic driving field.

10.2 Introduction

Quantum sensing is expected to become one of the key quantum technologies in the short/mid-term, with a wide variety of applications ranging from gravity mapping [28] to magnetic detection of single-neuron activity [29]. In this landscape, quantum resources such as entanglement or nonclassical states of light have been extensively studied as a way to outperform classical resources [25, 26]. In general terms, quantum metrology investigates procedures that accomplish some enhancement in precision, efficiency or simplicity of implementation by means of quantum effects [43]. For instance, it is now well established that quantum correlations among

the initial state of the probes in Ramsey interferometry may surpass the so-called *standard quantum limit* or *shot-noise limit* [25]. In this limit, the precision in parameter estimation scales as $1/\sqrt{N}$, where N is the resource count (number of probes in our case). Quantum effects may give rise to an increase in precision to reach the so-called *Heisenberg limit*, which scales as $1/N$. Frequently, however, these potential benefits are hindered by the effect of noise and decoherence over delicate quantum states [135, 170]. For example, the incoherent loss of a photon in a NOON state, well-known in optical interferometry for leading to a Heisenberg scaling, turns it into a useless mixed state [43].

In the last years, different protocols were conceived to produce robust sensing schemes, such as quantum illumination [171–174] or quantum error correction [175, 176]. Ideally, one would like to combine the enhancement given by the Heisenberg scaling with the robustness of classical states. On the one hand, although dissipation is typically considered as an obstacle, it may be turned into an asset to engineer advantageous states for quantum metrology. Useful symmetry properties and criticality exhibited by dissipative phase transitions have been proposed as useful resources for sensing purposes [177, 178]. This approach has the advantage that no initial state preparation is required and furthermore, the steady state may be naturally robust against noise, which is normally the key limiting factor in other schemes. On the other hand, one could exploit the correlations naturally developed in many-body systems as an alternative to the initial preparation of quantum correlations in Ramsey interferometry. In particular, lattice systems with local (nearest-neighbours) interactions are now within the state-of-the-art techniques, which enables the study of a rich variety of dissipative phase states and transitions [53, 179]. The potential benefits of local interactions and quantum phase transitions in closed systems have been already considered [144, 180]. In Fig. 10.1, all these ideas are schematically compared with the canonical Ramsey interferometer. Additionally, there have been proposals of nonlinear estimation strategies going beyond the $1/N$ Heisenberg-like scaling that rely on long-range many-body interactions as the generator of translations of the parameter to estimate [181–184]. A proper resource count showed that this was compatible with a Heisenberg limit based on the Margolus-Levitin bound [95, 96]. In this work the target parameter is incorporated in a linear

Hamiltonian and it is based on *nearest-neighbour* interactions between sites so that the resources scale with N.

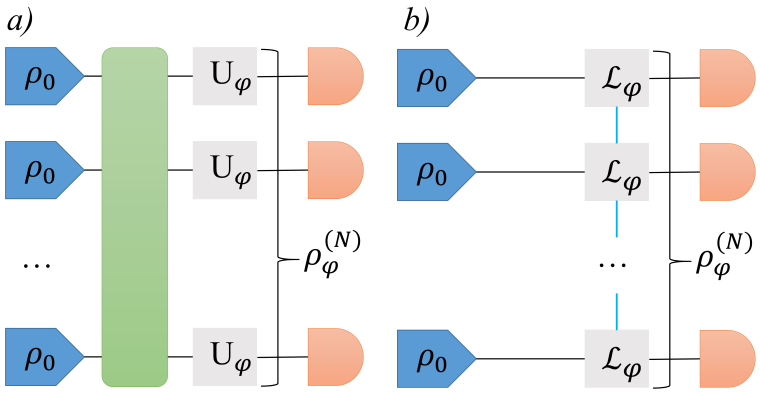

Figure 10.1: Comparison with Ramsey interferometry [43]. ρ_0 represents the initial state of N probes and local detections are performed at the end (orange semicircles). a) Entanglement among the probes (green box) is generated before they are fed into a unitary channel U_φ that leads to a joint state ρ_φ^N. b) Initial probe states evolve under a Markovian channel $\mathcal{L}_\varphi$ with first-neighbour interactions among them (blue lines). The state preparation and the interaction with the probes occur simultaneously.

This work presents the following results. (i) We introduce a specific dissipative model of N single qubit lasers with an effective dissipative-mediated coupling in first-neighbours. (ii) The steady state of this model is shown to be formally equivalent to a thermal state of the classical XY model subjected to an external field. (iii) Analytical expressions of optimal observables for estimating the amplitude and phase of a weak periodic driving as well as the corresponding Fisher information are presented. A Heisenberg scaling with the number of lattice sites is manifested as a result of *classical* long-range correlations in the lattice. These long-range correlations are naturally developed by the system dynamics with short-range interactions, typically present in networks of quantum optical systems such as superconducting circuits, cavity QED and trapped ions, on which our work is focused. As a result, even though the resources scale with N, one yet may achieve a quantum Fisher information scaling as N^2.

10.3 Lattice of single-qubit lasers

We shall study a chain of N identical coupled single-qubit lasers. This system is a generalization of our previous scheme in [177]. Every single-qubit laser consists of a bosonic mode a_j coupled by a Jaynes-Cummings interaction to a two-level system (qubit), with levels $|g\rangle$ and $|e\rangle$, subjected to incoherent pumping of the qubit and losses of the bosonic mode with rates γ and κ, respectively. These dissipative processes are well-described though appropriate master equations [61], for which the following notation for Lindbald super-operators (dissipators) will be employed,

$$\mathcal{L}_{\{O,\Gamma\}}(\rho) = \Gamma(2O\rho O^\dagger - O^\dagger O\rho - \rho O^\dagger O). \tag{10.1}$$

Each mode is additionally fed with a weak coherent periodic driving field whose amplitude $|\epsilon|$ and phase ϕ are aimed to be estimated. The qubit and the driving frequencies are in resonance with the bosonic modes.

We are interested in implementing an incoherent coupling of each qubit laser with its neighbours, which will induce classical correlations among them. Dissipative couplings appear naturally through evanescent modes in arrays of coupled macroscopic lasers [185–187]. However in microscopic systems of single-mode cavity arrays [53] or superconducting circuits [47], bosonic modes are coupled by coherent photon tunneling terms. To get a dissipative coupling from these coherent terms, we assume that the cavities are coupled by intermediate auxiliary modes b_k with a fast photon decay rate, $\tilde{\kappa}$ (see Fig. 10.2). The coherent hopping is given by the Hamiltonian term,

$$H^{\text{hop}} = -t\sum_{\langle k,j\rangle}(a_j^\dagger b_k + b_k^\dagger a_{j+1} + h.c.), \tag{10.2}$$

with t being the photon tunneling amplitude. The adiabatic elimination of these auxiliary modes results in an effective dissipative interaction. This can be shown by calculating the Heisenberg equations for b_k, yielding

$$\dot{b_k} = -it(a_j + a_{j+1}) - \tilde{\kappa}b_k, \tag{10.3}$$

where a_j and a_{j+1} are the neighbouring modes. In the case that b_k is a fast decaying mode, i.e., $\tilde{\kappa} \gg 1$, one may adiabatically eliminate it by taking $\dot{b_k} \approx 0$ and using its steady-state solution,

$$b_k = -\frac{it}{\tilde{\kappa}}(a_j + a_{j+1}). \tag{10.4}$$

The substitution of equation (10.4) in the complete dynamics will result in the effective elimination of the direct hopping (10.2), whereas the dissipator of the intermediate mode originates an effective dissipative-mediated coupling given by,

$$\mathcal{L}_{\{b_k,\tilde{\kappa}\}} \to \mathcal{L}_{\{a_j+a_{j+1},\frac{t^2}{\tilde{\kappa}}\}}. \tag{10.5}$$

In an interaction picture rotating at the mode frequency and performing such adiabatic elimination, the whole dynamics is described by the following master equation for the system density matrix ρ,

$$\dot{\rho} = -i[H,\rho] + \sum_j^N \left(\mathcal{L}_{\{\sigma_j^+,\gamma\}} + \mathcal{L}_{\{a_j,\kappa\}} + \mathcal{L}_{\{a_j+a_{j+1},\frac{t^2}{\tilde{\kappa}}\}}\right)(\rho) \tag{10.6}$$

where the Hamiltonian is given by,

$$\begin{aligned} H &= \sum_j^N H_j^{\mathrm{JC}} + \sum_j^N H_j^{\mathrm{d}}, \\ H_j^{\mathrm{JC}} &= g(\sigma_j^+ a_j + a^\dagger{}_j \sigma_j^-), \quad H_j^{\mathrm{d}} = \epsilon^* a_j + \epsilon a_j^\dagger, \end{aligned} \tag{10.7}$$

and $\epsilon = |\epsilon| e^{i\phi}$. Note that the last dissipator in equation (10.6) represents the effective dissipative-mediated coupling in first-neighbours. A mean field calculation of (10.6) predicts a dissipative phase transition to a lasing phase when the renormalized pumping parameter

$$\tilde{C}_{\mathrm{p}} = \frac{C_{\mathrm{p}}}{(1+3(t/\kappa)^2)} \tag{10.8}$$

satisfies $\tilde{C}_{\mathrm{p}} > 1$ ($C_{\mathrm{p}} \equiv g^2/(\kappa\gamma)$) (see appendix 10.9).

For sensing purposes, the single qubit laser will be prepared to work in a regime of large number of bosons [177]. This can be accomplished in a strong pumping regime of the two-level systems, i.e., $\gamma \gg g, \kappa, |\epsilon|$, in which the qubits can be adiabatically eliminated [54]. This leads to the following effective quartic master equation for the bosonic mode (see appendix 10.10 for details),

$$\begin{aligned} \dot{\rho}_f = &-i\sum_j^N [\epsilon^* a_j + \epsilon a_j^\dagger, \rho_f] + \sum_j^N \mathcal{L}_{\{a_j+a_{j+1},D\}}(\rho_f) \\ &+ \sum_j^N \left(\mathcal{L}_{\{a_j^\dagger,A\}} + \mathcal{L}_{\{a_j a_j^\dagger,B\}} - \mathcal{L}_{\{(a_j^\dagger)^2,B\}} + \mathcal{L}_{\{a_j,C-\frac{t^2}{\kappa}\}}\right)(\rho_f). \end{aligned} \tag{10.9}$$

We have introduced the coefficients $A = g^2/\gamma$, $B = 2g^4/\gamma^3$, $C = \kappa + D$, $D = t^2/\tilde{\kappa}$, and $\rho_f = \mathrm{Tr}_{\mathrm{qubit}}\{\mathcal{L}(\rho)\}$ is the reduced density matrix of the bosonic field. Equation (10.9) is valid below the critical point, $\tilde{C}_{\mathrm{p}} < 1$, and slightly above it, $C_{\mathrm{p}} \gtrsim 1$.

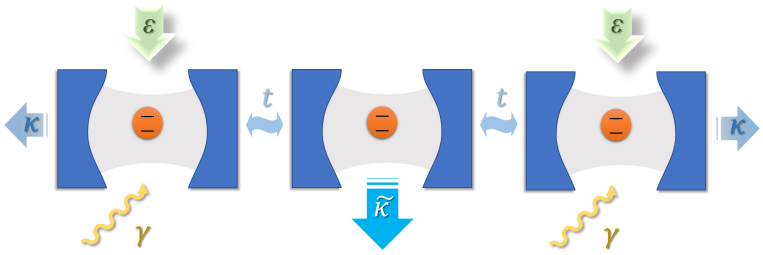

Figure 10.2: General scheme of the dissipative-mediated coupling. Neighbouring single qubit lasers are coupled through a coherent hopping term to a fast decaying mode at rate $\tilde{\kappa}$, which is adiabatically eliminated. Each single qubit laser is subjected to incoherent qubit pumping at rate γ, mode losses at rate κ and a periodic driving field ϵ.

10.4 Semi-classical limit

Equation (10.9) can be more conveniently expressed as an equation in phase space. Concretely, we shall use the *Glauber-Sudarshan P* representation [54] of the effective master equation, defined as

$$\rho(t) = \int d^2\alpha P(\alpha, \alpha^*, t)|\alpha\rangle\langle\alpha| \tag{10.10}$$

where $|\alpha\rangle$ is the coherent state $|\alpha\rangle = \exp(\alpha a^\dagger - \alpha^* a)|0\rangle$. The function $P(\alpha, \alpha^*)$ is a quasi-probability distribution over $|\alpha\rangle\langle\alpha|$, with the normalization condition $\int d^2\alpha P(\alpha, \alpha^*, t) = 1$ and expectation values given by $\langle (a^\dagger)^p a^q\rangle = \int d^2\alpha (\alpha^*)^p \alpha^q P(\alpha, \alpha^*)$. The conversion between the operator master equation (10.9) and its representation in phase space can be carried out thanks to the following equivalences 3.23 and 3.24. In a regime of large number of bosons $|\alpha|^2 \gg 1$, the substitution of this representation leads to an equation of motion for $P(\alpha, \alpha^*, t)$ (see Appendix 10.11 for derivation) with the form of the well-known Fokker-Planck equation [188],

$$\begin{aligned}\frac{\partial P}{\partial t} &= +2A\sum_j \frac{\partial^2 P}{\partial\alpha_j \partial\alpha_j^*} \\ &- \sum_{\langle j,k\rangle} \frac{\partial}{\partial\alpha_j}[(A - C - B|\alpha_j|^2)\alpha_j - D\alpha_k - \epsilon']P + c.c.,\end{aligned} \tag{10.11}$$

where $\epsilon' \equiv i\epsilon$ and $\langle j, k\rangle$ stands for first neighbours. Equation (10.11) presents the adequate structure so that the steady state may be analytically integrated using a certain detailed balance condition (see appendix 10.11). In polar coordinates

$\alpha_j = r_j e^{i\theta_j}$, the steady state reads as follows,

$$P(\vec{r},\vec{\theta}) = \frac{1}{Z}\exp\left(\sum_j(\mu r_j^2 - \lambda r_j^4 - 2\nu r_j \sin(\theta_j - \phi)) - \sum_{\langle j,k\rangle} 2\varsigma r_j r_k \cos(\theta_j - \theta_k)\right), \tag{10.12}$$

where we use the notation $\vec{r} = (r_1, r_2, \cdots, r_N)$ and $\vec{\theta} = (\theta_1, \theta_2, \cdots, \theta_N)$. We have also introduced the parameters $\lambda = B/2A$, $\mu = (A-C)/A$, $\nu = |\epsilon|/A$ and $\varsigma = D/A$, and Z is a normalization constant.

The radial components r_j are essentially associated to the number of bosons in each cavity $r_j^2 \approx n_j$. As the input signals ϵ_j are assumed to be weak, their major influence will be on the angular dynamics, while the radial components r_j will be settled on their steady-state values $r_j \approx r_0$. In this case, the dynamics of equation (10.11) will be dominated by the angular components for laser operation sufficiently far above threshold, and one can derive an effective equation for the angular variables $\vec{\theta}$. This can be done by assuming a P function of the form

$$P(\mathbf{r},\theta) = R(r_1)R(r_2)\cdots R(r_N)P'(\theta), \tag{10.13}$$

where each $R(r_j)$ is a Gaussian distribution properly normalized around r_0. The resulting equation reads (see appendix (10.11)),

$$\begin{aligned}\frac{\partial P'}{\partial t} = &+\frac{A}{2n_0}\sum_j \frac{\partial^2 P'}{\partial\theta_j^2} \\ &+\sum_{\langle j,k\rangle}\frac{\partial}{\partial\theta_j}\left((D\sin(\theta_k-\theta_j) + \frac{|\epsilon|}{\sqrt{n_0}}\cos(\theta_j-\phi))P'\right),\end{aligned} \tag{10.14}$$

in which $n_0 = r_0^2$ stands for the steady average number of bosons *per site*. Equation (10.14) can be related to the first-neighbours stochastic Kuramoto model of N identical oscillators [189, 190]. The Kuramoto model is paradigmatic in the study of synchronization, and it has gained renewed attention in the context of complex [190–192] and neural networks [193]. The steady state solution to equation (10.14) can be obtained by imposing $r_j = r_0$ in equation (10.12) and tracing over the radial part,

$$P'(\vec{\theta}) = \frac{1}{Z}\exp\left(-\sum_{\langle j,k\rangle} 2\varsigma n_0 \cos(\theta_j - \theta_k) - \sum_j 2\nu\sqrt{n_0}\sin(\theta_j - \phi)\right). \tag{10.15}$$

We identify the steady state (10.15) as formally equivalent to a thermal state of an antiferromagnetic classical XY model in the presence of an external field, with

an effective temperature

$$\beta_{\text{eff}} = \frac{n_0}{(C_{\text{p}}\kappa)}. \tag{10.16}$$

Our setup given by equation (10.6) is thus revealed as an alternative to simulate the XY model, which has been recently implemented in various platforms [194–198]. This has been proved to be particularly fruitful in the study of geometric frustration [194, 196]. In the context of machine learning, the XY model has also been suggested as an alternative to Markov chain Monte Carlo methods in order to speed up the computationally time-consuming Boltzmann sampling [197–201].

10.5 Quantum Fisher information and Heisenberg scaling

The maximal resolution that can be achieved by means of the lattice qubit laser for estimating the amplitude $|\epsilon|$ and phase ϕ can be systematically assessed in terms of the quantum Fisher information (QFI), F_Q [27]. This theory sets an ultimate lower bound on the resolution attainable when estimating certain parameter φ encoded in a density matrix ρ_φ through the well-known quantum *Cramer-Rao bound*,

$$\Delta^2\varphi \geq \frac{1}{F_Q[\rho_\varphi]}. \tag{10.17}$$

An observable that saturates this bound is said to be optimal. The so-called *symmetric logarithmic derivative* (SLD), L_φ, defined through the operator equation

$$\partial_\varphi \rho_\varphi = \frac{1}{2}(\rho_\varphi L_\varphi + L_\varphi \rho_\varphi), \tag{10.18}$$

gives us such optimal observable [154]. The QFI can then be obtained as $F_Q[\rho_\varphi] = Tr\left\{\rho_\varphi L_\varphi^2\right\}$. For the single-qubit laser, the optimal observables for estimating $|\epsilon|$ and ϕ in the steady state are the field quadratures

$$\hat{P}_\phi = i(ae^{-i\phi} - a^\dagger e^{i\phi}) \tag{10.19}$$

$$\hat{X}_\phi = (ae^{-i\phi} + a^\dagger e^{i\phi}) \tag{10.20}$$

respectively ($[\hat{X}_\phi, \hat{P}_\phi] = 2i$) [177].

We shall first focus on the amplitude estimation for a given phase. It is natural to suggest that the linear combination

$$\hat{P}^{\phi}_{\text{sum}} = \sum_j \hat{P}^{\phi}_j \tag{10.21}$$

may be the optimal observable for the lattice qubit laser, at least for weak couplings t between sites. By using such linear ansatz for the SLD, it can be shown (see appendix 10.13) that this assumption is correct as long as $\varsigma \ll 1$, a condition easily satisfied in our setup. The analytical expression of $\langle \hat{P}^{\phi}_{\text{sum}} \rangle$ can be calculated by using the distribution (10.15). A perturbative calculation in first order in $|\epsilon|$ is enough as we are assuming weak external forces. In that case, the average field quadrature $\langle \hat{P}^{\phi}_{\text{sum}} \rangle$ can be expressed in terms of the correlation function of the XY model with no external field ($\nu = 0$) (see appendix 10.12), namely

$$\langle \hat{P}^{\phi}_{\text{sum}} \rangle \approx \frac{2n_0|\epsilon|}{C_{\text{p}}\kappa} N \sum_j^N \langle \cos(\theta_i - \theta_j) \rangle_{\epsilon=0}. \tag{10.22}$$

The factor N in equation (10.22) is a trivial contribution from the fact that $\hat{P}^{\phi}_{\text{sum}}$ is a sum of N copies. The correlation function

$$G(|i-j|) = \langle \cos(\theta_i - \theta_j) \rangle, \tag{10.23}$$

on the contrary, represents a potentially non-trivial enhancement that arises from the correlations between sites.

The importance of the correlation function in the realm of parameter estimation lies in the possible *long-range order*, which in the thermodynamic limit (here $N \to \infty$) is defined as non-negligible correlations between infinitely distant sites, i.e. $\langle \cos(\theta_i - \theta_j) \rangle \neq 0$ for $|i-j| \to \infty$. If this relation held, it would imply a scaling of $\sum_j G(|i-j|)$ with the system size N, which in turn could result in a quadratic scaling N^2 of $\langle \hat{P}^{\phi}_{\text{sum}} \rangle$. This is eventually the mechanism behind the *spontaneous symmetry breaking* with order parameter given by $\langle \hat{P}^{\phi}_{\text{sum}} \rangle$, mathematically expressed as

$$\lim_{\epsilon \to 0} \lim_{N \to \infty} \langle \hat{P}^{\phi}_{\text{sum}} \rangle / N \neq 0. \tag{10.24}$$

Nevertheless, the Mermin-Wagner theorem rules out such phase transition for a lattice dimension D such that $D \leq 2$ [72, 202], where thermal fluctuations prevent

ordering even at zero temperature. Particularly for a $1D$ chain, the correlation function always adopts a generic exponential decay

$$G(|i-j|) \propto \exp\left(-|i-j|/\xi\right), \tag{10.25}$$

where ξ is the so-called *correlation length* [66]. Even so, we propose that finite-size long-range correlations can yet be implemented in a finite chain of size N. This can be done by properly tuning the parameters of the lattice qubit lasers such that the correlation length becomes greater than the system size, i.e., $N/\xi \ll 1$, so that the correlation function gives us then an extra N factor, $\sum_j G(|i-j|) \sim N$. To this purpose, the naturally antiferromagnetic sign obtained in equation (10.15) does not favour this positive correlation as the ferromagnetic case does. There are two alternatives to implement an effective ferromagnetic interaction in our model; first by alternating the coupling signs $\pm t$ with the intermediate adiabatically eliminated mode so that the effective dissipative coupling becomes

$$\mathcal{L}_{\{a_j + a_{j+1}, \frac{t^2}{\tilde{\kappa}}\}} \to \mathcal{L}_{\{a_j - a_{j+1}, \frac{t^2}{\tilde{\kappa}}\}}. \tag{10.26}$$

Second, by alternating the phase of periodic drivings such that $\phi_j = \phi + \pi j$ to achieve the same effect expressed in equation (10.26). An explicit calculation of the correlation length can be derived as the correlation functions of the classical $1D$-XY chain are well-known [203]. Hence, one obtains a condition for finite-size long-range correlations in the chain,

$$N \ln\left(\frac{I_0(4\varsigma n_0)}{I_1(4\varsigma n_0)}\right) \ll 1 \tag{10.27}$$

where $I_n(z)$ are the modified Bessel functions of the first kind. Crucially, equation (10.27) can be satisfied even for a weak coupling t by increasing the steady number of bosons n_0. Notice that an increment of n_0 can be achieved simply by increasing the incoherent qubit pumping γ (for a single qubit laser $n_0 \approx \gamma/\kappa$). Upon condition (10.27), the quantum Fisher information for $|\epsilon|$ becomes (see appendix 10.13),

$$F_Q[\rho_{|\epsilon|}] = \frac{2n_0 N^2}{C_{\mathrm{p}}\kappa}, \tag{10.28}$$

which indicates an enhancement of N^2 with respect to the single qubit laser [177].

An analogous procedure may be employed for estimating the phase ϕ for a given amplitude. Note that in this case the optimal observable for the single qubit laser,

$\hat{X}_\phi$ depends itself on the target parameter ϕ. A first estimation $\bar{\phi}$, such that $\delta\phi = (\bar{\phi}-\phi) \ll 1$, is thus required to work in the optimal operating regime. This condition is analogous to the optimal free precession time in Ramsey spectroscopy [156]. In this case the linear combination $\hat{X}^{\bar{\phi}}_{\text{sum}} = \sum_j \hat{X}^{\bar{\phi}}_j$ becomes the optimal observable for the lattice qubit laser. Upon condition (10.27), the QFI becomes,

$$F_Q[\rho_\phi] = \frac{2n_0 N^2 |\epsilon|^2}{C_{\text{p}}\kappa}, \tag{10.29}$$

showing again an enhancement of N^2.

The results (10.28) and (10.29) both show a Heisenberg scaling N^2 with the number of sites, not limited by the dissipation κ. This sort of scaling is typically associated with entanglement or nonclassicality in quantum metrology [43]. In contrast, here it arises solely as a result of the long-range correlations enabled by our many-body system. It is important to notice that here the resources scale with N even though we make use of many-body interactions. Yet we may achieve a quantum Fisher information scaling as N^2 thanks to the long-range correlations developed by the system dynamics, rather than the long-range correlations induced by a long-range interaction. This resource count is important in order to make proper comparisons between different schemes as noted in [95, 96]. Let us recall that the P function exhibits nonclassical behavior when it takes negative values or becomes more singular than the delta function [54]. Here notice that the distribution (10.15) is a regular and positive function. This result thus indicates that it is possible to attain a Heisenberg scaling with classically correlated systems exhibiting long-range correlations. The natural robustness of a classical steady state renders an advantageous implementation over schemes relying on quantum states highly sensitive to decoherence. Finally, as the steady state is similar to a Gaussian state, we can safely presume that the regime in which the Cramer-Rao bound becomes valid is rapidly reached.

Let us also discriminate the roles of the key aspects involved in the results (10.28) and (10.29). In our scheme the non-unitary evolution is responsible for reaching a steady state but it is not enough to induce long-range correlations. The latter actually arise from the interplay between nearest-neighbour couplings and local many-body interactions, which are also known to lead to a Heisenberg scaling in closed systems [180].

10.6 2D & 3D systems

Our setup benefits from having a higher dimensional lattice. In 2D lattices, the XY model is well-known to develop quasi-long range order for low temperatures through the Kosterlitz-Thouless transition [75, 204, 205] (2016 Nobel prize). This transition is driven by the energy cost to thermally break up pairs of vortex-antivortex configurations. The critical temperature is approximately located at $\beta_{\mathrm{c}}\varsigma = 2/\pi$. The effective temperature $\beta_{\mathrm{eff}} = n_0/(C_{\mathrm{p}}\kappa)$ implies that low temperatures are achieved close the the critical point ($C_{\mathrm{p}} \approx 1$) and large average number of bosons n_0. Hence, our regime of parameters readily guarantees that we work in an effective low temperature regime $n_0\varsigma > 2/\pi$. In this regime, the correlation function in equation (10.22) decays algebraically, *i.e,*

$$G(|i-j|) \propto |i-j|^{-\eta}, \tag{10.30}$$

which softens the condition imposed for achieving finite-size long-range correlations. Specifically, by using the spin wave approximation for the value of η [205], we have

$$N^{\frac{1}{2\pi n_0 \varsigma}} \approx 1. \tag{10.31}$$

In 3D lattices the XY model undergoes Spontaneous Symmetry Breaking and it naturally shows long-range order. Consequently conditions (10.27) and (10.31) are not necessary to achieve the enhancing N^2.

10.7 Conclusions

The model introduced in (10.6) may be implemented with single qubit photon laser using single atoms [158] or superconducting qubits [86, 159, 160]. The phononic excitations in ion traps can also play the role of the bosonic field [157, 161], in which case this systems allows the precise measurement of ultra-weak forces resonant with the trapping frequency [162, 163, 177, 206, 207]. A possible implementation of our model with trapped ions may be carried out by extending the implementation sketched in [177], in which it was shown that local sources of error such as heating or dephasing only result in a renormalization of the parameters.

The ideas exposed do not fundamentally rely on the XY model. They can be readily generalized to other setups that give rise to a dissipative dynamics in which

the steady state can be formally identified in terms of another classical Hamiltonian $H_{\rm c}$ of the form

$$H_{\rm c} = \varphi \sum_{j}^{N} H_j + t \sum_{\langle j,k \rangle} H_{i,j}, \tag{10.32}$$

like equation (10.12). It is important to notice that in these models the resources still scale with N, as we assume short-range interactions implied by the notation $\langle j,k \rangle$. If the target parameter φ is small enough, the Fisher information of the steady state will generically be expressed as

$$F_Q[\rho_\varphi] \propto N \sum_{j} G(|i-j|), \tag{10.33}$$

with G being the corresponding correlation function of the equivalent classical model $H_{i,j}$. Bearing in mind the fluctuation-dissipation theorem [66], this establishes a general link between a susceptibility $\chi \propto \sum_j G(|i-j|)$ and the Fisher information in the steady state, thereby showing the possibility of a metrological enhancement though long-range correlations in dissipative systems. An analogous result was recently exposed in [208], and it strengthens a connection between the fields of quantum metrology and condensed-matter Physics.

10.8 Acknowledgments

This paper was funded by the People Programme (Marie Curie Actions) of the European Union Seventh Framework Programme under REA Grant no: PCIG14-GA-2013-630955. We thank Pedro Nevado for fruitful discussions.

10.9 Appendix A: Mean field theory

Here we shall perform a mean-field analysis of equation (10.6), in the spirit of the well-known Maxwell-Bloch equations of a laser [61]. The mean-field ansatz assumes that the system density matrix ρ is separable in the qubit-field subspaces, i.e., $\rho \approx \rho_{\rm field} \otimes \rho_{\rm qubit}$. In practical terms, this allows us to approximate expectation values in such a way that $\langle \sigma a \rangle \approx \langle \sigma \rangle \langle a \rangle$. Furthermore, this avoids the infinite hierarchy of equations for the expectation values of moments of such observables. Namely, we can

write the following closed system of equations in terms of the variables $A_j \equiv \langle a_j \rangle$, $S_j \equiv -i\langle \sigma_j^- \rangle$ and $D_j \equiv \langle \sigma_j^z \rangle$,

$$\begin{aligned} \dot{A}_j &= -gS_j - CA_j - \frac{t^2}{\tilde{k}}(A_{j-1} + A_{j+1}) \\ \dot{S}_j &= gD_jA_j - \gamma S_j \\ \dot{D}_j &= -2g(S_j^* A_j + S_j A_j^*) - 2\gamma(D_j - 1), \end{aligned} \tag{10.34}$$

where periodic boundary conditions are assumed. The result (10.34) is achieved by means of the Heisenberg equations for such observables and using the commutation relations $[a^\dagger, a] = 1$, $\{\sigma^+, \sigma^-\} = 1$ and $[\sigma^z, \sigma^\pm] = \pm 2\sigma^\pm$. The set of nonlinear equations (10.34) represents an extension of the Maxwell-Bloch equations with an extra term describing the hoping of bosons between sites. This system of equations exhibits multiple and frequently complicated possible steady states depending on the regime of parameters studied. It is noticeable also that one can find chaotic behavior in some regions of the parametric space given by κ, g, t, γ. This should not be surprising as the Maxwell-Block equations can be shown to be equivalent to the well-known Lorentz equations [54]. Therefore, appropriate ansatzs for the steady state must be assumed for a certain regime of parameters.

We shall consider in the following that the laser operates in a regime such that the pumping of the qubits represents the smallest timescale in the problem, i.e., $\gamma >> \kappa, g, t$, which is consistent with the adiabatic elimination of the qubits. In this case, the fast variables S_j and D_j may be adiabatically eliminated to obtain an equation for A_j. Additionally, we shall assume that the system does not break the translation symmetry, hence $A_j = A$. In writing equation (10.34) in a basis of the chain normal modes with $A_q = \sum_j A_j e^{iqj}$, the only surviving mode is the fundamental mode $q_0 = 0$, hence $A_{q_0} = \sum_j A_j$. After using the adiabatic elimination, the equation for this mode adopts the form,

$$\frac{dA}{dt} = \left(\frac{NC_{\mathrm{p}}}{1 + \frac{|A|^2}{n_{\mathrm{mf}}}} - (C + \tilde{t}) \right) A, \tag{10.35}$$

with $C_{\mathrm{p}} = g^2/\kappa\gamma$ and $n_{\mathrm{mf}} = 2\gamma^2/g^2$. Equation (10.35) exhibits a Hopf bifurcation indicating a dissipative phase transition to a lasing phase for

$$\tilde{C}_{\mathrm{p}} = \frac{C_{\mathrm{p}}}{\left(1 + 3\left(\frac{t}{k}\right)^2\right)} > 1, \tag{10.36}$$

which has the stable solution $|A_{q_0}|^2 = Nn_{\rm mf}(\tilde{C}_p - 1)$. This result simply represents a renormalization of the pumping parameter $\tilde{C}_{\rm p}$ with respect to the single qubit laser ($t = 0$), in which the critical point is given by $C_{\rm p} = 1$ [61, 177].

10.10 Appendix B: Adiabatic elimination

In this section we shall derive the effective master equation claimed in equation (10.9). We shall use a straightforward generalization of the procedure employed for the single-qubit laser [177]. Firstly, we trace over the qubits from the master equation (10.6),

$$\begin{aligned}\dot{\rho}_f = &-ig\sum_j^N (a_j\rho_j^{ge} + a_j^\dagger\rho_j^{eg} - \rho_j^{ge}a_j - \rho_j^{eg}a_j^\dagger) - \\ &- i\sum_j^N (\epsilon a_j^\dagger\rho_f + \epsilon^* a_j\rho_f - \epsilon\rho_f a_j^\dagger - \epsilon^*\rho_f a_j^\dagger) + \\ &+ (\kappa + \frac{t^2}{\tilde{\kappa}})\sum_j^N (2a_j\rho_f a_j^\dagger - a_j^\dagger a_j\rho_f - \rho_f a_j^\dagger a_j) + \\ &+ \frac{t^2}{\tilde{\kappa}}\sum_j (2a_j\rho_f a_{j+1}^\dagger - a_{j+1}^\dagger a_j\rho_f - \rho_f a_{j+1}^\dagger a_j + c.c),\end{aligned} \tag{10.37}$$

where we introduced the notation $\rho_j^{ge} = \langle g_j|\rho|e_j\rangle$ and $\epsilon = |\epsilon|e^{i\phi}$. In order to obtain a closed equation for the reduced density matrix ρ_f, we have to eliminate the operators ρ_j^{ge}, ρ_j^{eg} from equation (10.37). By writing their corresponding equations of motion using equation (10.6),

$$\dot{\rho}_j^{ge} = -ig(a_j^\dagger\rho_j^{ee} - \rho_j^{gg}a_j^\dagger) - \gamma\rho_j^{ge}, \tag{10.38}$$

(where we have neglected the contributions from κ,ϵ and $t^2/\tilde{\kappa}$ in comparison with γ) the operators ρ_{ge} and ρ_{eg} can be adiabatically eliminated (in the limit $\gamma \gg \kappa, g, |\epsilon|$) from (10.37) by taking $\dot{\rho}_{ge} \approx 0$ in equation (10.38) and substituting in equation (10.37) their steady-state solutions,

$$\rho_j^{ge} = -i\frac{g}{\gamma}(a_j^\dagger\rho_j^{ee} - \rho_j^{gg}a_j^\dagger). \tag{10.39}$$

Likewise, the equations of motion of the operators ρ_{gg} and ρ_{ee} are required as the resulting equation still depends on them. These can be derived again from equation

(10.6), namely

$$\dot{\rho}_j^{ee} = -ig(a_j\rho_j^{ge} - \rho_j^{eg}a_j^\dagger) + 2\gamma\rho_j^{gg} \tag{10.40}$$

$$\dot{\rho}_j^{gg} = -ig(a_j^\dagger\rho_j^{eg} - \rho_j^{ge}a_j) - 2\gamma\rho_j^{gg} \tag{10.41}$$

where we again neglect terms with κ, ϵ and $t^2/\tilde{\kappa}$. A perturbative solution to the steady-states of Eqs. (10.40) and (10.41) may now be expressed in terms of the field density matrix ρ_f. To do so, let us adiabatically eliminate ρ_j^{gg} by taking $\dot{\rho}_j^{gg} \approx 0$ in equation(10.41), which gives

$$\rho_j^{gg} = -\frac{ig}{2\gamma}(a_j^\dagger\rho_j^{eg} - \rho_j^{ge}a_j) = \frac{g^2}{2\gamma^2}(2a_j^\dagger\rho_j^{ee}a_j - a\dagger a_j\rho_j^{gg} - \rho_j^{gg}a_j^\dagger a_j). \tag{10.42}$$

The ground state population of each qubit is expected to be negligible as a result of the fast pumping of the qubits ($\gamma \gg 1$). Thus, in first order we can assume $\rho_j^{gg} \approx 0$ and $\rho_j^{ee} = \rho_j - \rho_j^{gg} \approx \rho_j$. A second order correction is achieved by inserting this first order approximation into equation (10.42), hence

$$\rho_j^{gg} = \frac{g^2}{\gamma^2}a^\dagger\rho_j a \tag{10.43}$$

$$\rho_j^{ee} = \rho_j - \rho_j^{gg} = \rho_j - \frac{g^2}{\gamma^2}a^\dagger\rho_j a_j. \tag{10.44}$$

A closed equation for ρ_f is finally accomplished by inserting Eqs. (10.43) and (10.44) into equation (10.37), and bearing in mind that $\sum_j a_j\rho_j = \sum_j a_j\rho_f$

$$\begin{aligned}
\dot{\rho}_f = &-i\sum_j(\epsilon a_j^\dagger\rho_f + \epsilon^* aj\rho_f - \epsilon\rho_f a_j^\dagger - \epsilon^*\rho_f a_j)+ \\
&+\frac{g^2}{\gamma}\sum_j(2a_j^\dagger\rho_f a_j - a_j a_j^\dagger\rho_f - \rho_f a_j a_j^\dagger)+ \\
&+\frac{2g^4}{\gamma^3}\sum_j(a_j a_j^\dagger\rho_f a_j a_j^\dagger - a_j^{\dagger 2}\rho_f a_j^2)+ \\
&+(\kappa + \frac{t^2}{\tilde{\kappa}})\sum_j^N(2a_j\rho_f a_j^\dagger - a_j^\dagger a_j\rho_f - \rho_f a_j^\dagger a_j)+ \\
&+\frac{t^2}{\tilde{\kappa}}\sum_j(2a_j\rho_f a_{j+1}^\dagger - a_{j+1}^\dagger a_j\rho_f - \rho_f a_{j+1}^\dagger a_j + c.c).
\end{aligned} \tag{10.45}$$

which, written in compact notation, is the result presented in equation (10.9).

10.11 Appendix C: Fokker-Planck equation

Let us summarize the derivation of the Fokker-Planck equation (10.11), the angular Fokker-Planck equation (10.14) and their corresponding steady-state solutions

(10.12,10.15). Bearing in mind the coherent representation of a density matrix ρ,

$$\rho(t) = \int d^2\alpha P(\alpha, \alpha^*, t)|\alpha\rangle\langle\alpha|, \tag{10.46}$$

the master equation can be expressed as an equation of motion for $P(\alpha, \alpha^*, t)$ after an integration by parts with the assumption of zero boundary conditions at infinity. Note that this change introduces an extra minus sign for each differential operator ∂_α. The integrand of equation (10.46) is hence expressed as a product of $|\alpha\rangle\langle\alpha|$ and a c-number function of α, α^*, yielding a differential equation for $P(\alpha, \alpha^*, t)$. We shall focus in a regime in which the average number of bosons is large, which implies $|\alpha|^2 \gg 1$. As B is a very small coefficient compared to A, $B/A \propto (g/\gamma)^2 \ll 1$, we shall retain only the most important terms in B and drop any contribution smaller than $B|\alpha|^2\alpha$. By doing so, we arrive at the Fokker-Planck equation claimed in equation (10.11),

$$\begin{aligned}\frac{\partial P}{\partial t} &= +2A\sum_j \frac{\partial^2 P}{\partial\alpha_j\partial\alpha_j^*} \\ &\quad -\sum_{\langle j,k\rangle}\frac{\partial}{\partial\alpha_j}[(A-C-B|\alpha_j|^2)\alpha_j - D\alpha_k - \epsilon']P + c.c.,\end{aligned} \tag{10.47}$$

where $\epsilon' \equiv i\epsilon$. Let us rewrite equation (10.47) in Cartesian coordinates, with $\alpha_j = x_j^1 + ix_j^2$ and $\partial/\partial\alpha = 1/2(\partial/\partial x^1 - i\partial/\partial x^2)$,

$$\begin{aligned}\frac{\partial P}{\partial t} &= \frac{A}{2}\sum_j^N\sum_{i=1}^2 \frac{\partial^2 P}{\partial x_i^2} \\ &\quad -\sum_j^N\sum_{i=1}^2\frac{\partial}{\partial x_j^i}[(A-C-B\vec{x_j}^2)x_j^i - D(x_{j-1}^i + x_{j+1}^i) - \epsilon_i']P\end{aligned} \tag{10.48}$$

where we introduced the two-dimensional vectors $\vec{x} = (x_j^1, x_j^2)$ and $\vec{\epsilon'} = (\Re(\epsilon'), \Im(\epsilon'))$. The steady-state satisfies $\partial P/\partial t = 0$ and equation (10.48) can be written as $\sum_i \partial J_i/\partial x_i = 0$, with the current $\vec{J_j}$ defined as

$$J_j^i = [(A-C-B\vec{x_j}^2)x_j^i - D(x_{j-1}^i + x_{j+1}^i) - \epsilon_i'] - \frac{A}{2}\frac{\partial P}{\partial x_j^i}. \tag{10.49}$$

Fortunately, the drift vector $A_j^i \equiv [(A-C-B\vec{x}^2)x_j^i - D(x_{j-1}^i + x_{j+1}^i) - \epsilon_i']$ satisfies a detailed balance condition given by $\partial A_i/\partial x_j = \partial A_j/\partial x_i$, and the steady-state solution can be hence found by the condition $\vec{J} = 0$ [54]. This gives rise to a first

order differential equation for P that can be trivially integrated to give,

$$P(\vec{x}) = \frac{1}{Z}\exp\left\{\frac{1}{A}\left[\left(A - C - \frac{B}{2}\vec{x_j}^2\right)\vec{x_j}^2\right] - \frac{2}{A}\left[D\sum_{\langle j,k\rangle}\vec{x_j}\cdot\vec{x_k} - \vec{\epsilon'}\cdot\vec{x_j}\right]\right\}, \tag{10.50}$$

where Z is a normalization constant. This can be then expressed in polar coordinates $\alpha_j = r_j e^{i\theta_j}$ as follows,

$$P(\vec{r},\vec{\theta}) = \frac{1}{Z}\exp\left(\sum_j(\mu r_j^2 - \lambda r_j^4 - 2\nu r_j\sin(\theta_j - \phi)) - \right. \\ \left. - \sum_{\langle j,k\rangle} 2\varsigma r_j r_k\cos(\theta_j - \theta_k)\right), \tag{10.51}$$

where we introduced the notation $\vec{r} = (r_1, r_2, \cdots, r_N)$ and $\vec{\theta} = (\theta_1, \theta_2, \cdots, \theta_N)$, and defined the parameters $\lambda = B/2A$, $\mu = (A-C)/A$, $\nu = |\epsilon|/A$ and $\varsigma = D/A$.

One can derive from an equation solely for the angular variables $\vec{\theta}$ from equation (10.47). To do so, on has to admit the radial variables are settled around their steady-state values $r_j \approx r_0$, while the dynamics of equation (10.47) is hence dominated by the angular components. In that case, the P function may be assumed to take the form $P(\mathbf{r},\theta) = R(r_1)R(r_2)\cdots R(r_N)P'(\theta)$ where each $R(r_j)$ is a properly normalized Gaussian function around r_0,

$$R(r_j) = \frac{1}{N}\exp\left(-\frac{(r_j - r_0)^2}{2\sigma^2}\right) \tag{10.52}$$

Above threshold in a regime of large number of bosons, the normalization constant in (10.52) is given by

$$N = \int_0^\infty r dr\exp\left(-\frac{(r_j - r_0)^2}{2\sigma^2}\right) = \tag{10.53}$$

$$r_0\int_{-r_0\approx-\infty}^{\infty} dr'\exp\left(-\frac{r'^2}{2\sigma^2}\right) + \cancel{\int_{-r_0}^{\infty} r dr\exp\left(-\frac{r'^2}{2\sigma^2}\right)} = \tag{10.54}$$

$$= r_0\sqrt{2\pi\sigma^2}. \tag{10.55}$$

Our equations can be written in polar coordinates with the aid of the equivalences,

$$\frac{\partial}{\partial\alpha} = \frac{1}{2}e^{(-i\theta)}\left(\frac{\partial}{\partial r} - \frac{i}{r}\frac{\partial}{\partial}\right) \\ \frac{\partial}{\partial\alpha*} = \frac{1}{2}e^{(i\theta)}\left(\frac{\partial}{\partial r} + \frac{i}{r}\frac{\partial}{\partial}\right). \tag{10.56}$$

Equation (10.47) then reads as follows,

$$\frac{\partial P}{\partial t} = \frac{\prod_j \partial R_j}{\partial t} P' + \frac{\partial P'}{\partial t} \prod_j R_j = +\frac{A}{2} \sum_j \frac{\partial^2}{\partial \theta_j^2} P -$$
$$- \sum_j \left\{ \frac{1}{r_j} \frac{\partial}{\partial r_j} \left[r_j^2 (A - C - B r_j^2) P \right] + \frac{A}{2} \left[\frac{\partial^2}{\partial r_j^2} + \frac{1}{r_j^2} \frac{\partial}{\partial r_j} \right] P \right\} +$$
$$+ |\epsilon| \sum_j \sin(\theta_j - \phi) \frac{\partial P}{\partial r_j} + \sum_j \frac{|\epsilon|}{r_j} \cos(\theta_j - \phi) \frac{\partial P}{\partial \theta_j} +$$
$$+ D \sum_{\langle j,k \rangle} r_k \cos(\theta_k - \theta_j) \frac{\partial P}{\partial r_j} + D \sum_{\langle j,k \rangle} \frac{r_k}{r_j} \sin(\theta_k - \theta_j) \frac{\partial P}{\partial \theta_j}. \tag{10.57}$$

One can obtain a purely angular equation by integrating both sides of equation (10.57) in the radial variables $\int_0^\infty \vec{r} d\vec{r}$. On the one hand, the second line in (10.57) can be simplified (for $|\epsilon| \approx 0$) as $R(r_j)$ satisfies

$$\frac{\partial R_j}{\partial t} = - \left\{ \frac{1}{r_j} \frac{\partial}{\partial r_j} \left[r_j^2 (A - C - B r_j^2) R_j \right] + \frac{A}{2} \left[\frac{\partial^2}{\partial r_j^2} + \frac{1}{r_j^2} \frac{\partial}{\partial r_j} \right] R_j \right\} \tag{10.58}$$

On the other hand, the integration of the first derivative $\partial_r R$ is eliminated through the relation,

$$\begin{aligned} \int_0^\infty r dr \partial_r R &= -\frac{1}{N} \int_0^\infty r dr \frac{(r - r_0)}{\sigma^2} \exp\left(-\frac{(r - r_0)^2}{2\sigma^2} \right) = \\ &= -\frac{1}{N} \int_{-r_0}^\infty (r' + r_0) dr' \frac{(r')}{\sigma^2} \exp\left(-\frac{(r')^2}{2\sigma^2} \right) \approx \\ &\approx -\frac{1}{N} \int_{-\infty}^\infty dr' \frac{(r'^2)}{\sigma^2} \exp\left(-\frac{(r')^2}{2\sigma^2} \right) = \\ &= -\frac{1}{N} \sqrt{2\pi} \sigma = -\frac{1}{r_0}. \end{aligned} \tag{10.59}$$

After grouping terms, the resulting equation adopts the form claimed in equation (10.14),

$$\begin{aligned} \frac{\partial P'}{\partial t} &= +\frac{A}{2n_0} \sum_j \frac{\partial^2 P'}{\partial \theta_j^2} \\ &+ \sum_{\langle j,k \rangle} \frac{\partial}{\partial \theta_j} \left((D \sin(\theta_k - \theta_j) + \frac{|\epsilon|}{\sqrt{n_0}} \cos(\theta_j - \phi)) P' \right), \end{aligned} \tag{10.60}$$

The steady state state of (10.60) can be obtained by imposing a detail balance condition such that the current $\vec{J}_\theta = 0$ or simply by taking $r_j = r_0$ in (10.50) and grouping the radial part into the normalization constant Z, which gives

$$P'(\vec{\theta}) = \frac{1}{Z} \exp\left(-\sum_{\langle j,k \rangle} 2\varsigma n_0 \cos(\theta_j - \theta_k) - \sum_j 2\nu \sqrt{n_0} \sin(\theta_j - \phi) \right). \tag{10.61}$$

10.12 Appendix D: Correlation function in the XY chain

In this section we aim to show rigorously the expression of $\langle \hat{P}^{\phi}_{\text{sum}} \rangle = \langle \sum_j \hat{P}^{\phi}_j \rangle$ in first order in ϵ as claimed in equation (10.22) as well as the expresion for $\langle \hat{X}^{\bar{\phi}}_{\text{sum}} \rangle = \langle \sum_j \hat{X}^{\phi}_j \rangle$. Concretely, we will show how it can be written in terms of the correlation function of the classical XY model with no external field. The correlation functions of the XY chain are already well-known [203]. In particular, the only two-point non-zero correlation function of the Boltzmann distribution (10.51) with $\nu = 0$ is precisely $\langle \cos(\theta_i - \theta_j) \rangle$ which can expressed in terms of the modified Bessel functions of the first kind $I_n(z)$, namely

$$\langle \cos(\theta_1 - \theta_{j+1} \rangle = \frac{1}{Z_0} \sum_{n=-\infty}^{\infty} I^j_{n-1}(4r_0^2\varsigma) I^{N-j}_n(4r_0^2\varsigma). \tag{10.62}$$

In equation (10.62) we have assumed ferromagnetic sign. For distant sites, the correlation function in 1D systems is known to decay exponentially with a certain correlation length ξ (the typical scale of the correlations) [66], i.e.,

$$\langle \cos(\theta_1 - \theta_{1+j} \rangle \approx \left(\frac{I_1(4r_0^2\varsigma)}{I_0(4r_0^2\varsigma)} \right)^j \approx e^{-j/\xi}, \tag{10.63}$$

from which the correlation length is given by

$$\xi^{-1} = \ln \left(\frac{I_1(4r_0^2\varsigma)}{I_0(4r_0^2\varsigma)} \right). \tag{10.64}$$

A perturbative expression in first order of ϵ for $\hat{P}^{\phi}_{\text{sum}} = \sum_j \hat{P}^{\phi}_j$ can be derived by using the Boltzmann factor given by the angular P function calculated in equation (10.51). If we expand the exponential up to first order in ν, the average quadrature $\langle \hat{P}^{\phi}_{\text{sum}} \rangle$ is given by two contributions $\langle \hat{P}^{\phi}_{\text{sum}} \rangle \approx \langle \hat{P}^{\phi}_{\text{sum}} \rangle_0 + \delta \langle \hat{P}^{\phi}_{\text{sum}} \rangle$ in terms of the Boltzmann factor of the XY with no external field, i.e.,

$$P_0(\vec{\theta}) = \frac{1}{Z_1} \exp \left(4\varsigma \sum_j r_j r_{j+1} \cos(\theta_j - \theta_{j+1}) \right) \tag{10.65}$$

with $Z1$ being the partition function up to first order, $Z_1 = Z_0 + \delta Z$. It is straightforward to check that the first order contribution δZ is zero so $Z_0 = Z_1$. The zero order contribution is then,

$$\langle \hat{P}^{\phi}_{\text{sum}} \rangle_0 = \frac{1}{Z_0} \oint d\vec{\theta} (-2 \sum_j r_0 \sin(\theta_j - \phi)) P_0(\vec{\theta}) \tag{10.66}$$

while the first order contribution can be expressed as,

$$\delta\langle\hat{P}^{\phi}_{\text{sum}}\rangle = \frac{1}{Z_0}\oint d\vec{\theta}(-2\sum_j r_0\sin(\theta_j-\phi))(-2\nu\sum_k r_0\sin(\theta_k-\phi))P_0(\vec{\theta}). \tag{10.67}$$

The average quadrature is thus given by

$$\langle\hat{P}^{\phi}_{\text{sum}}\rangle \approx 4r_0^2\nu\sum_{i,j}\langle\sin(\theta_j-\phi)\sin(\theta_i-\phi)\rangle_{\epsilon=0}. \tag{10.68}$$

By using the trigonometric relation,

$$\sin(\theta_j-\phi)\sin(\theta_i-\theta_j) = \frac{1}{2}(\cos(\theta_i-\theta_j)-\cos(\theta_i+\theta_j+2\phi)), \tag{10.69}$$

we note that only the first term in equation (10.69) gives rise to a non-zero correlation contribution, thus the quadrature takes the form claimed in equation (10.22),

$$\langle\hat{P}^{\phi}_{\text{sum}}\rangle \approx \frac{2n_0|\epsilon|}{C_{\text{p}}\kappa}N\sum_j^N\langle\cos(\theta_i-\theta_j)\rangle_{\epsilon=0}. \tag{10.70}$$

The field quadrature $\hat{X}^{\bar{\phi}}_{\text{sum}} = \sum_j \hat{X}^{\phi}_j$ in first order, on the other hand, will be given by

$$\langle\hat{X}^{\bar{\phi}}_{\text{sum}}\rangle \approx 4r_0^2\nu\sum_{i,j}\langle\cos(\theta_j-\bar{\phi})\sin(\theta_i-\phi)\rangle_{\epsilon=0}. \tag{10.71}$$

As we assume $\delta\phi = (\bar{\phi}-\phi) \ll 1$, equation (10.71) can be further simplified by means of the trigonometric relation

$$\begin{aligned}\sin(\theta-\bar{\phi}) &= \cos(\theta-\phi)\cos\delta\phi + \sin(\theta-\phi)\sin\delta\phi \approx \\ &\approx \cos(\theta-\phi)+\sin(\theta-\phi)\delta\phi.\end{aligned} \tag{10.72}$$

Only the second term in (10.72) leads to a non-zero correlation function, so we finally arrive to

$$\begin{aligned}\langle\hat{X}^{\bar{\phi}}_{\text{sum}}\rangle &\approx \delta\phi 4r_0^2\nu\sum_{i,j}\langle\sin(\theta_i-\phi)\sin(\theta_j-\phi)\rangle_{\epsilon=0} = \\ &= \delta\phi 4r_0^2\nu\sum_{i,j}\langle\cos(\theta_i-\theta_j)\rangle_{\epsilon=0}.\end{aligned} \tag{10.73}$$

By imposing the condition $N/\xi \ll 1$, i.e.

$$N\ln\left(\frac{I_0(4\varsigma n_0)}{I_1(4\varsigma n_0)}\right) \ll 1, \tag{10.74}$$

relations (10.68,10.73) are further reduced,yielding

$$\langle \hat{P}^{\phi}_{\text{sum}} \rangle \approx 4n_0 \nu N^2 \tag{10.75}$$

$$\langle \hat{X}^{\bar{\phi}}_{\text{sum}} \rangle \approx \delta\phi 4n_0 \nu N^2, \tag{10.76}$$

where $n_0 = r_0^2$ symbolizes the steady average of bosons of each cavity.

10.13 Appendix E: Symmetric logarithmic derivative & quantum Fisher information

In this section we will obtain the optimal observables for the lattice-qubit laser, as well as the quantum Fisher information for them. To do that, we have to solve the operator equation for the symmetric logarithmic derivative, this is,

$$\partial_\varphi \rho_\varphi = \frac{1}{2}(\rho_\varphi L_\varphi + L_\varphi \rho_\varphi). \tag{10.77}$$

The P function (10.51) can be well approximated by the following Gaussian-like approximation (we treat directly the ferromagnetic case),

$$\begin{aligned} P(\vec{r},\vec{\theta}) = \frac{1}{Z}\exp\Bigg(-\sum_j \frac{(r_j - r_0)^2}{2\sigma^2} - \nu \sum_j r_j \sin(\theta_j - \phi) + \\ + 4\varsigma \sum_j r_j r_{j+1} \cos(\theta_j - \theta_{j+1}) \Bigg), \end{aligned} \tag{10.78}$$

where the radial components are assumed to be settled around their steady-state values r_0^2 with width σ^2. Using (10.78), the l.h.s of equation(10.77) reads,

$$\partial_{|\epsilon|} P(r,\theta) = \left(\partial_{|\epsilon|} \ln Z + \frac{i}{A} \sum_j (\alpha_j e^{-i\phi} - \alpha_j^* e^{i\phi}) \right) P. \tag{10.79}$$

It is straightforward to check that $\partial_{|\epsilon|} \ln Z$ is equivalent to the average of the sum of the field quadratures $\langle \hat{P}_\phi \rangle = \langle i \sum_j (a_j e^{-i\phi} - a_j^\dagger e^{i\phi}) \rangle$. This result suggests we introduce the ansatz $L_{|\epsilon|} = S_0 + \sum_j (S a_j + S^* a_j^\dagger)$, with S_0, S proper coefficients. Inserting this ansatz into the r.h.s of equation (10.77) and using the relations (3.23) and (3.24), we obtain

$$L_{|\epsilon|}\rho = \int_0^\infty \int_0^{2\pi} d\vec{\theta} d\vec{r} r_1 \dots r_N (S_0 + \sum_j (S\alpha_j + S^*(\alpha_j^* - \partial_{\alpha_j})))P \tag{10.80}$$

with analogous expression for $\rho L_{|\epsilon|}$. Well above threshold where $r_0 \gg \sigma$, we may further simplify the exact derivative ∂_α in equation (10.80) if we assume the radial component to be approximately constant and homogeneous so that $\alpha_j = r_j e^{i\theta_j} \approx r_0 e^{i\theta_j}$ (*after* taking the derivative). We may distinguish two contributions to the derivative. First, an on-site contribution given by the first two terms of the r.h.s in equation (10.78)

$$\partial_{\alpha_j} P_{\text{on}} = \frac{e^{-i\theta_j}}{2}\left(\frac{\partial}{\partial r_j} - \frac{i}{r_j}\frac{\partial}{\partial \theta_j}\right)P_{\text{on}} = \\ = \left(-\frac{\alpha_j^*}{2\sigma^2} + \frac{r_0}{2\sigma^2}e^{-i\theta_j} + \frac{i|\epsilon|}{A}e^{-i\phi}\right)P \approx \frac{i|\epsilon|}{A}e^{-i\phi}P_{\text{on}}. \quad (10.81)$$

Second, a contribution given by the neighbouring interaction,

$$\partial_{\alpha_j} P_{\text{int}} \approx 2\varsigma r_0 (e^{-i\theta_{j-1}} + e^{-i\theta_{j+1}})P_{\text{int}}. \quad (10.82)$$

Using the results (10.80), (10.81) and (10.82), we can identify terms from both sides of equation (10.77), leading to the following SLD,

$$L_\epsilon[\rho_{|\epsilon|}] = \frac{1}{A}\left(\frac{N\nu}{1-2\varsigma} - \sum_j \langle \hat{P}_j^\phi \rangle + \frac{\sum_j \hat{P}_j^\phi}{1-2\varsigma}\right) \quad (10.83)$$

The contribution of the first term of the r.h.s can be neglected in comparison with the contribution given by $\sum_j \hat{P}_\phi$. On the other hand, the SLD must fulfill the relation $\langle L_{|\epsilon|} \rangle = 0$ according to the definition (10.77). In our case, this implies that the result (10.83) is correct as long as $\varsigma \ll 1$, which is consistent with our scheme. In that case, the observable $\hat{P}^\phi_{\text{sum}} = \sum_j \hat{P}_j^\phi$ turns out to be the optimal observable for estimating $|\epsilon|$. A totally analogous procedure may be employed to prove that $\hat{X}^\phi_{\text{sum}} = \sum_j \hat{X}_j^\phi$ is the optimal observable for estimation $|\phi|$.

As the quantum Fisher information is obtained through the SLD, we may recover the results claimed in Eqs. (10.28) and (10.29) simply through the error propagation formula, for which the fluctuations $\Delta^2\langle \hat{P}^\phi_{\text{sum}} \rangle$, $\Delta^2\langle \hat{X}^{\bar{\phi}}_{\text{sum}} \rangle$ are additionally needed. These fluctuations can be written as,

$$\Delta^2\langle \hat{P}^\phi_{\text{sum}} \rangle = \sum_{i,j} \langle \hat{P}_i^\phi \hat{P}_j^\phi \rangle - \langle \sum_j \hat{P}_j^\phi \rangle^2 \quad (10.84)$$

and analogously for $\Delta^2\langle \hat{X}^{\bar{\phi}}_{\text{sum}} \rangle$. Notice that the thermal averages in (10.84) are *not* at zero external field ($\nu \neq 0$). The second term in equation (10.84) is directly given

by equation (10.75), which can be neglected as it leads to a second order contribution in $|\epsilon|$. The first term in turn may be straightforwardly derived with the aid of the following relation held by the partition function Z,

$$\frac{1}{Z}\frac{\partial^2 Z}{\partial \phi^2} = -\nu \sum_j \langle \hat{P}_j^{\phi} \rangle + \nu^2 \sum_{i,j} \langle \hat{X}_i^{\phi} \hat{X}_j^{\phi} \rangle. \tag{10.85}$$

The partition function Z is not expected to explicitly depend on the phase ϕ, hence we infer the following useful relation

$$\sum_{i,j} \langle \hat{P}_i^{\phi} \hat{P}_j^{\phi} \rangle = \sum_{i,j} \langle \hat{X}_i^{\phi} \hat{X}_j^{\phi} \rangle = \nu^{-1} \langle \sum_j \hat{P}_j^{\phi} \rangle. \tag{10.86}$$

On the other hand, the result (10.72) leads to

$$\sum_{i,j} \langle \hat{X}_i^{\bar{\phi}} \hat{X}_j^{\bar{\phi}} \rangle \approx \sum_{i,j} \langle \hat{P}_i^{\phi} \hat{P}_j^{\phi} \rangle. \tag{10.87}$$

Consequently, by putting together the relations (10.86), (10.75), (10.76) and (10.87), we readily find the QFI.

$$F_Q[\rho_{|\epsilon|}] = \frac{\left(\frac{\partial \langle \hat{P}_{\rm sum}^{\phi} \rangle}{\partial |\epsilon|}\right)^2}{\Delta^2 \langle \hat{P}_{\rm sum}^{\phi} \rangle} \approx \frac{2 n_0 N^2}{C_{\rm p} \kappa}, \tag{10.88}$$

$$F_Q[\rho_{\phi}] = \frac{\left(\frac{\partial \langle \hat{X}_{\rm sum}^{\bar{\phi}} \rangle}{\partial \delta \phi}\right)^2}{\Delta^2 \langle \hat{X}_{\rm sum}^{\bar{\phi}} \rangle} \approx \frac{2 n_0 N^2 |\epsilon|^2}{C_{\rm p} \kappa}. \tag{10.89}$$

Part V

Discussion of results

Chapter 11

Conclusions and outlook

11.1 Conclusions

In this thesis I have applied theoretical tools inspired in the field of condensed matter physics that have potential applications in the quantum simulation of models hosting topological order, and also the design of robust sensing schemes in quantum optical dissipative systems. Loosely speaking, we have seen that the use of symmetry principles in many-body systems helps us to understand and interpret topological effects in quantum simulation, and also diverse enhancements in precision for dissipative quantum sensing. Furthermore, criticality has been revealed as an ally for improving sensing schemes in dissipative environments. To be more specific, the main conclusions that can be drawn from the results presented are:

1. **Periodically driven systems may generate topological order:** It has been shown that proper arrangements of periodic driving fields acting on the Ising model produce effective spin-spin interactions that are directionally dependent. In this way we managed to effectively reproduce the quantum compass model on a square lattice, in which the interactions depend on the orientation of the bonds and the twofold ground state hosts topological order.

2. **Adiabatic preparation of topological phases may depend non-trivially on the system size**: for the quantum compass model, an analytical study concerning the adiabatic preparation of the ground state based on the system symmetries reveals that the adiabatic passage crucially depends on the parity

of the lattice size.

3. **Critical points of dissipative phase transitions are optimal points for sensing**: criticality has been established as a resource for sensing in dissipative systems . For the single qubit laser, the optimality of the lasing critical point is evidenced by the analytical and numerical results for both optimal and non-optimal measurement schemes. Specifically we analyzed the field quadratures and the number of bosons in the steady state, both showing higher quantum Fisher information as the critical point is approached ($C_p \to 1$). In networks of qubit lasers, only the optimal scheme (quadratures) was analyzed with the same result, and the extension for using the number of photons as observable would be almost straightforward.

4. **Active mediums and strong incoherent pumping may be used to enhance the precision in parameter estimation**: we may take advantage of an active medium (networks of qubit lasers) in two different ways with potential benefits for sensing. First, the precision in parameter estimation increases with the incoherent pumping γ acting on the qubit, with a quantum Fisher information that scales linearly $F_Q \propto \gamma$. Secondly, the range of correlations in N coupled qubit lasers can be extended in finite size systems so as to achieve long-range correlations that ultimately leads to a quantum Fisher information scaling quadratically with the number of probes $F_Q \propto N^2$.

5. **Networks of single qubit lasers can be mapped onto the classical XY model**: the steady state of a system consisting of a lattice of single qubit lasers that exchange photons through incoherent hopping can be mapped onto the classical XY model. The effective temperature is essentially regulated by the incoherent pumping γ and the proximity to the lasing critical point $C_{\mathrm{p}} = 1$, which allows the observation of the Kosterlitz-Thouless transition. This is valid in a regime of strong incoherent pumping $\gamma \gg 1$ where only the laser phases are relevant degrees of freedom. The dissipative exchange of photons between neighbouring qubit lasers can be implemented by means of an intermediate lossy cavity that is adiabatically eliminated.

6. **Spontaneous symmetry breaking as a resource for sensing**: the pres-

ence of spontaneous symmetry breaking (SSB) in a system can be understood as an advantage to increase the precision in parameter estimation when the measurement scheme coincides with the order parameter describing the symmetry breaking. In this thesis we have seen this idea in two different scenarios. First, for a single qubit laser the SSB of the lasing steady state occurs in the limit of large number of photons $n \to \infty$, which leads to a quantum Fisher information that scales with the system size $F_Q \propto n$. Second, for networks of N single qubit lasers in three dimensions, the steady state also experience SSB as we take the system size N into the thermodynamic limit $N \to \infty$, giving rise to a quantum Fisher information scaling quadratically with the system size $F_Q \propto N^2$. In both cases the optimal measurement schemes (field quadratures) coincide with the order parameter that characterize the SSB (the coherent component $\langle a \rangle$).

7. **Long-range correlations as a resource for sensing in dissipative systems**: I have shown that classical long-range correlations in quantum optical dissipative lattice systems produce an enhancement on the precision in parameter estimation. The capacity of a many-body system for hosting long-range order is limited by the Mermin-Wagner theorem, yet one may induce long-range correlations in finite systems by proper tuning of the parameters. In $2D$ lattices this tuning may be facilitated by the existence of topological defects and quasi-long range order, while in $3D$ one may naturally expect long-range order and SSB.

8. **A Heisenberg scaling with the number of probes may be achieved in models with nearest-neighbour interactions**: a main consequence of the previous point show that a Heisenberg scaling with the number of probes can be achieved in dissipative systems when there exists long-range correlations in finite systems, or long-range order in systems with SSB. These correlations are dynamically induced and they only assumed nearest-neighbour interactions between the probes, which is the normal scenario in quantum optical systems. In contrast to previous results [181–184] where the resources scale with N^2, here the resources scale with N. While previously long-range correlations have been introduced *a priori* by long-range interactions in closed systems,

here they are naturally developed by the system dynamics with short-range interactions.

11.2 Outlook

The results presented in this thesis pose interesting questions and invite to further research and applications of the results. Firstly, the use of periodically driven systems can be extended to the quantum simulation of additional models with intriguing topological properties, like topological insulators in trapped ions as proposed in [209]. Moreover, it is feasible to apply the same tools in the context of quantum optical dissipative systems to simulate possible dissipative topological quantum models. Some proposals of periodically driven dissipative systems have already indicated its potential benefits in this direction [86, 143].

Secondly, there is no reason to think that the general ideas of using criticality and symmetry breaking as a resource for sensing are exclusive of the system analyzed in this work. One could think of other systems in which the same working principles are displayed in the form of alternative dissipative phase transitions and order parameters. Conversely, one might use general symmetry principles as a guide to design a model where experimentally convenient observables coincide with the order parameter describing the symmetry breaking. Our experience now suggests that this sort of scheme is likely to become the optimal measurement scheme for estimating a certain system parameter. For example, while our results exploit the symmetry breaking of the underlying $U(1)$ global symmetry of the steady stete, one could think of other symmetry groups that could lead to advantageous schemes. A possibility is the symmetry breaking of certain spatio-temporal or time reversal symmetries that end in spatial patterns containing the information for the parameter estimation. Additionally, it might be interesting to extend criticality for dynamical quantum phase transitions [210, 211].

In this work we have explored the consequences of a dissipative-mediated interaction in a square lattice of single qubit lasers. However, alternative arrangements or interactions in the lattice system may also lead to new interesting models and phenomena for quantum sensing and quantum simulation. For example, if instead of

a dissipative (incoherent) coupling of the lasers the exchange of photons is given directly by a coherent hopping, we expect to find a net photonic current associated to a Josephson effect that can be used for estimating a phase difference between sites. Also, the combination of both incoherent and coherent hopping terms is expected to conceal interesting results for the study of quantum synchronization, as there could be a dissipative phase transition between a synchronized and desynchronized phase. It seems feasible to extend our results to the estimation of gradients of phases along the lattice, with potential applications in quantum imaging. Moreover, the formalism in phase space established to describe the dynamics invites to consider time-dependent Fokker-Planck equations, which could extend our ideas to estimation of static fields or frequencies. This might be a fertile land to exploit classical effects from statistical mechanics, such as stochastic resonance [212] or ratchet effects [213], in the light of quantum interactions and quantum noise.

Last, but not least, it is important to clarify how the use of interacting systems and non-linear strategies may lead or not to an overall advantage over previous schemes relying on quantum correlations, like in the Ramsey interferometer. It seems clear nowadays that in the case of a collection of non-interacting probes, quantum resources like entanglement (if used appropriately) lead to an enhancement in precision (Heisenberg scaling). In order to make meaningful comparisons in the most general case, this is, considering both interacting and non-interacting as well as quantum and classical correlations, one needs to take into account two factors at the same time: spatial resources, like the number of probes, and time resources, particularly the time it takes the system to acquire the information of the parameter to estimate. In our scheme, that would involve the need to consider the transient times before reaching the steady state.

Bibliography

[1] Andrea De Mauro, Marco Greco, and Michele Grimaldi. A formal definition of Big Data based on its essential features. *Libr. Rev.*, 65(3):122–135, 2016.

[2] Gyu Myoung Lee, Noel Crespi, Jun Kyun Choi, and Matthieu Boussard. *Internet of Things*, volume 12. Springer, 2013.

[3] Stuart Russell and Peter Norving. Artificial intelligence: A modern approach. 2005.

[4] A. Galindo and M. A. Martín-Delgado. Information and computation: Classical and quantum aspects. *Rev. Mod. Phys.*, 74(2):347–423, 2002.

[5] Michael A. Nielsen and Issac L. Chuang. Quantum Computation and Quantum Information, 2011.

[6] P Goy, J M Raimond, M Gross, and S Haroche. Observation of cavity enhanced single atom spontaneous emission . *Phys. Rev. Lett.*, 50(24):1903–1907, 1983.

[7] Jean-Michel Raimond, M Brune, and Serge Haroche. Manipulating quantum entanglement with atoms and photons. *Rev. Mod. Phys.*, 73(3):1–18, 2001.

[8] Serge Haroche. Controlling photons in a box and exploring the quantum to classical boundary. *Ann. Phys.*, 525(10-11):753–776, 2013.

[9] M Brune, J M Raimond, F Schmidt-Kaler, A Maali, J Dreyer, E Hagley, and S Haroche. Quantum Rabi nutation in vacuum and coherent fields: a direct test of field quantization in a cavity. *Summ. Pap. Present. Quantum Electron. Laser Sci. Conf.*, 76(11):2–5, 1996.

[10] Carl E. Wieman, David E. Pritchard, and David J. Wineland. Atom cooling, trapping, and quantum manipulation. *Rev. Mod. Phys.*, 71(2):S253–S262, 1999.

[11] D. Leibfried, R. Blatt, C. Monroe, and D. Wineland. Quantum dynamics of single trapped ions. *Rev. Mod. Phys.*, 75(1):281–324, 2003.

[12] David J Wineland. Nobel Lecture: Superposition, entanglement, and raising Schrödinger's cat. *Rev. Mod. Phys.*, 85(3):1103, 2013.

[13] R. Blatt and C. F. Roos. Quantum simulations with trapped ions. *Nat. Phys.*, 8(4):277–284, 2012.

[14] Immanuel Bloch, Jean Dalibard, and Wilhelm Zwerger. Many-body physics with ultracold gases. *Rev. Mod. Phys.*, 80(3):885–964, 2008.

[15] Thilo Stöferle, Henning Moritz, Christian Schori, Michael Köhl, and Tilman Esslinger. Transition from a strongly interacting 1D superfluid to a Mott insulator. *Phys. Rev. Lett.*, 92(13):130403, 2004.

[16] Rudolf Grimm, Matthias Weidemüller, and Yurii B. Ovchinnikov. Optical Dipole Traps for Neutral Atoms. *Adv. At. Mol. Opt. Phys.*, 42(C):95–170, 2000.

[17] Dario Gil. The future is quantum - IBM Blog Research, 2017.

[18] Miguel Herrero-Collantes and Juan Carlos Garcia-Escartin. Quantum random number generators. *Rev. Mod. Phys.*, 89(1):015004, feb 2017.

[19] Davide Castelvecchi and Others. Quantum cloud goes commercial, 2017.

[20] Paul Marks. Quantum cryptography to protect Swiss election. *New Sci.*, 2007.

[21] Nicolas Gisin, Grégoire Ribordy, Wolfgang Tittel, and Hugo Zbinden. Quantum cryptography. *Rev. Mod. Phys.*, 74(1):145–195, mar 2002.

[22] Elizabeth Gibney. Billion-euro boost for quantum tech, 2016.

[23] P. John K. Bongs, V. Boyer, M. A. Cruise, A. Freise, M. Holynski, J. Hughes, A. Kaushik, Y.-H. Lien, A. Niggebaum, M. Perea-Ortiz, P. Petrov, S. Plant,

Y. Singh, A. Stabrawa, D. J. Paul, M. Sorel, D. R. S. Cumming, J. H. Marsh, R. W. Bowtell, M. G. Bason, R. P. B. UK National Quantum Technology Hub in Sensors and Metrology. In Jürgen Stuhler and Andrew J. Shields, editors, *UK Natl. Quantum Technol. Program.*, volume 9900, page 990009. SPIE, International Society for Optics and Photonics, jun 2015.

[24] C. W. Chou, D. B. Hume, J. C.J. Koelemeij, D. J. Wineland, and T. Rosenband. Frequency comparison of two high-accuracy Al+ optical clocks. *Phys. Rev. Lett.*, 104(7):70802, 2010.

[25] Vittorio Giovannetti, Seth Lloyd, and Lorenzo Maccone. Quantum Enhanced Measurement: Beating the Standard Quantum Limit. *Sci.*, 306(November):1330–6, 2004.

[26] Axel André, A S Sørensen, and M D Lukin. Stability of Atomic Clocks Based on Entangled Atoms. *Phys. Rev. Lett.*, 92(23):4, 2008.

[27] M Jarzyna and J Kołodyński. Quantum limits in optical interferometry. *Prog. Opt.*, 60:345–435, 2003.

[28] S. Abend, M. Gebbe, M. Gersemann, H. Ahlers, H. Müntinga, E. Giese, N. Gaaloul, C. Schubert, C. Lämmerzahl, W. Ertmer, W. P. Schleich, and E. M. Rasel. Atom-chip fountain gravimeter. *Phys. Rev. Lett.*, 117(20):1–7, 2016.

[29] J. F. Barry, M. J. Turner, J. M. Schloss, D. R. Glenn, Y. Song, M. D. Lukin, H. Park, and R. L. Walsworth. Optical magnetic detection of single-neuron action potentials using quantum defects in diamond. *Proc. Natl. Acad. Sci.*, 113(49):14133–14138, 2016.

[30] S. Stringari. Superfluid gyroscope with cold atomic gases. *Phys. Rev. Lett.*, 86(21):4725–4728, 2001.

[31] E. Hodby, S. A. Hopkins, G. Hechenblaikner, N. L. Smith, and C. J. Foot. Experimental observation of a superfluid gyroscope in a dilute bose-einstein condensate. *Phys. Rev. Lett.*, 91(9):090403, 2003.

[32] J. M. Taylor, P. Cappellaro, L. Childress, L. Jiang, D. Budker, P. R. Hemmer, A. Yacoby, R. Walsworth, and M. D. Lukin. High-sensitivity diamond magnetometer with nanoscale resolution. *Nat. Phys.*, 4(10):810–816, 2008.

[33] Mikhail I. Kolobov. *Quantum imaging.* Springer Science & Business Media, 2007.

[34] G. Brida, M. Genovese, and I. Ruo Berchera. Experimental realization of sub-shot-noise quantum imaging. *Nat. Photonics*, 4(4):227–230, 2010.

[35] C. Simon, M. Afzelius, J. Appel, A. Boyer de la Giroday, S. J. Dewhurst, N. Gisin, C. Y. Hu, F. Jelezko, S. Kröll, J. H. Müller, J. Nunn, E. S. Polzik, J. G. Rarity, H. De Riedmatten, W. Rosenfeld, A. J. Shields, N. Sköld, R. M. Stevenson, R. Thew, I. A. Walmsley, M. C. Weber, H. Weinfurter, J. Wrachtrup, and R. J. Young. Quantum memories. *Eur. Phys. J. D*, 58(1):1–22, may 2010.

[36] Félix Bussières, Nicolas Sangouard, Mikael Afzelius, Hugues De Riedmatten, Christoph Simon, and Wolfgang Tittel. Prospective applications of optical quantum memories. *J. Mod. Opt.*, 60(18):1519–1537, 2013.

[37] P.W. Shor. Algorithms for quantum computation: discrete logarithms and factoring. In *Proc. 35th Annu. Symp. Found. Comput. Sci.*, pages 124–134. Ieee, 1994.

[38] Lov K. Grover. A fast quantum mechanical algorithm for database search. In *Proc. twenty-eighth Annu. ACM Symp. Theory Comput. - STOC '96*, pages 212–219. ACM, 1996.

[39] J. Ignacio Cirac and Peter Zoller. Goals and opportunities in quantum simulation. *Nat. Phys.*, 8(4):264–266, 2012.

[40] I. M. Georgescu, S. Ashhab, and Franco Nori. Quantum simulation. *Rev. Mod. Phys.*, 86(1):153–185, mar 2014.

[41] M. Schuld, I. Sinayskiy, and F. Petruccione. An introduction to quantum machine learning. *Contemp. Phys.*, 56(2), 2014.

[42] Maria Schuld, Ilya Sinayskiy, and Francesco Petruccione. The quest for a Quantum Neural Network. *Quantum Inf. Process.*, 13(11):2567–2586, 2014.

[43] Vittorio Giovannetti, Seth Lloyd, and Lorenzo MacCone. Advances in quantum metrology. *Nat. Photonics*, 5(4):222–229, 2011.

[44] D. A. Lidar and Todd A. Brun. *Quantum error correction*. Cambridge University Press, 2013.

[45] J. J. Sakurai. Modern Quantum Mechanics, Revised Edition, 1995.

[46] R. J. Schoelkopf and S. M. Girvin. Wiring up quantum systems. *Nature*, 451(7179):664–669, 2008.

[47] Andrew A. Houck, Hakan E. Türeci, and Jens Koch. On-chip quantum simulation with superconducting circuits. *Nat. Phys.*, 8(4):292–299, apr 2012.

[48] Sei Suzuki, Jun-ichi Inoue, and Bikas K Chakrabarti. *Quantum Ising Phases and Transitions in Transverse Ising Models*, volume 862. Springer, 2013.

[49] Zohar Nussinov and Jeroen Van Den Brink. Compass models: Theory and physical motivations. *Rev. Mod. Phys.*, 87(1), 2015.

[50] Alexei Kitaev. Anyons in an exactly solved model and beyond. *Ann. Phys. (N. Y).*, 321(1):2–111, 2006.

[51] Kliment I Kugel' and D I Khomski. The Jahn-Teller effect and magnetism: transition metal compounds. *Sov. Phys. Uspekhi*, 25(4):231–256, 1982.

[52] Henrik Bruus and Karsten Flensberg. *Many-Body Quantum Theory in Condensed Matter Physics: An Introduction*. Oxford University Press, 2004.

[53] Michael J. Hartmann, Fernando G.S.L. Brandão, and Martin B. Plenio. Quantum many-body phenomena in coupled cavity arrays. *Laser Photonics Rev.*, 2(6):527–556, 2008.

[54] Leonard Mandel and Emil Wolf. *Optical Coherence and Quantum Optics*. Cambridge university press, 1995.

[55] Kerson Huang. *Introduction to Statistical Physics*. CRC press, 2001.

[56] H P Carmichael. *Statistical Methods in Quantum Optics: Master equations and Fokker-Planck equations*. Springer, 1998.

[57] Daniel Adam Steck. Quantum and atom optics. 2007.

[58] Ian Stewart and Martin Golubitsky. *Fearful symmetry: is God a geometer?* Courier Corporation, 2010.

[59] Guillermo Velarde. *Mecánica Cuántica*. Universidad Politécnica de Madrid, Escuela técnica superior de ingenieros industriales, Sección de publicaciones, 2004.

[60] Pedro Nevado and Diego Porras. Rabi Lattice models with discrete gauge symmetry: phase diagram and implementation in trapped ion quantum simulators. *Phys. Rev. A*, 013624(1):1–10, 2015.

[61] H.-P Breuer and F Pettruccione. *The Theory of Open Quantum Systems*. Oxford, 2006.

[62] R. Islam, C. Senko, W. C. Campbell, S. Korenblit, J. Smith, A. Lee, E. E. Edwards, C. C.J. Wang, J. K. Freericks, and C. Monroe. Emergence and frustration of magnetism with variable-range interactions in a quantum simulator. *Science (80-.).*, 340(6132):583–587, 2013.

[63] M. Born and R. Oppenheimer. Zur Quantentheorie der Molekeln. *Ann. Phys.*, 389(20):457–484, 1927.

[64] Subir Sachdev. *Quantum Phase Transitions*. Cambridge University Press, 2011.

[65] Markus Greiner, Olaf Mandel, Tilman Esslinger, TW Hänsch, and Immanuel Bloch. Quantum phase transition from a super fluid to a Mott insulator in a gas of ultracold atoms. *Nature*, 415(6867):39–44, 2002.

[66] J J Binney, N J Dowrick, A J Fisher, and M Newman. *The Theory of Critical Phenomena: An Introduction to the Renormalization Group*. Oxford University Press, Inc., 1992.

[67] Steven Strogatz. *Nonlinear dynamics and chaos: with applications to physics, biology, chemistry, and engineering*. CRC Press, 2018.

[68] C C Lin and Frank H Shu. On the spiral structure of disk galaxies. In *Sel. Pap. CC Lin with Comment. Vol. 1 Fluid Mech. Vol. 2 Astrophys.* World Scientific, 1987.

[69] A. V. Getling. *Rayleigh-Benard convection : structures and dynamics*. World Scientific, 1998.

[70] A Brandstater and Harry L Swinney. Strange attractors in weakly turbulent Couete-Taylor flow. *Phys. Rev. A*, 35(5):2207, 1987.

[71] Darcy Wentworth and others Thompson. *On growth and form*. Cambridge Univ. Press, 1942.

[72] N D Mermin and H Wagner. Absence of ferromagnetism or antiferromagnetism in one- or two- dimensional isotropic Heisemberg models. *Phys. Rev. Lett.*, 17(22):1133–1136, 1966.

[73] Zohar Nussinov and Gerardo Ortiz. A symmetry principle for topological quantum order. *Ann. Phys. (N. Y).*, 324(5):977–1057, 2009.

[74] Horst L. Stormer, Daniel C. Tsui, and Arthur C. Gossard. The fractional quantum Hall effect. *Rev. Mod. Phys.*, 71(2):S298–S305, 1999.

[75] Kosterlitz J. M.; Thouless D. J. Ordering, metastability and phase transitions in two-dimensional systems. *J. Phys. C Solid State Phys.*, 6(7):1181, 1973.

[76] Gerard Milburn. *Quantum Optics*. Cambridge university press, 2007.

[77] Hermann. Haken. *Laser Theory*. Springer Berlin Heidelberg, 1983.

[78] Yoshihisa Yamamoto and Atac Imamoglu. *Mesoscopic Quantum Optics*. John Wiley and Sons, 1999.

[79] J F Scott, M Sargent, and C D Cantrell. Laser-phase transition analogy: Application to first-order transitions. *Opt. Commun.*, 15(1):13–16, 1975.

[80] Matthias Troyer and Uwe-Jens Wiese. Computational complexity and fundamental limitations to fermionic quantum Monte Carlo simulations. *Phys. Rev. lett.*, 94(17):170201, 2004.

[81] Richard P Feynman, Pinchas Birnbaum, and Eran Tromer. Simulating Physics with Computers. *Int. J. Theor. Phys.*, 21(6):467–488, 1982.

[82] D. Porras and J. I. Cirac. Effective quantum spin systems with ion traps. *Phys. Rev. Lett.*, 92(20):207901, 2004.

[83] André Eckardt, Christoph Weiss, and Martin Holthaus. Superfluid-insulator transition in a periodically driven optical lattice. *Phys. Rev. Lett.*, 95(26):260404, 2005.

[84] Alejandro Bermudez, Tobias Schaetz, and Diego Porras. Synthetic gauge fields for vibrational excitations of trapped ions. *Phys. Rev. Lett.*, 107(15):150501, 2011.

[85] Alejandro Bermudez, Tobias Schaetz, and Diego Porras. Photon-assisted-tunneling toolbox for quantum simulations in ion traps. *New J. Phys.*, 14(5):053049, 2012.

[86] Carlos Navarrete-Benlloch, Juan José García-Ripoll, and Diego Porras. Inducing nonclassical lasing via periodic drivings in circuit quantum electrodynamics. *Phys. Rev. Lett.*, 113(19):193601, 2014.

[87] Ch Schneider, Diego Porras, Tobias Schaetz, Tobias Schaetz, Chris R Monroe, and Tilman Esslinger. Experimental quantum simulations of many-body physics with trapped ions. *New J. Phys.*, 15(15):24401, 2013.

[88] Govinda Clos, Diego Porras, Ulrich Warring, and Tobias Schaetz. Time-Resolved Observation of Thermalization in an Isolated Quantum System. *Phys. Rev. Lett.*, 117(17):170401, 2016.

[89] C. E. Creffield and G. Sierra. Finding zeros of the Riemann zeta function by periodic driving of cold atoms. *Phys. Rev. A*, 91(6):063608, 2015.

[90] Iulia Buluta and Franco Nori. Quantum simulators. *Science (80-.).*, 326(5949):108–111, 2009.

[91] A. Friedenauer, H. Schmitz, J. T. Glueckert, D. Porras, and T. Schaetz. Simulating a quantum magnet with trappedions. *Nat. Phys.*, 4(10):757–761, 2008.

[92] JJ García-Ripoll and JI Cirac. Spin dynamics for bosons in an optical lattice. *New J. Phys.*, 76(1):76, 2003.

[93] D. Porras, F. Marquardt, J. Von Delft, and J. I. Cirac. Mesoscopic spin-boson models of trapped ions. *Phys. Rev. A*, 78(1), 2008.

[94] C. L. Degen, F. Reinhard, and P. Cappellaro. Quantum sensing. *Rev. Mod. Phys.*, 89(3):035002, jul 2017.

[95] Marcin Zwierz, Carlos A. Perez-Delgado, and P Kok. Optimality of the Heisenberg limit for continuous-variable quantum metrology. *Phys. Rev. Lett.*, 105(18):4, 2010.

[96] Marcin Zwierz, Carlos A. Pérez-Delgado, and Pieter Kok. Ultimate limits to quantum metrology and the meaning of the Heisenberg limit. *Phys. Rev. A*, 85(4):042112, 2012.

[97] M. Napolitano, M. Koschorreck, B. Dubost, N. Behbood, R. J. Sewell, and M. W. Mitchell. Interaction-based quantum metrology showing scaling beyond the Heisenberg limit. *Nature*, 471(7339):486–489, 2011.

[98] Peter W. Shor. Scheme for reducing decoherence in quantum computer memory. *Phys. Rev. A*, 52(4):R2493, 1995.

[99] A. Yu Kitaev. Fault-tolerant quantum computation by anyons. *Ann. Phys. (N. Y).*, 303(1):2–30, 2003.

[100] B. Douçot and L. B. Ioffe. Physical implementation of protected qubits. *Reports Prog. Phys.*, 75(7):072001, 2012.

[101] B. Doucot, M. V. Feigel'man, L. B. Ioffe, and a. S. Ioselevich. Protected Qubits and Chern Simons theories in Josephson Junction Arrays. *Physics (College. Park. Md).*, 71(2):20, 2004.

[102] Julien Dorier, Federico Becca, and Frédéric Mila. Quantum compass model on the square lattice. *Phys. Rev. B*, 72(2):024448, 2005.

[103] Han-Dong Chen, Chen Fang, Jiangping Hu, and Hong Yao. Quantum phase transition in the quantum compass model. *Phys. Rev. B*, 75(14):144401, 2007.

[104] Román Orús, Andrew C. Doherty, and Guifré Vidal. First order phase transition in the anisotropic quantum orbital compass model. *Phys. Rev. Lett.*, 102(7):077203, 2009.

[105] Sergey Gladchenko, David Olaya, Eva Dupont-Ferrier, Benoit Douçot, Lev B. Ioffe, and Michael E. Gershenson. Superconducting nanocircuits for topologically protected qubits. *Nat. Phys.*, 5(1):48–53, 2009.

[106] L. M. Duan, E. Demler, and M. D. Lukin. Controlling Spin Exchange Interactions of Ultracold Atoms in Optical Lattices. *Phys. Rev. Lett.*, 91(9):090402, 2003.

[107] Jonathan Simon, Waseem S. Bakr, Ruichao Ma, M. Eric Tai, Philipp M. Preiss, and Markus Greiner. Quantum Simulation of Antiferromagnetic Spin Chains in an Optical Lattice. *Nature*, 472(7343):307, 2011.

[108] J. Struck, M. Weinberg, C. Ölschläger, P. Windpassinger, J. Simonet, K. Sengstock, R. Höppner, P. Hauke, A. Eckardt, M. Lewenstein, and L. Mathey. Engineering Ising-XY spin-models in a triangular lattice using tunable artificial gauge fields. *Nat. Phys.*, 9(11):738–743, 2013.

[109] Hendrik Weimer, Markus Müller, Igor Lesanovsky, Peter Zoller, and Hans Peter Büchler. A Rydberg quantum simulator. *Nat. Phys.*, 6(5):382–388, 2010.

[110] Alpha Gaëtan, Yevhen Miroshnychenko, Tatjana Wilk, Amodsen Chotia, Matthieu Viteau, Daniel Comparat, Pierre Pillet, Antoine Browaeys, and Philippe Grangier. Observation of collective excitation of two individual atoms in the Rydberg blockade regime. *Nat. Phys.*, 5(2):115–118, 2009.

[111] M. Viteau, M. G. Bason, J. Radogostowicz, N. Malossi, D. Ciampini, O. Morsch, and E. Arimondo. Rydberg excitations in Bose-Einstein condensates in quasi-one-dimensional potentials and optical lattices. *Phys. Rev. Lett.*, 107(6):060402, 2011.

[112] Alexander W. Glaetzle, Marcello Dalmonte, Rejish Nath, Christian Gross, Immanuel Bloch, and Peter Zoller. Designing frustrated quantum magnets with laser-dressed Rydberg atoms. *Phys. Rev. Lett.*, 114(17):173002, 2015.

[113] Olaf Mandel, Markus Greiner, Artur Widera, Tim Rom, Theodor W. Hänsch, and Immanuel Bloch. Coherent Transport of Neutral Atoms in Spin-Dependent Optical Lattice Potentials. *Phys. Rev. Lett.*, 91(1):010407, 2003.

[114] Philipp Hauke, Olivier Tieleman, Alessio Celi, Christoph Ölschläger, Juliette Simonet, Julian Struck, Malte Weinberg, Patrick Windpassinger, Klaus Sengstock, Maciej Lewenstein, and André Eckardt. Non-Abelian gauge fields and topological insulators in shaken optical lattices. *Phys. Rev. Lett.*, 109(14):145301, 2012.

[115] J. Struck, C. Olschläger, M. Weinberg, P. Hauke, J. Simonet, A. Eckardt, M. Lewenstein, K. Sengstock, and P. Windpassinger. Tunable gauge potential for neutral and spinless particles in driven optical lattices. *Phys. Rev. Lett.*, 108(22):225304, 2012.

[116] M. Aidelsburger, M. Atala, M. Lohse, J. T. Barreiro, B. Paredes, and I. Bloch. Realization of the hofstadter hamiltonian with ultracold atoms in optical lattices. *Phys. Rev. Lett.*, 111(18):185301, 2013.

[117] Hirokazu Miyake, Georgios A. Siviloglou, Colin J. Kennedy, William Cody Burton, and Wolfgang Ketterle. Realizing the harper hamiltonian with laser-assisted tunneling in optical lattices. *Phys. Rev. Lett.*, 111(18):185302, 2013.

[118] N. Goldman, G. Juzeliunas, P. Öhberg, and I. B. Spielman. Light-induced gauge fields for ultracold atoms. *Reports Prog. Phys.*, 77(12):126401, 2014.

[119] Alejandro Bermudez and Diego Porras. Interaction-dependent photon-assisted

tunneling in optical lattices: A quantum simulator of strongly-correlated electrons and dynamical Gauge fields. *New J. Phys.*, 17(10):103021, 2015.

[120] M. Aidelsburger, M. Lohse, C. Schweizer, M. Atala, J. T. Barreiro, S. Nascimbène, N. R. Cooper, I. Bloch, and N. Goldman. Measuring the Chern number of Hofstadter bands with ultracold bosonic atoms. *Nat. Phys.*, 11(2):162–166, 2015.

[121] J. Almeida, P. C. De Groot, S. F. Huelga, A. M. Liguori, and M. B. Plenio. Probing quantum coherence in qubit arrays. *J. Phys. B At. Mol. Opt. Phys.*, 46(10):104002, 2013.

[122] Wen Long You, Guang Shan Tian, and Hai Qing Lin. The low-energy states and directional long-range order in the two-dimensional quantum compass model. *J. Phys. A Math. Theor.*, 43(27):275001, 2010.

[123] M. S. Sarandy, L. A. Wu, and D. A. Lidar. Consistency of the adiabatic theorem. *Quantum Inf. Process.*, 3(6):331–349, 2004.

[124] S. Trotzky, P. Cheinet, S. Fölling, M. Feld, U. Schnorrberger, A. M. Rey, A. Polkovnikov, E. A. Demler, M. D. Lukin, and I. Bloch. Time-resolved observation and control of superexchange interactions with ultracold atoms in optical lattices. *Science (80-.).*, 319(5861):295–299, 2008.

[125] S. Nascimbène, Y. A. Chen, M. Atala, M. Aidelsburger, S. Trotzky, B. Paredes, and I. Bloch. Experimental realization of plaquette resonating valence-bond states with ultracold atoms in optical superlattices. *Phys. Rev. Lett.*, 108(20):205301, 2012.

[126] Takeshi Fukuhara, Adrian Kantian, Manuel Endres, Marc Cheneau, Peter Schauß, Sebastian Hild, David Bellem, Ulrich Schollwöck, Thierry Giamarchi, Christian Gross, Immanuel Bloch, and Stefan Kuhr. Quantum dynamics of a mobile spin impurity. *Nat. Phys.*, 9(4):235–241, 2013.

[127] Diego Porras, Peter A. Ivanov, and Ferdinand Schmidt-Kaler. Quantum simulation of the cooperative Jahn-Teller transition in 1D ion crystals. *Phys. Rev. Lett.*, 108(23):235701, 2012.

[128] Fernando Quijandría, Diego Porras, Juan José García-Ripoll, and David Zueco. Circuit QED bright source for chiral entangled light based on dissipation. *Phys. Rev. Lett.*, 111(7):073602, 2013.

[129] Carlton M. Caves. Quantum-mechanical noise in an interferometer. *Phys. Rev. D*, 23(8):1693–1708, 1981.

[130] Samuel L. Braunstein and Carlton M. Caves. Statistical distance and the geometry of quantum states. *Phys. Rev. Lett.*, 72(22):3439–3443, 1994.

[131] B. C. Sanders and G. J. Milburn. Optimal quantum measurements for phase estimation. *Phys. Rev. Lett.*, 75(16):2944–2947, 1995.

[132] Wayne M Itano, D J Wineland, and D J Heinzen. Optimal frequency measurements with maximally correlated sources. *Phys. Rev. A*, 54(6):4649–4652, 1996.

[133] S. F. Huelga, C. Macchiavello, T. Pellizzari, A. K. Ekert, M. B. Plenio, and J. I. Cirac. Improvement of frequency standards with quantum entanglement. *Phys. Rev. Lett.*, 79(20):3865–3868, 1997.

[134] B. M. Escher, R. L. De Matos Filho, and L. Davidovich. General framework for estimating the ultimate precision limit in noisy quantum-enhanced metrology. *Nat. Phys.*, 7(5):406–411, 2011.

[135] Rafał Demkowicz-Dobrzański, Jan Kołodyński, and Madalin Gua. The elusive Heisenberg limit in quantum-enhanced metrology. *Nat. Commun.*, 3(1):1063, 2012.

[136] Alex W. Chin, Susana F. Huelga, and Martin B. Plenio. Quantum metrology in non-markovian environments. *Phys. Rev. Lett.*, 109(23):233601, 2012.

[137] Andrea Smirne, Jan Kołodyński, Susana F. Huelga, and Rafał Demkowicz-Dobrzański. Ultimate precision limits for noisy frequency estimation. *Phys. Rev. Lett.*, 116(12):120801, 2016.

[138] J. Majer, J. M. Chow, J. M. Gambetta, Jens Koch, B. R. Johnson, J. A. Schreier, L. Frunzio, D. I. Schuster, A. A. Houck, A. Wallraff, A. Blais, M. H.

Devoret, S. M. Girvin, and R. J. Schoelkopf. Coupling superconducting qubits via a cavity bus. *Nature*, 449(7161):443–447, 2007.

[139] M. H. Devoret and R. J. Schoelkopf. Superconducting circuits for quantum information: An outlook. *Science (80-.).*, 339(6124):1169–1174, 2013.

[140] Frank Verstraete, Michael M. Wolf, and J. Ignacio Cirac. Quantum computation and quantum-state engineering driven by dissipation. *Nat. Phys.*, 5(9):633–636, 2009.

[141] Julio T. Barreiro, Markus Müller, Philipp Schindler, Daniel Nigg, Thomas Monz, Michael Chwalla, Markus Hennrich, Christian F. Roos, Peter Zoller, and Rainer Blatt. An open-system quantum simulator with trapped ions. *Nature*, 470(7335):486–491, 2011.

[142] Emanuele G. Dalla Torre, Johannes Otterbach, Eugene Demler, Vladan Vuletic, and Mikhail D. Lukin. Dissipative preparation of spin squeezed atomic ensembles in a steady state. *Phys. Rev. Lett.*, 110(12):120402, 2013.

[143] Alejandro González-Tudela and Diego Porras. Mesoscopic entanglement induced by spontaneous emission in solid-state quantum optics. *Phys. Rev. Lett.*, 110(8):080502, 2013.

[144] Paolo Zanardi, Matteo G.A. Paris, and Lorenzo Campos Venuti. Quantum criticality as a resource for quantum estimation. *Phys. Rev. A*, 78(4):042105, 2008.

[145] Teng Long Wang, Ling Na Wu, Wen Yang, Guang Ri Jin, Neill Lambert, and Franco Nori. Quantum Fisher information as a signature of the superradiant quantum phase transition. *New J. Phys.*, 16(6):063039, 2014.

[146] Giulio Salvatori, Antonio Mandarino, and Matteo G.A. Paris. Quantum metrology in Lipkin-Meshkov-Glick critical systems. *Phys. Rev. A*, 90(2):022111, 2014.

[147] Katarzyna Macieszczak, Mdlin Gu, Igor Lesanovsky, and Juan P. Garrahan. Dynamical phase transitions as a resource for quantum enhanced metrology. *Phys. Rev. A*, 93(2):022103, 2016.

[148] Klaus Mølmer. Optical coherence: A convenient fiction. *Phys. Rev. A*, 55(4):3195–3203, apr 1997.

[149] V. Degiorgio and Marlan O. Scully. Analogy between the laser threshold region and a second-order phase transition. *Phys. Rev. A*, 2(4):1170–1177, oct 1970.

[150] Li Tuo Shen, Zhen Biao Yang, Huai Zhi Wu, and Shi Biao Zheng. Quantum phase transition and quench dynamics in the anisotropic Rabi model. *Phys. Rev. A*, 95(1):013819, 2017.

[151] Gian-Carlo Rota. *Handbook of stochastic methods*, volume 55. Springer Berlin, 1985.

[152] H. Haken. Cooperative phenomena in systems far from thermal equilibrium and in nonphysical systems. *Rev. Mod. Phys.*, 47(1):67–121, 1975.

[153] Jonathan P. Dowling and Kaushik P. Seshadreesan. Quantum optical technologies for metrology, sensing and imaging. *J. Light. Technol.*, 33(12):2359–2370, 2014.

[154] Samuel L. Braunstein, Carlton M. Caves, and G. J. Milburn. Generalized uncertainty relations: Theory, examples, and Lorentz invariance. *Ann. Phys. (N. Y).*, 247(1):135–173, 1996.

[155] Alex Monras. Phase space formalism for quantum estimation of Gaussian states. *arXiv:1303.3682*, 2013.

[156] N. Poli, C. W. Oates, P. Gill, and G. M. Tino. Optical atomic clocks. *Riv. del Nuovo Cim.*, 36(12):555–624, 2013.

[157] K. Vahala, M. Herrmann, S. Knünz, V. Batteiger, G. Saathoff, T. W. Hänsch, and Th Udem. A phonon laser. *Nat. Phys.*, 5(9):682–686, 2009.

[158] J Mckeever, A Boca, A D Boozer, J R Buck, and H J Kimble. Experimental realization of a one atom laser in the regime of strong coupling. *Nature*, 425(6955):268, 2003.

[159] O. Astafiev, K. Inomata, A. O. Niskanen, T. Yamamoto, Yu A. Pashkin, Y. Nakamura, and J. S. Tsai. Single artificial-atom lasing. *Nature*, 449(7162):588–590, 2007.

[160] Julian Hauss, Arkady Fedorov, Carsten Hutter, Alexander Shnirman, and Gerd Schön. Single-qubit lasing and cooling at the rabi frequency. *Phys. Rev. Lett.*, 100(3):037003, 2008.

[161] Ivan S. Grudinin, Hansuek Lee, O. Painter, and Kerry J. Vahala. Phonon laser action in a tunable two-level system. *Phys. Rev. Lett.*, 104(8):083901, 2010.

[162] Michael J. Biercuk, Hermann Uys, Joe W. Britton, Aaron P. Vandevender, and John J. Bollinger. Ultrasensitive detection of force and displacement using trapped ions. *Nat. Nanotechnol.*, 5(9):646–650, 2010.

[163] Sydney Schreppler, Nicolas Spethmann, Nathan Brahms, Thierry Botter, Maryrose Barrios, and Dan M. Stamper-Kurn. Optically measuring force near the standard quantum limit. *Science (80-.).*, 344(6191):1486–1489, 2014.

[164] Peter A. Ivanov, Kilian Singer, Nikolay V. Vitanov, and Diego Porras. Quantum sensors assisted by spontaneous symmetry breaking for detecting very small forces. *Phys. Rev. Appl.*, 4(5):054007, 2015.

[165] Ravid Shaniv and Roee Ozeri. Quantum lock-in force sensing using optical clock Doppler velocimetry. *Nat. Commun.*, 8:14157, feb 2017.

[166] M. D. Barrett, B. DeMarco, T. Schaetz, V. Meyer, D. Leibfried, J. Britton, J. Chiaverini, W. M. Itano, B. Jelenković, J. D. Jost, C. Langer, T. Rosenband, and D. J. Wineland. Sympathetic cooling of 9 Be + and 24 Mg + for quantum logic. *Phys. Rev. A*, 68(4):042302, oct 2003.

[167] D. Porras and J. I. Cirac. Bose-Einstein Condensation and Strong-Correlation Behavior of Phonons in Ion Traps. *Phys. Rev. Lett.*, 93(26):263602, dec 2004.

[168] Shinsuke Haze, Yusuke Tateishi, Atsushi Noguchi, Kenji Toyoda, and Shinji Urabe. Observation of phonon hopping in radial vibrational modes of trapped ions. *Phys. Rev. A*, 85(3):031401, 2012.

[169] D. Kielpinski, B. E. King, C. J. Myatt, C. A. Sackett, Q. A. Turchette, W. M. Itano, C. Monroe, D. J. Wineland, and W. H. Zurek. Sympathetic cooling of trapped ions for quantum logic. *Phys. Rev. A - At. Mol. Opt. Phys.*, 61(3):8, 2000.

[170] Takafumi Ono and Holger F. Hofmann. Effects of photon losses on phase estimation near the Heisenberg limit using coherent light and squeezed vacuum. *Phys. Rev. A*, 81(3):033819, 2010.

[171] Seth Lloyd. Enhanced sensitivity of photodetection via quantum illumination. *Science (80-.).*, 321(5895):1463–1465, 2008.

[172] E. D. Lopaeva, I. Ruo Berchera, I. P. Degiovanni, S. Olivares, G. Brida, and M. Genovese. Experimental realization of quantum illumination. *Phys. Rev. Lett.*, 110(15):153603, 2013.

[173] M. Sanz, U. Las Heras, J. J. García-Ripoll, E. Solano, and R. Di Candia. Quantum Estimation Methods for Quantum Illumination. *Phys. Rev. Lett.*, 118(7):1–8, 2017.

[174] Quntao Zhuang, Zheshen Zhang, and Jeffrey H. Shapiro. Optimum Mixed-State Discrimination for Noisy Entanglement-Enhanced Sensing. *Phys. Rev. Lett.*, 118(4):040801, jan 2017.

[175] E. M. Kessler, I. Lovchinsky, A. O. Sushkov, and M. D. Lukin. Quantum error correction for metrology. *Phys. Rev. Lett.*, 112(15):1–8, 2014.

[176] G. Arrad, Y. Vinkler, D. Aharonov, and A. Retzker. Increasing sensing resolution with error correction. *Phys. Rev. Lett.*, 112(15):150801, 2014.

[177] Samuel Fernández-Lorenzo and Diego Porras. Quantum sensing close to a dissipative phase transition: Symmetry breaking and criticality as metrological resources. *Phys. Rev. A*, 96(1):013817, 2017.

[178] Meghana Raghunandan, Jörg Wrachtrup, and Hendrik Weimer. High-Density Quantum Sensing with Dissipative First Order Transitions. *Phys. Rev. Lett.*, 120(15):1–6, 2018.

[179] R. Rota, F. Storme, N. Bartolo, R. Fazio, and C. Ciuti. Critical behavior of dissipative two-dimensional spin lattices. *Phys. Rev. B*, 95(13):134431, 2017.

[180] Michael Skotiniotis, Pavel Sekatski, and Wolfgang Dür. Quantum metrology for the Ising Hamiltonian with transverse magnetic field. *New J. Phys.*, 17(7):073032, 2015.

[181] S. M. Roy and Samuel L. Braunstein. Exponentially enhanced quantum metrology. *Phys. Rev. Lett.*, 100(22):220501, 2008.

[182] S. Choi and B. Sundaram. Bose-Einstein condensate as a nonlinear Ramsey interferometer operating beyond the Heisenberg limit. *Phys. Rev. A*, 77(5):053613, 2008.

[183] Sergio Boixo, Steven T. Flammia, Carlton M. Caves, and JM Geremia. Generalized Limits for Single-Parameter Quantum Estimation. *Phys. Rev. Lett.*, 87131(9):1–4, 2006.

[184] Daniel Maldonado-Mundo and Alfredo Luis. Metrological resolution and minimum uncertainty states in linear and nonlinear signal detection schemes. *Phys. Rev. A - At. Mol. Opt. Phys.*, 80(6):063811, 2009.

[185] R. A. Oliva and Steven H. Strogatz. Dynamics of a Large Array of Globally Coupled Lasers With Distributed Frequencies. *Int. J. Bifurc. Chaos*, 11(09):2359–2374, 2001.

[186] Vardit Eckhouse, Moti Fridman, Nir Davidson, and Asher A. Friesem. Loss enhanced phase locking in coupled oscillators. *Phys. Rev. Lett.*, 100(2):024102, 2008.

[187] Micha Nixon, Moti Friedman, Eitan Ronen, Asher A. Friesem, Nir Davidson, and Ido Kanter. Synchronized cluster formation in coupled laser networks. *Phys. Rev. Lett.*, 106(22):223901, 2011.

[188] Hannes Risken. *Fokker-planck equation*. Springer, 1984.

[189] Juan A. Acebrón, L. L. Bonilla, Conrad J.Pérez Vicente, Félix Ritort, and Renato Spigler. The Kuramoto model: A simple paradigm for synchronization phenomena. *Rev. Mod. Phys.*, 77(1):137–185, 2005.

[190] Francisco A. Rodrigues, Thomas K.D.M. Peron, Peng Ji, and Jürgen Kurths. The Kuramoto model in complex networks. *Phys. Rep.*, 610:1–98, 2016.

[191] Strogatz SH. Exploring complex networks. *Nature*, 410(6825):268–276, 2001.

[192] Alex Arenas, Albert Díaz-Guilera, and Conrad J. Pérez-Vicente. Synchronization reveals topological scales in complex networks. *Phys. Rev. Lett.*, 96(11):114102, 2006.

[193] D Cumin and C P Unsworth. Generalising the Kuramoto model for the study of neuronal synchronization in the brain. *Phys. D*, 226(2):181–196, 2007.

[194] J Struck, C Ölschläger, R Le Targat, P Soltan-Panahi, A Eckardt, M Lewenstein, P Windpassinger, and K Sengstock. Quantum simulation of frustrated classical magnetism in triangular optical lattices. *Science*, 333(6045):996–9, aug 2011.

[195] Natalia G. Berloff, Matteo Silva, Kirill Kalinin, Alexis Askitopoulos, Julian D. Töpfer, Pasquale Cilibrizzi, Wolfgang Langbein, and Pavlos G. Lagoudakis. Realizing the classical XY Hamiltonian in polariton simulators. *Nat. Mater.*, 16(11):1120–1126, sep 2017.

[196] Micha Nixon, Eitan Ronen, Asher A. Friesem, and Nir Davidson. Observing geometric frustration with thousands of coupled lasers. *Phys. Rev. Lett.*, 110(18):184102, 2013.

[197] Y Takeda, S Tamate, Y Yamamoto, H Takesue, T Inagaki, and S Utsunomiya. Boltzmann sampling for an XY model using a non-degenerate optical parametric oscillator network. *Quantum Sci. Technol.*, 3(1):014004, jan 2018.

[198] Shuhei Tamate, Yoshihisa Yamamoto, Alireza Marandi, Peter McMahon, and Shoko Utsunomiya. Simulating the classical XY model with a laser network. *arXiv Prepr. arXiv1608.00358*, 2016.

[199] Dh Ackley, Ge Hinton, and Tj Sejnowski. A learning algorithm for boltzmann machines. *Cogn. Sci.*, 9(1):147–169, 1985.

[200] Richard S. Zemel, Christopher K. I. Williams, and Michael C. Mozer. Lending Direction to Neural Networks 2 Stochastic Directional Unit Boltzmann Machines. *Neural Networks*, 8(4):503–512, 1995.

[201] Pierre Baldi and Ronny Meir. Computing with Arrays of Coupled Oscillators: An Application to Preattentive Texture Discrimination. *Neural Comput.*, 2(4):458–471, 1990.

[202] Sidney Coleman. There are no Goldstone bosons in two dimensions. *Commun. Math. Phys.*, 31(4):259–264, 1973.

[203] Daniel C. Mattis. Transfer matrix in plane-rotator model. *Phys. Lett. A*, 104(6-7):357–360, 1984.

[204] V L Berezinskii. Destruction of long-range order in one-dimensional and two-dimensional systems having a continuous symmetry group I. classical systems. *Sov. Phys. JETP*, 32(3):493, 1971.

[205] J. Zittartz. Phase transition of the two-dimensional classicalXY-model. *Zeitschrift fr Phys. B Condens. Matter Quanta*, 23(1):55–62, 1976.

[206] P. a. Ivanov and D. Porras. Adiabatic quantum metrology with strongly correlated quantum optical systems. *Phys. Rev. A*, 88(2):023803, 2013.

[207] Ravid Shaniv, Nitzan Akerman, and Roee Ozeri. Atomic Quadrupole Moment Measurement Using Dynamic Decoupling. *Phys. Rev. Lett.*, 116(14):140801, 2015.

[208] Esteban A. Martinez, Christine A. Muschik, Philipp Schindler, Daniel Nigg, Alexander Erhard, Markus Heyl, Philipp Hauke, Marcello Dalmonte, Thomas Monz, Peter Zoller, and Rainer Blatt. Real-time dynamics of lattice gauge theories with a few-qubit quantum computer. *Nature*, 534(7608):516–519, 2016.

[209] Pedro Nevado, Samuel Fernández-Lorenzo, and Diego Porras. Topological Edge States in Periodically Driven Trapped-Ion Chains. *Phys. Rev. Lett.*, 119(21):210401, 2017.

[210] A. A. Zvyagin. Dynamical quantum phase transitions. *Low Temp. Phys.*, 42(11):971–994, 2017.

[211] Utso Bhattacharya, Souvik Bandyopadhyay, and Amit Dutta. Mixed state dynamical quantum phase transitions. *Phys. Rev. B*, 96(18):180303, 2017.

[212] Luca Gammaitoni, Istituto Nazionale, Dipartimento Fisica, Sezione Perugia, I Perugia, D Augsburg, Peter Jung, Fabio Marchesoni, and I Camerino. Stochastic resonance. *Rev. Mod. Phys.*, 70(1):223–287, 1998.

[213] R. Dean Astumian and Peter Hänggi. *Brownian motors*, volume 55. 2002.